UNIVERSITY OF CALIFORNIA

Santa Barbara

Mechanisms and Attribution of Changes in Austral Summer Precipitation related to the South Atlantic Convergence Zone

A dissertation submitted in partial satisfaction
of the requirements for the degree Doctor of Philosophy
in
Geography
by
Marcia Terezinha Zilli

Committee in charge:

Professor Leila M. V. Carvalho, Chair
Professor Keith Clarke
Professor Qinghua Ding
Dr. Brant Liebmann, National Oceanic and Atmospheric Administration

September 2017

The dissertation of Marcia Terezinha Zilli is approved.

_____

Brant Liebmann

_____

Keith Clarke

_____

Qinghua Ding

_____

Leila M. V. Carvalho, Committee Chair

September 2017

Mechanisms and attribution of changes in austral summer precipitation related to the South Atlantic Convergence Zone

ACKNOWLEDGEMENTS

I would like to express my deepest gratitude to the chair of my committee, Leila Carvalho, not only for her priceless scientific and professional advices, but mostly for her endless care and support. Your serenity and clear-mindedness guided me through all the hardships I faced during my doctorate. More than an advisor, I have you as part of my family and I will be forever thankful for all the time you were by my side, helping me at each step of the way.

I would like to thank my committee members, Professor Keith Clarke, Professor Qinghua Ding, and Dr. Brant Liebmann, for their understanding of my capacities and limitations. Your dedication in helping me improve this research is very much appreciated.

I would like to show my appreciation to the Brazilian National Council of Scientific Research (CNPq) and the Science without Borders program for the financial support throughout my doctorate. I would also like to thank the Department of Geography and the Earth Research Institute for their support.

I own my deepest gratitude to my family, and especially to my mother Maria Tereza, for understanding my career option and for supporting me even when this meant that we would only be able to spend together only a few weeks per year.

Special thanks also to all the past and current members of the CLIVAC lab, and to all my friends for their support.

CURRICULUM VITAE: MARCIA TEREZINHA ZILLI

August 2017

Education

Ph.D. Geography – University of California, Santa Barbara, September 2017 (expected). Mechanisms and Attribution of Changes in Austral Summer Precipitation related to the South Atlantic Convergence Zone

M.Sc. Water Resources and Environmental Engineering – Federal University of Parana, Curitiba, Brazil, February 2008. Interannual variability of rainfall in spring and summer in South America, their interconnections and their impact on major Brazilian hydroelectric power plants' reservoirs.

B.Sc. Environmental Engineering – Federal University of Parana, Curitiba, Brazil, February 2005. Interannual variations of rainfall in South America and the nature of SACZ-Subtropics oscillation in summer rainfall.

Teaching experience

Teaching Assistant – UC Santa Barbara, Dept. of Geography

- Economic Geography – Geog109 (2017)
- Land, Water, and Life – Geog 3B (2016)
- Geography of Surfing – Geog 20 (2016)
- Environmental Hydrology – Geog 112 (2015)

Teaching Assistant – UC Santa Barbara, Dept. of Environmental Studies

- Science and Policy of Climate Change – ENVS117 (2017)

Reader – UC Santa Barbara, Dept. of Geography

- Mountain Weather and Climate – Geog 195LC (2014)
- Climate Change – Geog 119 (2013)

Lecturer – Federal University of Parana, Curitiba, BR, Dept. of Hydraulics and Sanitation

- Urban and Environmental Sanitation (2012)
- Urban Sanitation Structures (2012)

Lecturer – Anchieta College of Parana, Curitiba, BR, Dept. of Environmental Engineering

- Introduction to Environmental Engineering (2011)
- Climatology and Meteorology (2011)
- Applied Hydraulics (2012)
- Atmospheric Pollution (2012)
- Water Supply Systems (2011)

Publications

Zilli, M.T., L. Carvalho, B. Lintner. 2017: Observed decadal variability in precipitation and circulation over South America during austral summer. *Climate Dynamics* (in review)

Zilli, M.T., L. Carvalho, B. Liebmann, M. A. Silva Dias. 2017: A comprehensive analysis of trends in extreme precipitation over Southeastern Brazil. *International Journal of Climatology*, 37, 2269-2279. DOI: 10.1002/joc.4840

Grimm, A. M., **M.T. Zilli.** 2009: Interannual Variability and Seasonal Evolution of Summer Monsoon Rainfall in South America. Journal of Climate, 22, 2257-2275. DOI: http://dx.doi.org/10.1175/2008JCLI2345.1

Grimm, A.M., **M.T. Zilli**, I.F.A. Cavalcanti. 2007: Do seasonal forecasts reproduce the link between early and peak monsoon rainfall in South America? CLIVAR Exchanges. , 12, 16-17.

Publications in Preparation

Zilli, M.T., L. Carvalho, B. Lintner, Q. Ding. 2017: Detection and Attribution of Causes of the Poleward Shift of the South Atlantic Convergence Zone in CMIP-5 simulations

Awards

National Council for Scientific and Technological Development (CNPq), Brazil – Science without Borders Graduate Student Fellowship (202691/2011-0). *The South Atlantic Convergence Zone Variability and the Natural Disasters occurrence over Southeastern Brazil.* (Sept. 2012-Aug. 2016)

UCSB Earth Research Institute – Summer Research Fellowship (2013, 2014, 2015, 2016)

Earth Research Institute Travel Scholarship (2013, 2014, 2015, 2016)

Jack and Laura Dangermond Travel Scholarship (2013, 2014, 2015, 2016)

Brazilian Meteorological Society 3rd International Symposium on Climatology – Featured article (2009)

Federal University of Parana XIII Undergraduate Research Event – 1st Place award: Applied Physics (2005)

Service

Journal Referee: Journal of Geophysical Research, Water, and Meteorological Applications

Dept. of Geography UCSB, Graduate Student Representative (2013-2016) Representative at department faculty meetings

Conference and Workshop Participation

American Geophysical Union: Annual Meeting – San Francisco, CA (2013, 2014, 2015, 2016)

University of Minnesota: 4th Workshop on Understanding Climate Change from Data – Boulder, CO (June 30- July 2, 2014)

Brazilian Meteorological Society: 3rd International Symposium on Climatology – Canela, RS, BR (October 18-21, 2009)

Brazilian Meteorological Society: XV Brazilian Meteorology Conference – São Paulo, SP, BR (August 24-29, 2008)

Brazilian Water Resources Association: XVII Brazilian Symposium on Water Resources. São Paulo, SP, BR (November 25-29, 2007)

American Meteorological Society: International Conference on South Hemisphere Meteorology and Oceanography, Foz do Iguassu, PR, BR (April 24-28, 2006)

Brazilian Meteorological Society: XIV Brazilian Meteorology Congress, Florianópolis, SC, BR, (November 27-December 1, 2006)

ABSTRACT

Mechanisms and attribution of changes in austral summer precipitation related to the South Atlantic Convergence Zone

By

Marcia Terezinha Zilli

Austral summer (DJF) precipitation over tropical South America (SA) is characterized by the South American Monsoon System (SAMS) and the South Atlantic Convergence Zone (SACZ). The increase in atmospheric temperature and water vapor content over the SA during the last decades of the 20th century could affect the duration and amplitude of the SAMS and the intensity of the SACZ. This research examines the spatial variability of precipitation trends over SE Brazil, focusing on the SACZ. More specifically, this study investigates trends in precipitation over Southeastern Brazil (SE Brazil) and examines changes in the position and intensity of the SACZ. SE Brazil is the most densely populated region in the country with a large portion of this population living in urban centers. The SACZ is important for agriculture and water supply for millions of people. One of the main goals of this research is to identify mechanisms associated with the observed changes in the characteristics of the SACZ during the last three decades of the 20th century, and examine the relative contribution of natural and anthropogenic forcing to precipitation trends. The first chapter investigates the pattern of spatial variability of precipitation trends over the coastal region of SE Brazil. This study shows that over the southern portion of the study area, precipitation is increasing due to the increase in the frequency and intensity of extreme events. Over the northern portion of the area, while the intensity of extreme events is increasing, the number of precipitating days is decreasing. This spatial pattern of

precipitation trends suggests a poleward shift of the SACZ, which is investigated in the second chapter. Chapter 2 focuses on the underlying mechanisms associated with changes in precipitation intensity related to the position of the SACZ. Decadal variations in the mean state of the atmosphere suggest that the observed changes in precipitation over SE Brazil are associated with a weakening of the poleward winds along the eastern Brazilian coast that reduces the dynamic support necessary for convection along the equatorward margin of the SACZ. Additionally, this analysis also identifies a decrease in low-to-mid troposphere (700hPa) moisture over the tropical Atlantic in the recent decade that further reduces the moisture transported into the convective margin of the SACZ. Both mechanisms contribute to reducing precipitation over eastern tropical Brazil and characterize the poleward shift of the SACZ. The final chapter focuses on evaluating the contribution of natural variability and anthropogenic-related forcings to the poleward shift of the SACZ and drying conditions over eastern Brazil at the end of 20th century. Simulations from different scenarios of the Coupled Model Intercomparison Project phase 5 (CMPI5) models capable of reproducing the SACZ climatology suggest significant contribution of anthropogenic forcing on the SACZ-related precipitation trends. Despite the large discrepancies in the simulated precipitation trends, similarities among the ensemble members provide compelling evidence that the poleward shift of the SACZ in the last three decades of the 20^{th} century is largely enhanced by anthropogenic forcing. Collectively, the three chapters of this dissertation characterize the recent changes in precipitation related to a poleward shift of the SACZ and give novel insights into the influence of anthropogenic-related forcing on these changes. These findings advance the scientific understanding of the consequences of recent climate variability and change over eastern tropical South America, particularly over the SACZ.

TABLE OF CONTENTS

LIST OF FIGURES

LIST OF TABLES

Introduction

In 2013, the Intergovernmental Panel on Climate Change (IPCC) released its Fifth Assessment Report (AR5) communicating an increase in global temperature since the last century, both over land and ocean, with the last three decades being warmer than any other previous decades in instrumental records (Hartmann et al. 2013). As the troposphere warms up atmospheric water vapor content also increases, following the Clausius-Clapeyron law (Held and Soden 2006). Despite the large confidence in the spatial distribution and magnitude of the temperature and water vapor trends, their effects on the precipitation occurrence are spatially complex and not completely understood. In addition to the interplay of different mechanisms resulting in changes in precipitation, the confidence in these results is low due to data sparsity and quality or lack of agreement among the available data. Over Brazil, the confidence in an uptrend in precipitation is medium, but with large spatial variability (Hartmann et al. 2013).

Changes in precipitation over Southeastern Brazil (SE Brazil; Figure 1, top left) are of particular interest since this is the most urbanized region of the country (Figure 1, top right). Approximately 93% of the 86 million inhabitants of SE Brazil live in urban areas, and are responsible for about 55.2% of the national gross product (IBGE 2012). The population density is also large over the region (Figure 1, bottom), and largely concentrated on areas of complex topography (Figure 1, top left). Due to the economic and social importance of this region, there is a great concern regarding population's vulnerability and exposure to water scarcity and precipitation-related disasters.

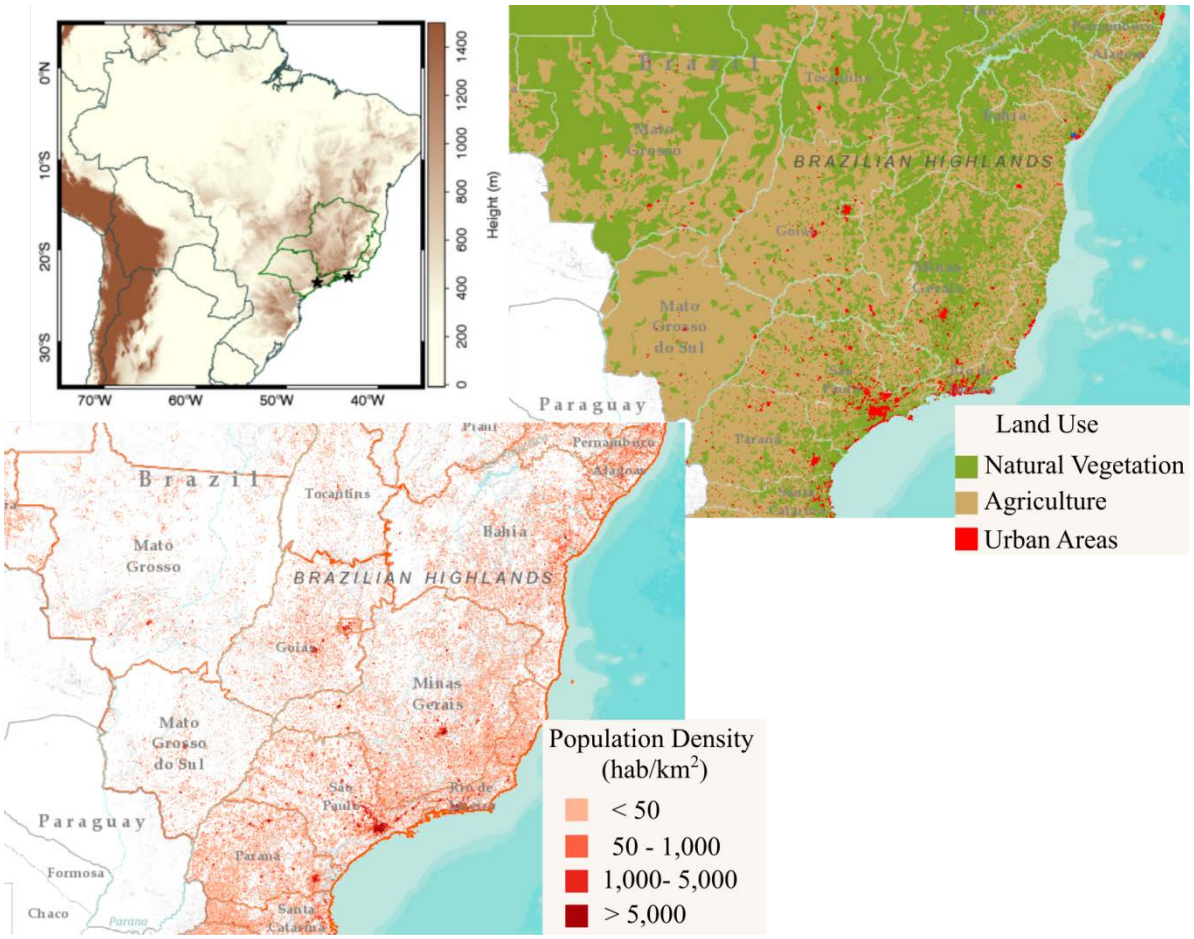

Figure 1 — Top left: Location of SE Brazil (green line), the cities (stars) of São Paulo (23.6°S, 46.6°W) and Rio de Janeiro (22.9°S, 43.2°W), and local topography (shades; 1km resolution DEM from SRTM; USGS 2004). Top right: Land use (source: IBGE 2017a). Bottom: population density (source: IBGE 2017b)

In 2016, the Brazilian government released the Third National Communication of Brazil to the United Nation Framework Convention on Climate Change, addressing the impacts of future climate change on Brazilian strategic sectors (Brazil 2016). Among the main impacts caused by changes in precipitation regimes, the communication emphasizes a reduction in water availability and daily runoff and an increase in the area with negative water balance over central and eastern Brazil, which can potentially affect the agricultural production and hydroelectric energy generation. On the other hand, the communication also addresses the risk of increase in extreme precipitation events in the first half of the 21st

century that could result in increased vulnerability to floods, flash floods, and landslides over SE Brazil. Other studies also show the large socio-climatic vulnerability of the region, particularly in metropolitan regions (São Paulo and Rio de Janeiro, stars in Figure 1, top left) and mostly related to population density and, to a less extent, to social and economic inequalities (Nobre et al. 2010; Torres et al. 2012; Cavalcanti et al. 2017; Debortoli et al. 2017).

SE Brazil is the Brazilian region most exposed to natural disasters related to intense precipitation such as floods, flash floods, and landslides (Figure 2; CEDEP UFSC 2013a), with the austral summer (December to February) concentrating about 76% of the occurrences registered since 1991. After 2001, these events have become more frequent over the region, which could be attributed to an increase in the urban population living in risk areas, and also, to some extent, to an improvement in the notification system (CEDEP UFSC 2013a; CEDEP UFSC 2013c). Most of these events occurred in urbanized areas along the coast and with complex topography.

Austral summer of 2009-10 has the largest number of floods in the region since the beginning of the records in 1991 (CEDEP UFSC 2013b, c). Between December 31st and January 1st, a 400mm rain event occurred along the coastal area of Rio de Janeiro state (RJ), causing landslides in the city of Angra dos Reis (Figure 3) that resulted in 53 fatalities, affected 4,000 people and caused approximately US$270 million in damages (Folha de São Paulo 2010; CEDEP UFSC 2013b). On the same day, the city of São Luiz do Paraitinga, São Paulo state (SP; Figure 3), was affected by heavy precipitation that resulted in massive floods that damaged almost 80% of the heritage buildings of this historical city and affected 9,000 of its 10,500 inhabitants (Pagnan 2010). Later in the season, on January 20th-21st, the

metropolitan region of São Paulo registered 479mm of precipitation during an active South Atlantic Convergence Zone (SACZ) event that caused floods and disrupted traffic in more than 110 areas, according to the Sao Paulo State Emergency Response Agency (available at http://www.cgesp.org/v3/alagamentos.jsp).

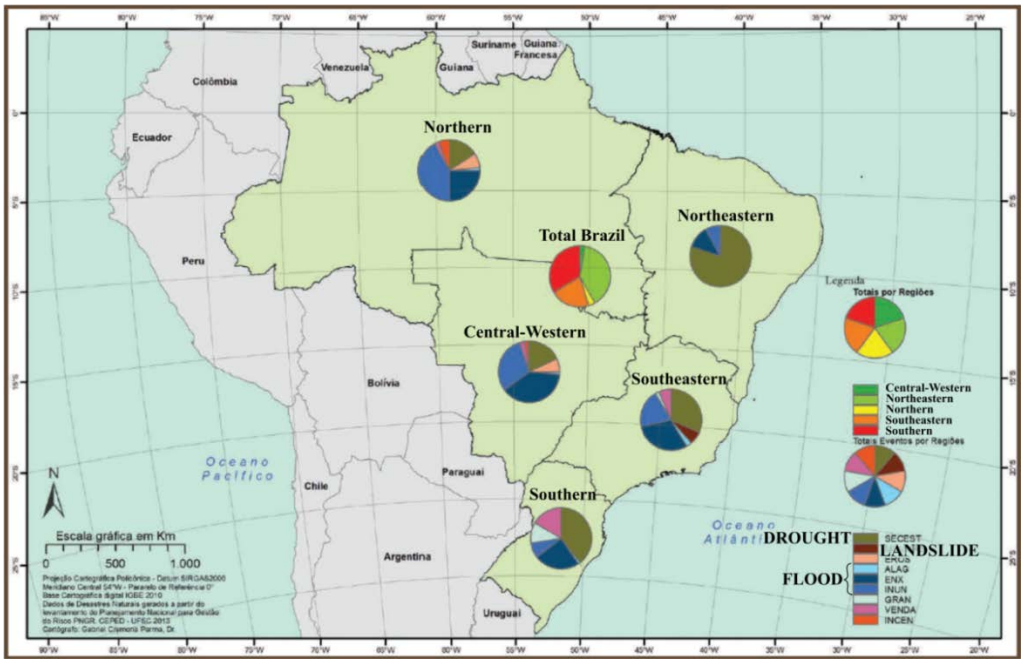

Figure 2 — Occurrence of natural disasters in Brazil separated according to the region: drought (green), landslides (brown), floods and flash floods (shades of blue), winds (magenta), and hail (cyan). (Adapted from CEDEP UFSC 2013a)

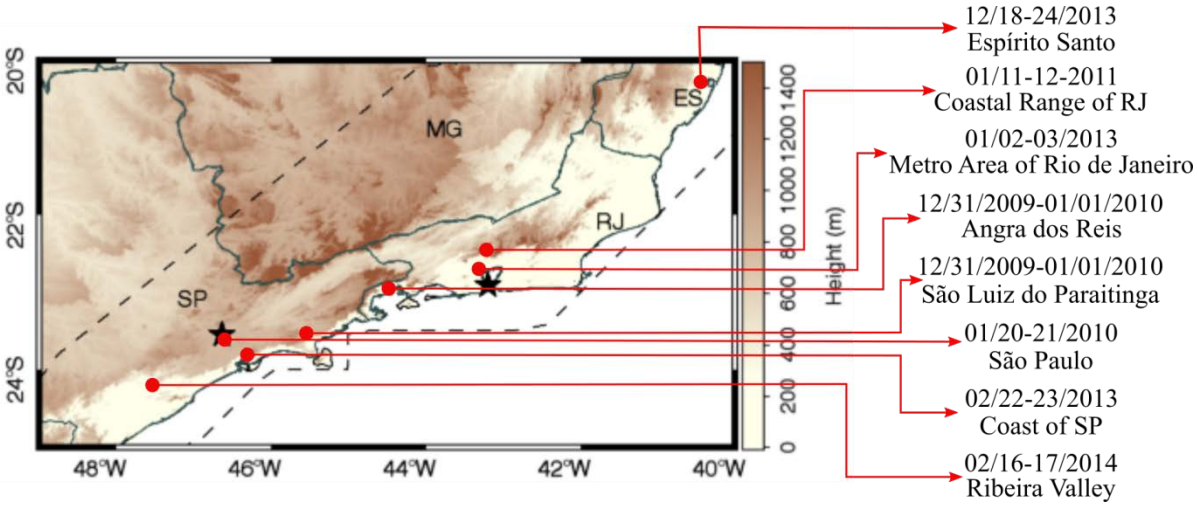

Figure 3 — Location of the main natural disasters registered since 2010 over SE Brazil.

In the summer of the next year (2010-11), RJ reported the worst natural disaster registered in Brazilian history. On January 11th-12th, an active SACZ event caused intense precipitation over the Coastal Range region of the state (Figure 3), with accumulated precipitation above 200mm in 24 hours, resulting in massive landslides and mudslides. The event affected 12 cities, causing 916 fatalities and displacing more than 35,000 people (Canedo et al. 2011; Brazil 2016). Two years later, localized storms caused landslides and flooding in the metropolitan area of Rio de Janeiro (January 02nd-03rd, 2013; Figure 3; Época 2013) and at the coastal area of SP (February 22nd-23rd; Figure 3; Maciel 2013). In December 2013, a sequence of SACZ events caused intense precipitation over the state of Espírito Santo (ES; Figure 3), resulting in accumulated precipitation of 300mm above the climatology for the month. The strongest events occurred between December 18th and 24th, with some rain gauges registering more than 300mm accumulated in this period. By the end of the month, 54 of 78 cities of the state were under an emergency situation, with more than 61,000 people displaced and 24 fatalities (Nascimento 2013). The 2013-14 summer season finished with another generalized flood on the south coast of SP, in the Ribeira Valley (Figure 3) on February 15th-17th, which displaced more than 1,000 people (Tomazela 2014).

On the other hand, the years of 2014 and 2015 were extremely dry over SE Brazil due to the absence of active SACZ during the rainy seasons (Coelho et al. 2016). SP was the most affected state, where the water supply reservoirs for the Metropolitan Area of São Paulo were below 25% at the end of the summer season (ANA/DAEE 2015).

This highly contrasting situation, with years characterized by record breaking total precipitation followed by years with severe droughts, highlights the importance of understanding the variability of precipitation, including extremes, over SE Brazil. The

majority of intense precipitation events occurring in the region are associated with the SACZ active phase, when atmospheric conditions favor convergence of winds and advection of moisture to the region (Liebmann et al. 2001; Carvalho et al. 2002, 2004; Seluchi and Chou 2009; Lima et al. 2010; Cavalcanti 2012). Conversely, the absence of these conditions for prolonged periods results in deficits of precipitation and even droughts. Global warming may increase precipitation variability in many regions of the world (IPCC AR5). Improving the understanding of the changes in the distribution and intensity of precipitation events, particularly in densely populated areas such as SE Brazil, largely contributes to the adaptation and preparedness to natural disasters and water scarcity.

Summer climate variability and the South Atlantic Convergence Zone

The atmospheric mechanisms associated with intense precipitation on SE Brazil are the South American Monsoon System (SAMS; Figure 4) and the South Atlantic Convergence Zone (SACZ; Figure 4). The SAMS is active from October through March and is described as a reversal in the wind anomalies over the continent and onset of large-scale convection over the continent (Barros et al. 2000; Zhou and Lau 2001; Vera et al. 2006b). The onset of the SAMS occurs between mid-September and mid-October (Silva and Carvalho 2007; Carvalho et al. 2011), when deep convective areas located over equatorial Amazon warm the troposphere and favor the establishment of the Bolivian High (Figure 5) over the Andes Altiplano (Lenters and Cook 1997). This increases the upper-level east-west pressure gradient and drives the upper levels monsoonal returning circulation (Figure 5), with the southerly winds over the continent turning clockwise toward east Africa after crossing the equator (Zhou and Lau 1998).

At lower levels, the deep convection and the differential land heating (Figure 5)

enhance the continental low pressure, increasing the land-ocean pressure gradient and accelerating the northeasterly trade winds. After crossing the Amazon, these winds are deflected southward by the Andes, forming a poleward flow along the eastern flank of the mountains (Figure 5; Zhou and Lau 1998), with intense episodes define as Low Level Jets (LLJ; Vera et al. 2006a). As the flow approaches the Chaco Low region over Argentina (Figure 5), it is redirected, advecting moisture toward SE Brazil or Southeastern South America (SESA; green area in Figure 4).

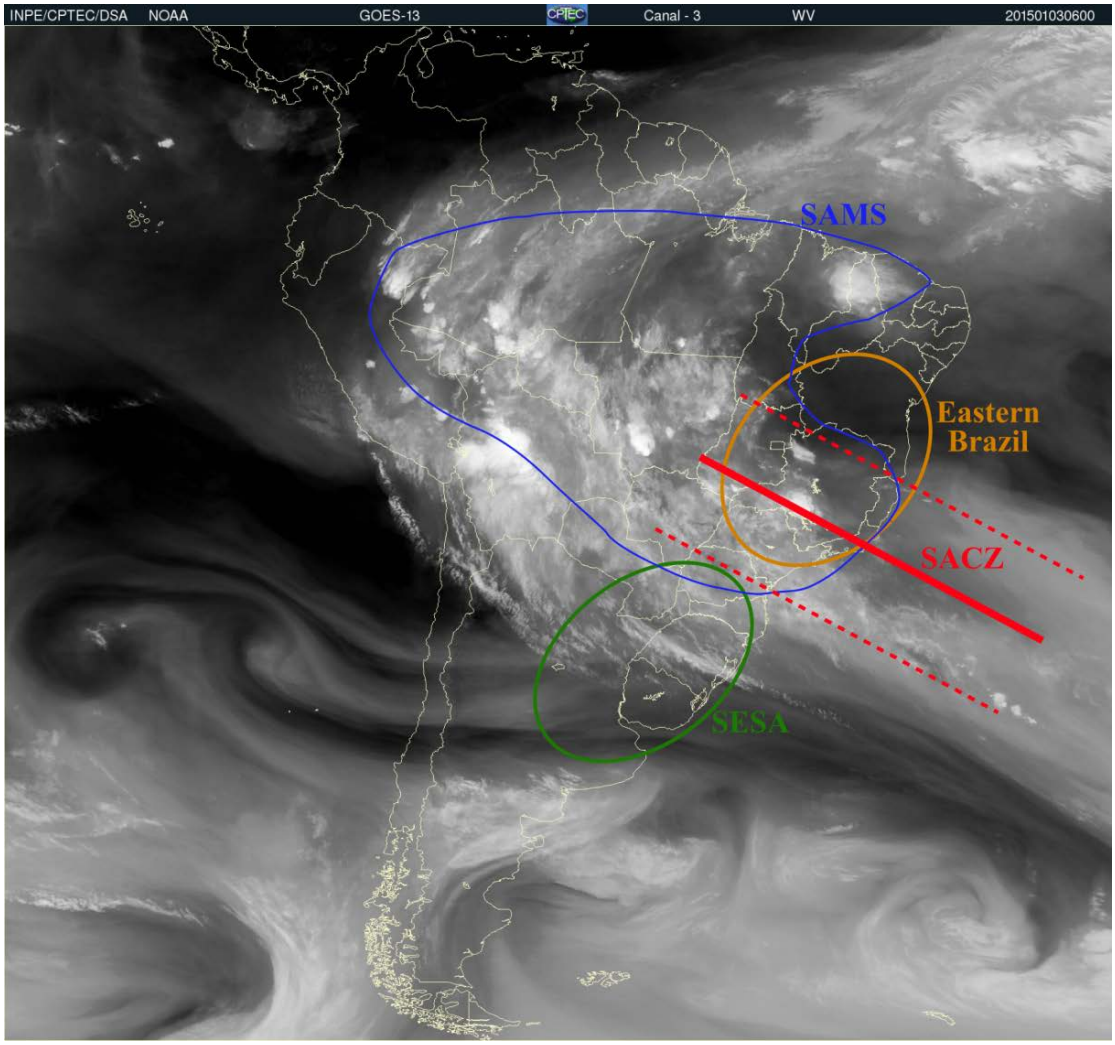

Figure 4 — NOAA GOES 13 Water Vapor image over South America (INPE/CPTEC/DSA) for Jan 03, 2015 0600UTC; South American Monsoon System (SAMS) in blue; South Atlantic Convergence Zone (SACZ) in red; Eastern Brazil in orange; and Southeastern South America (SESA) in green.

During the peak of the monsoon season, the deep convective heating over tropical South America intensifies the poleward flow along the eastern flank of the Andes through the Sverdrup balance, closing the anticyclonic circulation around the South Atlantic Subtropical High (SASH, Figure 5; Rodwell and Hoskins 2001; Liu et al. 2004; Wu et al. 2009). Moreover, the deep convection extends toward SE Brazil, where the local topography further intensifies the precipitation by mechanical uplift (Grimm et al. 2007; Kodama et al. 2012). The latent heat released by the increased precipitation warms the troposphere and increases the temperature gradient between the continent and the South Atlantic Ocean, sustaining the circulation (Zhou and Lau 1998).

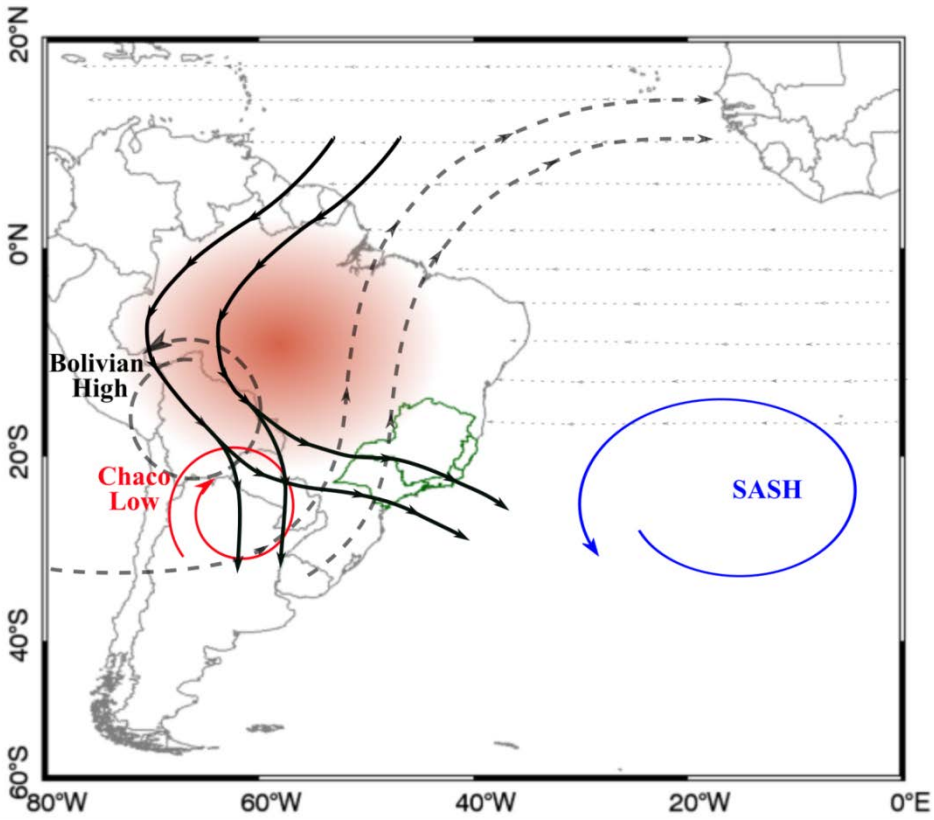

Figure 5 — Main circulation features of the SAMS: upper-level Bolivian High (counterclockwise dashed gray circulation); upper level monsoonal returning circulation (dashed gray lines); low level monsoonal flow (solid black line); Chaco Low (clockwise solid red circulation); SASH (counterclockwise solid blue circulation); trade winds region (dotted gray lines); and areas with deep convection heating (red shades)

The southeastward extension of the convective activity toward SE Brazil and subtropical South Atlantic Ocean is denominated South Atlantic Convergence Zone (SACZ; Figure 4) and is one of the main features of the SAMS (Kodama 1992, 1993; Zhou and Lau 1998; Liebmann et al. 2001; Carvalho et al. 2002, 2004; Raia and Cavalcanti 2008; Muza et al. 2009). Kodama (1992, 1993) described the SACZ as a baroclinic structure located eastward of a trough in the subtropical jet. It is formed by moisture converging from two different regions: low-level northerly inflow originated in the western periphery of the SASH; and westerly flows along the convergence zone, increasing in intensity with height and forming part of the subtropical jet in upper levels. These two components are essential for the development and strengthening of the convergence zone through frontogenesis intensification and convective instability generation (Kodama 1993).

Mechanisms associated with the SACZ spatial and temporal variability

The spatial variability of the SAMS summer precipitation is dominated by a dipole-like pattern, recurrent in time scales ranging from intraseasonal to decadal (Zhou and Lau 1998; Nogués-Paegle et al. 2000; Liebmann et al. 2004a; Carvalho et al. 2002, 2004, 2011; Grimm and Zilli 2009; Grimm and Saboia 2015). This dipole is present during both spring and summer and is characterized by an inversion in the signal of precipitation anomalies over eastern Brazil and SESA. During SAMS active phase (Figure 6, left), the monsoonal circulation advects moisture from the Amazon toward eastern Brazil. On the subtropics, the Chaco Low deepens, increasing the east-west pressure gradient and favoring the moisture transport from the South Atlantic toward the continent. These two circulations come together over SE Brazil, forming cyclonic anomalies related to ascending motion over the SACZ and causing intense moisture convergence and convective activity, with compensatory

subsidence to the southwest, over SESA. When the SACZ is inactive (Figure 6, right), the moisture flux from the Amazon is deflected southward due to the intensification of the LLJ. The SASH is displaced westward toward the continent, advecting moisture toward SESA, where it converges with the northwesterly branch from the Amazon, causing intense convection and precipitation over the area. In this case, the compensatory subsidence is over eastern Brazil (Barros et al. 2000; Nogués-Paegle and Mo 2002; Todd et al. 2003; Carvalho et al. 2002, 2004, 2011; Liebmann et al. 2004a; Grimm and Zilli 2009).

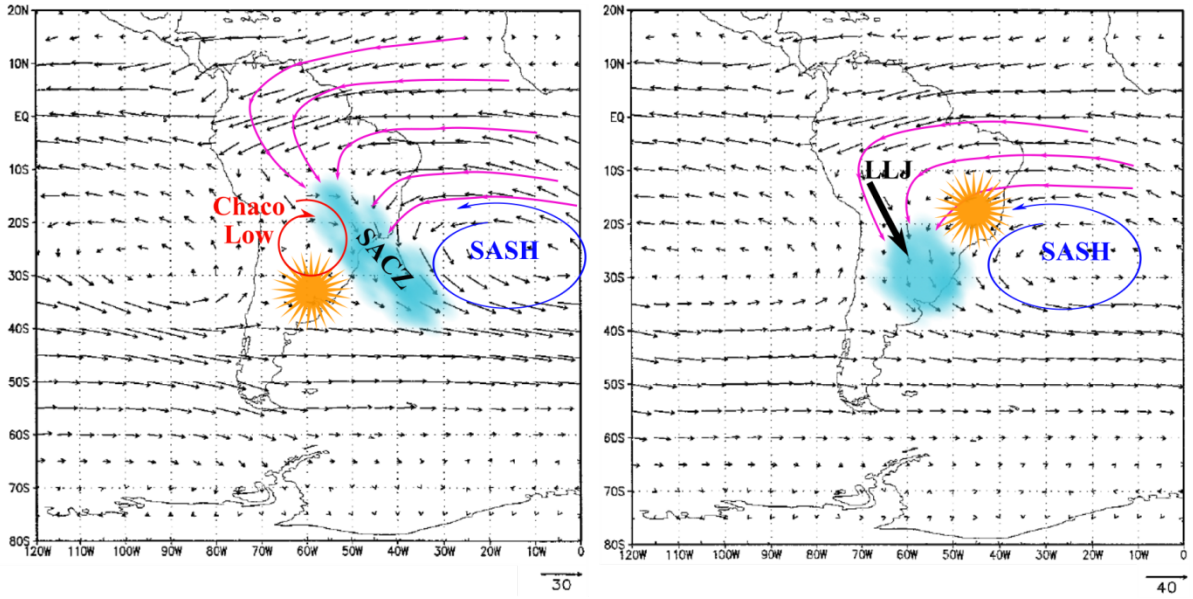

Figure 6 — Characteristics of the active (left) and inactive (right) phases of the SACZ: location of deep convection (blue shades) and subsidence (sun pattern); Chaco low (red solid circulation); SASH (blue solid circulation); LLJ (thick black arrow); and schematic circulation (magenta lines). Background: vertically integrated moisture flux from NCEP/NCAR reanalysis data (Adapted from Nogués-Paegle and Mo 1997)

In addition to characterizing the precipitation variability within each season, the dipole pattern also characterizes the reversal on the precipitation anomaly signal from spring to summer. Grimm and Zilli (2009) demonstrated that antecedent soil conditions during spring over eastern Brazil could influence the regional circulation, reversing the signal of the

precipitation anomaly during summer: during austral spring, positive (negative) precipitation anomalies increase (decrease) the soil moisture content and reduce (increase) the surface temperature over eastern Brazil; on late spring, the temperature anomalies induce anticyclonic (cyclonic) circulation anomalies that redirect the moisture flux from the Amazon toward SESA (eastern Brazil), resulting in negative (positive) precipitation anomalies in the region during austral summer (Grimm et al. 2007; Grimm and Zilli 2009). More recently, Grimm and Saboia (2015) confirmed that this inter-seasonal relationship also occurs on decadal time scales and are partially influenced by large-scale climatic modes, such as the Atlantic Multidecadal Oscillation (AMO) and the Interdecadal Pacific Oscillation (IPO).

As mention before, the dipolar pattern of precipitation anomalies over South America is related to active and suppressed SACZ phases, which depend on different large-scale mechanisms at various timescales. At synoptic to submonthly time scales (2-30 days), the cloudiness field related to enhanced convection is forced by a wavelike feature propagating from the extratropical Pacific across the southern tip of South America and then northeastward toward SE Brazil, characteristic of an mid-latitude Rossby wave train (Liebmann et al. 1999; Cunningham and Cavalcanti 2006). On intraseasonal scale (30-90 days), the Madden Julian Oscillation (MJO) also plays a role in triggering the Rossby wave train, with SACZ active phase related to suppressed convection over western Pacific and the Maritime continent and enhanced convection in central Pacific (Liebmann et al. 2004a; Carvalho et al. 2004, 2011; Cunningham and Cavalcanti 2006; Muza et al. 2009). The interannual variability is modulated by the El Niño Southern Oscillation (ENSO), with reduced (enhanced) precipitation anomalies over eastern Brazil and positive (negative)

anomalies over SESA during El Niño (La Niña) events (e.g., Grimm 2003; Drumond and Ambrizzi 2006; Grimm et al. 2007; Krishnamurthy and Misra 2010). On decadal time scales, positive (negative) phases of the PDO are associated with positive (negative) precipitation anomalies over eastern Brazil (Krishnamurthy and Misra 2011), intensifying the effects of ENSO when both oscillations are in phase (Kayano and Andreoli 2007).

The SACZ positioning and intensity is influenced by atmospheric-oceanic interactions associated with South Atlantic Dipole (SAD; Venegas et al. 1997; Bombardi et al. 2011; 2013). The SAD negative (positive) phase is characterized by negative (positive) SST anomalies over southwest subtropical South Atlantic and positive (negative) ones south of 40°S, and positive (negative) sea level pressure (SLP) anomalies over South Atlantic. During the negative SAD phase, the cold SST anomalies to the north are sustained by reduced incoming solar energy due to enhanced cloud cover related to active SACZ, possibly reinforcing it and increasing the SACZ persistence. Warmer SST anomalies over mid-latitudes are also favored by weaker westerlies, which reduce the ocean surface heat loss through evaporation (Robertson and Mechoso 2000; Chaves and Nobre 2004; Bombardi et al. 2013, 2014).

Climate change over SACZ and SE Brazil

According to the Clausius-Clapeyron law, the amount of water vapor in the troposphere increases linearly with temperature, favoring the thermodynamic component of the circulation and increasing moisture availability. However, changes in the dynamic component, related to horizontal and vertical advection, are spatially more variable and can offset the precipitation response (Schneider et al. 2010; Cherchi et al. 2011; Kitoh et al. 2013). Over South America, studies based on reanalyses and on simulations of the historical

scenario of global climate models located areas with large warming over the Amazon and central Brazil (Carvalho and Jones 2013; de Barros Soares et al. 2017) that are possibly affecting the position and intensity of the SASH (Li et al. 2013) and increasing the duration and amplitude of the SAMS over the continent (Jones and Carvalho 2013; Rao et al. 2014). In turn, changes in the SASH can influence the intensity and amount of relatively more stable air advected from the tropical South Atlantic into the northern margin of the SACZ, increasing its ventilation and reducing the support to precipitation formation (Lintner and Neelin 2010; Ma et al. 2011). There is also evidence that these trends will persist in the future (Seth et al. 2010; Carvalho and Jones 2013; Jones and Carvalho 2013; Li et al. 2013; Hsu et al. 2013; Kitoh et al. 2013), displacing the SACZ southward (Seth et al. 2010).

These changes in circulation and in the intensity and position of the SACZ affect the precipitation dipolar mode, changing the frequency and intensity of precipitation over eastern Brazil and SESA. Over SESA, observational studies identified an increase in total precipitation due to more frequent intense events (Haylock et al. 2006; Barros et al. 2008; Skansi et al. 2013). These trends were correctly reproduced by the historical (Vera et al. 2006c; Chou et al. 2014a; Diaz and Vera 2017) and future simulations of global climate models (Junquas et al. 2012, 2013; Chou et al. 2014b; Sanchez et al. 2015), indicating that the positive trends are likely to persist along the 21st century.

Over Eastern Brazil, long-term trends are less coherent, with positive trends in rainfall intensity observed in the states of RJ (Teixeira and Satyamurty 2011) and SP (Liebmann et al. 2004b; Dufek and Ambrizzi 2008; Marengo et al. 2010, 2013; Teixeira and Satyamurty 2011; Silva Dias et al. 2013; Obregón et al. 2014). On the urban areas of São Paulo, observational studies indicate a decrease in the number of rainy days and light rainy days, but

an increase in the number of heavy precipitation (Xavier et al. 1994; Dufek and Ambrizzi 2008; Sugahara et al. 2009; Silva Dias et al. 2013; Marengo et al. 2013; Raimundo et al. 2014). However, the global climate models are not able to correctly simulate the SACZ variability, resulting in large uncertainties on the signal of the trends over the region (Carvalho and Jones 2013; Diaz and Vera 2017; de Barros Soares et al. 2017).

Dissertation objectives

This research seeks to advance the scientific understanding of the consequences of climate change over eastern tropical South America with particular emphasis to the South Atlantic Convergence Zone to ultimately improve preparedness to precipitation-related natural disasters and water security. ***The specific objectives of this dissertation are:***

1. Provide a comprehensive analysis of the spatial variability of trends in observed precipitation over Southeastern Brazil focusing on regional and local scales (Chapter 1).
2. Investigate decadal changes in circulation and moisture related to the position and intensity of the South Atlantic Convergence Zone that influence dynamic and thermodynamic processes related to convection and precipitation over Eastern and Southeastern Brazil (Chapter 2).
3. Determine the contribution of natural variability and anthropogenic-related forcing on precipitation trends through the evaluation of various global climate model simulations (Chapter 3).

The first paper of this dissertation investigates trends in observed precipitation over the Southeastern coast of Brazil during the wet season (October to March), using rain gauge stations and gridded precipitation data with more than 70 years (Zilli et al. 2017a). By

utilizing robust statistical analyses, this work identified a positive trend in both average and extreme precipitation over the study region. This research is unique relative to previous studies because it detected spatial variability of these trends, and a tendency to more rainy days on the south portion of the study area, while the north portion shows a tendency for fewer but more intense precipitation events. The study provides a novel and detailed understanding of the precipitation variability, including extremes, in a very populated area of South America. The spatial pattern of the observed precipitation trends also suggests a poleward shift of the SACZ, favoring (inhibiting) convective activity over the southern (northern) portion of the study region.

The second chapter focuses on identifying mechanisms associated with the observed trends in precipitation over Southeastern Brazil (Zilli et al. 2017b, in review). It expands the study area, including also the eastern portion of the country, with the objective of capturing changes occurring along both margins of the South Atlantic Convergence Zone and providing evidence of the poleward shift of the convective activity. By comparing decadal averages of precipitation and other atmospheric fields during austral summer (December to March), this research identified changes in the circulation that have not been described previously: the weakening of the poleward winds along the eastern Brazilian coast and drying of the low-to-mid troposphere (700hPa). These changes affect the SACZ convergence and result in a decrease in average precipitation along the northern margin of the convergence zone. These results provide invaluable insights on mechanisms related to the SACZ intensity and positioning that are crucial to evaluate climate change over populated areas in Brazil.

The third chapter of this dissertation has the objective of attributing the causes of the

observed changes in precipitation related to the poleward shift of the SACZ. This work is based on the evaluation of precipitation trends simulated by a set of state-of-art global climate models capable of correctly reproducing the observed precipitation variability over the region. To accomplish these goals, this study compared precipitation trends obtained from coupled global climate model simulations that comprise the archives of the Coupled Model Intercomparison Project Phase 5 (CMIP5) perturbed only by natural variability (such as solar radiation and volcanic eruptions) with trends obtained from simulations forced by the 20th century anthropogenic-related changes in atmospheric composition and land use change. This study focused on identifying precipitation trends along the margins of the South Atlantic Convergence Zone. This is the first work to examine in detail the attribution of the poleward shift in the convergence zone to anthropogenic forcing, contributing to improve the current understanding of the expected changes in precipitation over the region.

References

ANA/DAEE (2015, Mar 12th) Boletim diário ANA/DAEE de monitoramento do Sistema Cantareira. http://arquivos.ana.gov.br/saladesituacao/BoletinsDiarios/DivulgacaoSiteSabesp_12-3-2015.pdf. Accessed in Jul, 16th 2017 (in Portuguese)

Barros V, Doyle ME, Camilloni IA (2008) Precipitation trends in southeastern South America: relationship with ENSO phases and with low-level circulation. Theor Appl Cimatol 93:19-33. doi: 10.1007/s00704-007-0329-x

Barros V, Gonzalez M, Liebmann B, Camilloni I (2000) Influence of the South Atlantic Convergence Zone and South Atlantic sea surface temperature on interannual summer rainfall variability in Southeastern South America. Theor Appl Cimatol 67:123-133

Brazil (2016) Third National Communication of Brazil to the United Nations Framework Convention on Climate Change – Volume II. Ministry of Science, Technology and Innovation. Brasília, Brazil

Bombardi RJ, Carvalho LMV (2011) The South Atlantic Dipole and Variations in the Characteristics of the South American Monsoon in the WCRP-CMIP3 Multi-Model

Simulations. Clim Dyn 36:2091-2102. doi: 10.1007/s00382-010-0836-9

Bombardi R, Carvalho LMV, Jones C (2013) Precipitation over eastern South America and the South Atlantic Sea surface temperature during neutral ENSO periods. Clim Dyn 42:1553-1568. doi: 10.1007/s00382-013-1832-7

Bombardi R, Carvalho LMV, Jones C (2014) Simulating the influence of the South Atlantic Dipole on the South Atlantic Convergence Zone during neutral ENSO. Theor Appl Cimatol 118:251-269. doi: 10.1007/s00704-013-1056-0

Canedo P, Ehrlich M, Lacerda WA (2011) Chuvas na região serrana do Rio de Janeiro. Sugestões para ações de engenharia e planejamento. Rio de Janeiro, Brazil: Instituto Alberto Luiz Coimbra de Pos-Graduação e Pesquisa de Engenharia – COPPE, Federal University of Rio de Janeiro, RJ (in Portuguese)

Carvalho LMV, Jones C (2013) CMIP5 simulations of low level tropospheric temperature and moisture over tropical Americas. J Clim 26:6257-6286. doi: 10.1175/JCLI-D-12-00532.1

Carvalho LMV, Jones C, Liebmann B (2002) Extreme precipitation events in Southeastern South America and large-scale convective patterns in the South Atlantic Convergence Zone. J Clim 15:2377-2394

Carvalho LMV, Jones C, Liebmann B (2004) The South Atlantic Convergence Zone: intensity, form, persistence and relationships with intraseasonal to interannual activity and extreme rainfall. J Clim 17:88-108

Carvalho LMV, Silva AE, Jones C, Liebmann B, Silva Dias PL, Rocha HR (2011) Moisture transport and intraseasonal variability in the South America Monsoon System. Clim Dyn 36:1865-1880. doi: 10.1007/s00382-010-0806-2

Cavalcanti I FA (2012) Large Scale and Synoptic Features Associated with Extreme Precipitation Over South America: A Review and Case Studies for the First Decade of the 21st Century. Atmos Res 118:27-40. doi: 10.1016/j.atmosres.2012.06.012

Cavalcanti IFA, Nunes L, Marengo J, Gomes J, Silveira V, Castellano M (2017) Projections of Precipitation Changes in Two Vulnerable Regions of São Paulo State, Brazil. Am J Clim Change, 6:268-293. doi: 10.4236/ajcc.2017.62014

CEDEP UFCS (2013a) Atlas Brasileiro de Desastres Naturais: 1991 a 2012, Volume Brasil. Centro Universitário de Estudos e Pesquisas sobre Desastres, Universidade Federal de Santa Catarina 2nd ed. Florianópolis, Brazil (in Portuguese)

CEDEP UFCS (2013b) Atlas Brasileiro de Desastres Naturais: 1991 a 2012, Volume Rio de Janeiro. Centro Universitário de Estudos e Pesquisas sobre Desastres Universidade Federal de Santa Catarina 2nd ed. Florianópolis, Brazil (in Portuguese)

CEDEP UFCS (2013c) Atlas Brasileiro de Desastres Naturais: 1991 a 2012, Volume São Paulo. Centro Universitário de Estudos e Pesquisas sobre Desastres Universidade Federal de

Santa Catarina 2nd ed. Florianópolis, Brazil (in Portuguese)

Chaves RR, Nobre P (2004) Interactions between sea surface temperature over the South Atlantic Ocean and the South Atlantic Convergence Zone. Geophys Res Lett, 31:L03204. doi: 10.1029/2003GL018647

Cherchi A, Alessandri A, Masina S, Navarra A (2011) Effects of increased CO_2 level on monsoons. Clim Dyn 37:83-101. doi: 10.1007/s00382-010-0801-7

Chou S, Lyra A, Mourão C, Dereczynski C, Pilotto I, Gomes J, Bustamante J, Tavares P, Silva A, Rodrigues D, Campos D, Chagas D, Sueiro G, Siqueira G, Nobre P, Marengo J (2014a) Evaluation of the Eta simulations nested in three Global Climate Models. Am J Clim Change 3:438-454. doi: 10.4236/ajcc.2014.35039

Chou S, Lyra A, Mourão C, Dereczynski C, Pilotto I, Gomes J, Bustamante J, Tavares P, Silva A, Rodrigues D, Campos D, Chagas D, Sueiro G, Siqueira G, Nobre P, Marengo J. (2014b) Assessment of climate change over South America under RCP 4.5 and 8.5 downscaling scenarios. Am J Clim Change 3:512-527. doi: 10.4236/ ajcc.2014.35043

Coelho C, Oliveira C, Ambrizzi T, Reboita M, Carpenedo C, Campos J, Tomaziello A, Pampuch L, Custodio M, Dutra L, Rocha R, Rehbein A (2016) The 2014 Southeast Brazil austral summer drought: regional scale mechanisms and teleconnections. Clim Dyn 46:3737-3752. doi: 10.1007/s00382-015-2800-1

Cunningham CAC, Cavalcanti IFA (2006) Intraseasonal modes of variability affecting the South Atlantic Convergence Zone. Int J Climatol 26:1165-1180. doi: 10.1002/joc.1309

de Barros Soares D, Lee H, Loikith PC, Barkhordarian A, Mechoso CR (2017) Can significant trends be detected in surface air temperature and precipitation over South America in recent decades? Int J Climatol 37:1483–1493. doi:10.1002/joc.4792

Debortoli NS, Camarinha PIM, Marengo JA, Rodrigues RR (2017) An index of Brazil's vulnerability to expected increases in natural flash flooding and landslide disasters in the context of climate change. Nat Hazards. doi: 10.1007/s11069-016-2705-2

Díaz LB, Vera CS (2017) Austral summer precipitation interannual variability and trends over Southeastern South America in CMIP5 models. Int J Climatol. doi: 10.1002/joc.5031

Drumond ARM, Ambrizzi T (2006) Inter-ENSO variability and its influence over the South American Monsoon System. Adv Geosci 6:167-171

Dufek AS, Ambrizzi T (2008) Precipitation variability in São Paulo state, Brazil. Theor Appl Climatol 93:167-178. doi: 10.1007/s00704-007-0348-7

Época (2013, Jan 04th). Morre segunda vítima das chuvas no Rio de Janeiro. Época. http://revistaepoca.globo.com/Sociedade/noticia/2013/01/morre-segunda-vitima-das-chuvas-no-rio-de-janeiro.html. Accessed Jul 16th, 2017 (in Portuguese)

Folha de São Paulo (2010, Feb 01st) Um mês após tragédia, Angra tem 4.000 desalojados; cidade terá

sistema meteorológico. Folha de São Paulo. http://www1.folha.uol.com.br/folha/cotidiano/ult95u687698.shtml. Accessed Jul 16th, 2017 (in Portuguese)

Grimm AM (2003) The El Niño impact on the summer monsoon in Brazil: regional processes versus remote influences. J Clim 16:263-280

Grimm AM, Pal JS, Giorgi F (2007) Connection between Spring Conditions and Peak Summer Monsoon Rainfall in South America: Role of Soil Moisture, Surface Temperature and Topography in Eastern Brazil. J Clim 20:5929-5945. doi: 10.1175/2007JCLI1684.1

Grimm AM, Saboia J (2015) Interdecadal variability of the South American precipitation in the monsoon season. J Clim 28:755-775. doi: 10.1175/JCLI-D-14-00046.1

Grimm AM, Zilli MT (2009) Interannual variability and seasonal evolution of summer monsoon rainfall in South America. J Clim 22:2257-2275. doi: 10.1175/2008JCLI2345.1

Hartmann DL et al (2013) Observations: Atmosphere and Surface. In: Stocker TF et al (Eds.), Climate Change 2013: The Physical Science Basis. Contribution of Working Group I to the Fifth Assessment Report of the Intergovernmental Panel on Climate Change, Chapter 2. Cambridge University Press, New York, pp 159-254

Haylock MR et al (2006): Trends in total and extremes South American rainfall in 1960-2000 and links with sea surface temperature. J Clim 19:1490-1512. doi: 10.1175/JCLI3695.1

Held IM, Soden BJ (2006) Robust response of the hydrological cycle to global warming. J Clim 19:5686-5699.

Hsu PC, Li T, Murakami H, Kitoh A (2013) Future change of the global monsoon revealed from 19 CMIP5 models. J Geophys Res – Atmos 118:1247-1260. doi: 10.1002/jgrd.50145

IBGE (2012) Contas regionais do Brasil 2012. Contas nacionais número 42. Rio de Janeiro. ftp://ftp.ibge.gov.br/Contas_Regionais/2012/pdf/contas_regionais_2012.pdf. Accessed Jul 16th, 2017 (in Portuguese).

IBGE (2017a) Land use map, 1:5,000,000, Brazilian Institute of Geography and Statistics, Brasília, Brazil, 2006. http://arcg.is/0anrrD. Accessed Jul 16th, 2017 (in Portuguese).

IBGE (2017b) Population Density, 1km, Brazilian Institute of Geography and Statistics, Brasília, Brazil, 2010. http://arcg.is/D8PjG. Accessed Jul 16th, 2017 (in Portuguese).

Jones C, Carvalho LMV (2013) Climate change in the South American Monsoon System: present climate and CMIP5 projections. J Clim 26:6660-6678. doi: 10.1175/JCLI-D-12-00412.1

Junquas C, Vera CS, Li L, LeTreut H (2012) Summer precipitation variability over Southeastern South America in a global warming scenario. Clim Dyn 38:1867-1883. doi: 10.1007/s00382-011-1141-y

Junquas C, Vera CS, Li L, LeTreut H (2013) Impact of projected SST changes on summer rainfall in Southeastern South America. Clim Dyn 40:1569-1589. doi: 10.1007/s00382-013-

1695-y

Kayano MT, Andreoli RV (2007) Relations of South American summer rainfall interannual variations with the Pacific Decadal Oscillation. Int J Climatol 27:531-540. doi: 10.1002/joc.1417

Kitoh A, Endo H, Kumar K, Cavalcanti I, Goswami P, Zhou T (2013) Monsoons in a changing world: a regional perspective in a global context. J Geophys Res – Atmos 118:3053-3065. doi: 10.1002/jgrd.50258

Kodama YM (1992) Large-scale common features of subtropical precipitation zones (the Baiu Frontal Zone, the SPCZ and the SACZ) Part I: characteristics of subtropical frontal zones. J Meteorol Soc Jpn 70:813-835

Kodama YM (1993) Large-scale common features of subtropical convergence zones (the Baiu Frontal Zone, the SPCZ and the SACZ). Part II: conditions of the circulations for generating the STCZs. J Meteorol Soc Jpn 75:581-610

Kodama YM, Sagawa T, Ishida S (2012) Roles of Brazilian Plateau in the Formation of the SACZ. J Clim 25:1745-1758. doi: 10.1175/2011JCLI3785.1

Krishnamurthy V, Misra V (2010) Observed ENSO teleconnection with the South American Monsoon System. Atmos Sci Let 11:7-12. doi: 10.1002/asl.245

Krishnamurthy V, Misra V (2011) Daily atmospheric variability in the South American Monsoon System. Clim Dyn 37:803-819. doi: 10.1007/s00382-010-0881-4

Lenters JD, Cook DR (1997) On the origin of the Bolivian High and related circulation features of the South American climate. J Atmos Sci 54:656-677

Li W, Li L, Ting M, Deng Y, Kushnir Y, Liu Y, Lu Y, Wang C, Zhang P (2013) Intensification of the Southern Hemisphere summertime subtropical anticyclones in a warming climate. Geophys Res Lett 40:5959–5964, doi:10.1002/2013GL058124

Liebmann B, Jones C, Carvalho LMV (2001) Interannual variability of daily extreme precipitation events in the state of São Paulo, Brazil. J Clim 14:208-218

Liebmann B, Kiladis GN, Marengo JA, Ambrizzi T, Glick JD (1999) Submonthly convective variability over South America and the South Atlantic Convergence Zone. J Clim 12:1877-1891

Liebmann B, Kiladis GN, Vera CS, Saulo C, Carvalho LMV (2004a) Subseasonal variations of rainfall in South America in the vicinity of the low-level jet east of the Andes and comparison to those in the South Atlantic Convergence Zone. J Clim 17:3829-3842

Liebmann B, Vera CS, Carvalho LMV, Camilloni A, Hoerling MP, Allured D, Barros VR, Baez J, Bidegain M (2004b) An observed trend in central South American precipitation. J Clim 17:4357-4367

Lima KC, Satyamurty P, Fernandes JPR (2010) Large-scale atmospheric conditions associated with heavy rainfall episodes in Southeast Brazil. Theor Appl Cimatol 101:121-135. doi: 10.1007/s00704-009-0207-9

Lintner BR, Neelin JD (2010) Tropical South America-Atlantic sector convective margins and their relationship to low-level inflow. J Clim 23:2671-2685. doi: 10.1175/2009JCLI3301.1

Liu YM, Wu GX, Ren R (2004) Relationship between the subtropical anticyclone and diabatic heating. J Clim 17:682–698

Ma HY, Ji X, Neelin J, Mechoso C (2011) Mechanisms for precipitation variability of the eastern Brazil/SACZ convective margin. J Clim 24:3445-3456. doi: 10.1175/2011JCLI4070.1

Maciel C (2013, Feb 25th) Baixada Santista registra 330 desabrigados devido a fortes chuvas. Agência Brasil. http://www.ebc.com.br/noticias/brasil/2013/02/baixada-santista-registra-330-desabrigados-devido-a-fortes-chuvas. Accessed Jul, 16th 2017 (in Portuguese)

Marengo JA, Rusticucci M, Penalba O, Renom M (2010) An intercomparison of observed and simulated extreme rainfall and temperature events during the last half of the twentieth century: part 2: historical trends. Clim Change 98:509-529. doi: 10.1007/s10584-009-9743-7

Marengo JA, Valverde MC, Obregón GO (2013) Observed and projected changes in rainfall extremes in the Metropolitan Area of São Paulo. Clim Res 57:61-72. doi: 10.3354/cr01160

Muza MN, Carvalho LMV, Jones C, Liebmann B (2009) Intraseasonal and interannual variability of extreme dry and wet events over Southeastern South America and the Subtropical Atlantic during austral summer. J Clim 22:1682-1699. doi: 10.1175/2008JCLI2257.1

Nascimento L (2013, Dec 28th) Chuvas provocam 24 mortes no Espirito Santo; 54 cidades foram atingidas. Agência Brasil. http://www.ebc.com.br/noticias/brasil/2013/12/chuvas-provocam-24-mortes-no-espirito-santo-54-cidades-foram-atingidas. Accessed Jul, 16th 2017 (in Portuguese)

Nobre CA, Young AF, Saldiva P, Marengo JA, Nobre AD, Alves Júnior SP, Silva GCM, Lombardo M (2010) Vulnerability of Brazilian Megacities to Climate Change: The São Paulo Metropolitan Region (RMSP). In: Motta RW, Hargrave J, Luedemann G, Gutierrez MBS (Eds.). Climate Change in Brazil, economic, social and regulatory aspects. IPEA, Brasília, Brazil, pp 197-219

Nogués-Paegle J, Byerle LA, Mo KC (2000) Intraseasonal modulation of South American summer precipitation. Mon Weather Rev 128:837-850

Nogués-Paegle J, Mo KC (1997) Alternating Wet and Dry Conditions over South America During Summer. Mon Weather Rev 125:279-291

Nogués-Paegle J, Mo KC (2002) Linkages between summer rainfall variability over South America and sea surface temperature anomalies. J Clim 15:1389-1407

Obregón GO, Marengo JA, Nobre CA (2014) Rainfall and Climate Variability: Long-Term Trends in the Metropolitan Area of São Paulo in the 20th Century. Clim Res 61:93-107. doi: https://doi.org/10.3354/cr01241

Pagan R (2010, Feb 02nd) São Luiz do Paraitinga deve perder 80% de área histórica. Folha de São Paulo. http://www1.folha.uol.com.br/folha/cotidiano/ult95u674239.shtml. Accessed Jul 16th, 2017 (in Portuguese)

Rao V, Franchito S, Gan M, Gerolamo R (2014) Duration of the South America summer monsoon is increasing. Atmos Sci Lett 15:110-113. doi: 10.1002/asl2.476

Raia A, Cavalcanti I (2008) The Life Cycle of the South American Monsoon System. J Clim 21:6227-6246. doi: 10.1175/2008JCLI2249.1

Raimundo CC, Sansigolo CA, Molion LCB (2014) Trends of rainfall classes in the metropolitan region of São Paulo. Rev Bras Meteorol 29:397-408. doi: 10.1590/s0102-778620130655 (in Portuguese)

Robertson AW, Mechoso CR (2000) Interannual and interdecadal variability of the South Atlantic Convergence Zone. Mon Weather Rev 128:2947-2957

Rodwell MJ, Hoskins BJ (2001) Subtropical anticyclones and summer monsoons. J Clim 14:3192-3211

Sanchez E, Solman S, Remedio A, Berbery H, Samuelsson P, Rocha R, Mourão C, Li L, Marengo J, Castro M, Jacob D (2015) Regional climate modeling in CLARIS-LPB: a concerted approach towards twenty-first century projections of regional temperature and precipitation over South America. Clim Dyn 45:2193-2212. doi: 10.1007/s00382-014-2466-0

Schneider T, O'Gorman PA, Levine XJ (2010) Water vapor and the dynamics of climate changes. Rev Geophys 48:RG3001. doi: 10.1029/2009RG000302

Seluchi ME, Chou SC (2009) Synoptic patterns associated with landslide events in the Serra do Mar, Brazil. Theor Appl Cimatol 98:67-77. doi: 10.1007/s00704-008-0101-x

Seth A, Rojas M, Rauscher SA (2010) CMIP3 projected changes in the annual cycle of the South American Monsoon. Clim Change 98:331-357. doi: 10.1007/s10584-009-9736-6

Silva AE, Carvalho LMV (2007) Large-scale Index for South America Monsoon (LISAM). Atmos Sci Lett 8:51-57. doi: 10.1002/asl.150

Silva Dias MAF, Dias J, Carvalho LMV, Freitas ED, Silva Dias PL (2013) Changes in extreme daily rainfall for São Paulo, Brazil. Clim Change 116:705-722. doi: 10.1007/s10584-012-0504-7

Skansi MM et al (2013) Warming and wetting signals emerging from analysis of changes in

climate extreme indices over South America. Glob Planet Change 100:295-307. doi: 10.1016/j.gloplacha.2012.11.004

Sugahara S, Rocha RP, Silveira R (2009) Non-stationary frequency analysis of extreme daily rainfall in São Paulo, Brazil. Int J Climatol 29:1339-1349. doi: 10.1002/joc.1760

Teixeira MS, Satyamurty P (2011) Trends in the frequency of intense precipitation events in Southern and Southeastern Brazil during 1960-2004. J Clim 24:1913-1921. doi: 10.1175/2011JCLI3511.1

Todd MC, Washington R, James T (2003) Characteristics of summer time daily rainfall variability over South America and the South Atlantic Convergence Zone. Meteorol Atmos Phys 83:89-108. doi: 10.1007/s00703-002-0563-9

Tomazela JM (2014, Feb 17th) Mais de mil são afetados por chuvas no Vale do Ribeira. Exame. http://exame.abril.com.br/brasil/noticias/mais-de-mil-sao-afetados-por-chuvas-no-vale-do-ribeira. Accessed Jul 16th, 2017 (in Portuguese)

Torres RR, Lapola DM, Marengo JA, Lombardo MA (2012) Socio-climatic hotspots in Brazil. Clim Change 1:1-13. doi: 10.1007/s10584-012-0461-1

USGS (2004) Shuttle Radar Topography Mission, 30 Arc Second, Global Land Cover Facility, University of Maryland, College Park, Maryland, February 2000

Venegas SA, Mysak LA, Straub DN (1997) Atmosphere-Ocean coupled variability in the South Atlantic. J Clim 10:2904-2920

Vera C, Baez J, Douglas M, Emmanuel C, Marengo J, Meitin J, Nicolini M, Nogués-Paegle J, Paegle J, Penalba O, Salio P, Saulo C, Silva Dias MAF, Silva Dias P, Zipser E (2006a) The South American Low Level Jet Experiment. Bull Am Meteorol Soc 87:63-77. doi: 10.1175/BAMS-87-1-63

Vera C, Higgins W, Amador J, Ambrizzi T, Garreaud R, Gochis D, Gutzler D, Letternmater D, Marengo JA, Mechoso CR, Nogués-Paegle J, Silva Dias PL, Zhang C (2006b) Toward a unified view of the American Monsoon System. J Clim 19:4977-5000

Vera C, Silvestri G, Liebmann B, Gonzales P (2006c) Climate Change Scenarios for Seasonal Precipitation in South America from IPCC-AR4 Models. Geophys Res Lett 33:L13707. doi: 10.1029/2006GL025759

Wu GX, Liu Y, Zhu X, Li W, Ren R, Duan A, Liang X (2009) Multi-scale forcing and the formation of subtropical desert and monsoon. Ann Geophys 27:3631-3644. doi: 10.5194/angeo-27-3631-2009

Xavier TMBS, Xavier AFS, Silva Dias MAF (1994) Evolução da precipitação diária num ambiente urbano: o caso da cidade de São Paulo. Rev Bras Meteorol 9:44-53 (in Portuguese)

Zhou J, Lau KM (1998) Does a monsoon climate exist over South America? J Clim 11:1020-1040

Zhou J, Lau KM (2001) Principal modes of interannual and decadal variability of summer rainfall over South America. Int J Climatol 21:1623-1644. doi: 10.1002/joc.700

Zilli MT, Carvalho LMV, Liebmann B, Silva Dias MA (2017a) A comprehensive analysis of trends in extreme precipitation over southeastern coast of Brazil. Int J Climatol 37:2269-2279. doi: 10.1002/joc.4840

Zilli MT, Carvalho LMV, Lintner BR (2017b) The poleward shift of South Atlantic Convergence Zone in recent decades. Clim Dyn, in review.

Chapter 1: A Comprehensive Analysis of Trends in Extreme Precipitation over Southeastern Coast Of Brazil

Marcia T.Zilli[1], Leila M. V. Carvalho[1,2], Brant Liebmann[3], Maria A. Silva Dias[4]

[1] Department of Geography, University of California, Santa Barbara, CA, USA

[2] Earth Research Institute, University of California, Santa Barbara, CA, USA

[3] CIRES, National Oceanic and Atmospheric Administration (NOAA), Boulder, CO, USA

[4] Department of Atmospheric Sciences, University of Sao Paulo, SP, Brazil.

1.1. Abstract

Southeastern Brazil (SE Brazil) is the most densely populated region in Brazil. Previous studies have shown evidence of positive trends in average precipitation and extreme events in a few locations, suggesting the increase in rainfall-related hazards with potential impacts to urbanized areas of the region. This study provides a comprehensive analysis of the spatial variability of trends in extreme precipitation over SE Brazil focusing on regional and local scales. We evaluate two precipitation datasets with more than 70 years of data: individual stations and gridded observed precipitation data. Our results indicate an increase in total seasonal and average daily precipitation over São Paulo State related to an increase in the frequency and intensity of extreme events. Additionally, individual stations indicate negative trends in the number of light rainy days over large urbanized areas in the state of São Paulo. Over Rio de Janeiro and Espirito Santo, both datasets evidence a positive trend in intensity and frequency of heavy rain events. Station analysis indicates negative trends in the percentage of rainy days and in the number of light rainy days, not evident in the gridded dataset. We suggest that these trends are influenced by local topography and the proximity of

large urban centers.

1.2. Introduction

SE Brazil, with more than 85 million inhabitants, is the most populous region in the country and is responsible for about 55.2% of the gross national product (IBGE 2012). The dominant climatic features of SE Brazil are the pronounced seasonal cycle in precipitation, moisture, and circulation that is controlled by the South American Monsoon System (SAMS) (Zhou and Lau 2001). The South Atlantic Convergence Zone (SACZ), one of the main features of the SAMS is characterized by a northwest-southeast rain band extending from the Amazon across SE Brazil toward the subtropical South Atlantic (Kodama 1992, 1993) and is related to the occurrence of extreme precipitation events in SE Brazil (Liebmann et al. 2001; Carvalho et al. 2002, 2004; Muza et al. 2009; Cavalcanti 2012).

In 2013, the Intergovernmental Panel on Climate Change (IPCC) released its Fifth Assessment Report (AR5) confirming that the increase in global temperature since the last century is certain both over land and ocean, with the last three decades being warmer than any other previous decades in instrumental records (Hartmann et al. 2013). Following the Clausius-Clapeyron law, atmospheric moisture content should increase in a warmer atmosphere with complex and non-uniform impacts on precipitation (Held and Soden 2006).

Previous studies based on various indices identified positive trends in precipitation primarily over Southeastern South America (SESA), including some locations in Southern, and Southeastern Brazil (SE Brazil; Haylock et al. 2006; Marengo et al. 2010; Silva Dias et al. 2013). Over SESA, these positive trends were related to intensification of heavy rainfall rather than an increase in the frequency of wet days (Skansi et al. 2013). Over SE Brazil (Figure 1.1, inlet), long-term trends in precipitation are less coherent, with some positive

trends in rainfall intensity observed in the states of Rio de Janeiro (RJ; Teixeira and Satyamurty 2011) and São Paulo (SP; Liebmann et al. 2004; Dufek and Ambrizzi 2008; Marengo et al. 2010, 2013; Teixeira and Satyamurty 2011; Silva Dias et al. 2013). Silva Dias et al. (2013) observed that trends in heavy rainfall in the city of Sao Paulo were positively correlated to coupled modes of variability in the Pacific (Pacific Decadal Oscillation) and Atlantic (North Atlantic Oscillation) oceans, as well as with the South American Monsoon System (SAMS) and SST anomalies along the SE coast of Brazil during the wet season.

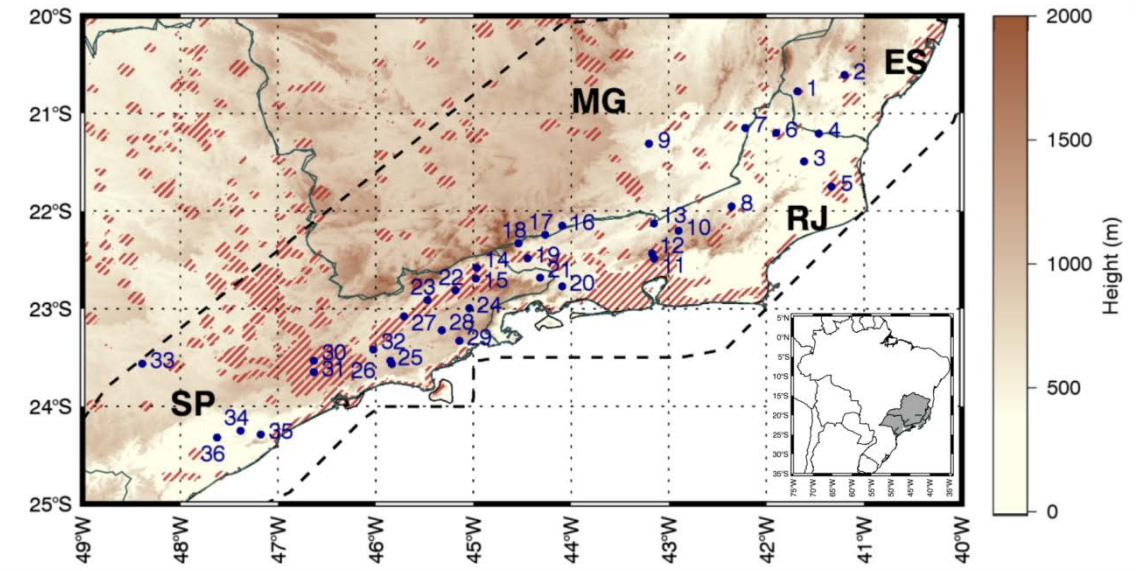

Figure 1.1 — Inlet: Location of SE Brazil (gray) and study area (dashed line) in Brazil. Main map: Location of the study area (dashed line) at SE Brazil; stations analyzed ("●"); local topography (shades; 1km resolution DEM from SRTM; USGS 2004); and urban areas (red cross-hatching; GRUMPv1 dataset, Balk et al. 2006). Information about stations is provided in Table 1.1

In addition, some studies have shown an increase in the number of consecutive dry days and a decrease in the number of light rainy days (less than 5mm/day) in the city of São Paulo (Xavier et al. 1994; Dufek and Ambrizzi 2008; Sugahara et al. 2009; Silva Dias et al. 2013; Marengo et al. 2013). Raimundo et al. (2014) observed that stations with negative trends in light rainy days were located in more urbanized areas while those located to the

east, north, and northeast of the city, in rural areas, actually showed positive trends for the index.

Most studies that investigated trends in precipitation over SE Brazil were based on rain gauge data with low spatial density (Haylock et al. 2006; Dufek and Ambrizzi 2008; Marengo et al. 2010; Teixeira and Satyamurty 2011) or focused on specific locations such as the metropolitan area of São Paulo (Xavier et al. 1994; Sugahara et al. 2009; Silva Dias et al. 2013; Marengo et al. 2013; Raimundo et al. 2014). The objective of this study is to provide a comprehensive analysis of the spatial variability of trends in extreme precipitation over SE Brazil focusing on regional and local scales. Information about the datasets used is provided in Section 1.3. Methodology is described in Section 1.4. Results are presented in Section 1.5 and final conclusions in Section 1.6.

1.3. Data

We examine precipitation records from two datasets: daily gridded precipitation from the Physical Sciences Division (PSD), Earth System Research Laboratory (Figure 1.2; Liebmann and Allured 2005); and data from individual stations, operated by different Brazilian agencies (Figure 1.1 and Table 1.1). While gridded precipitation offers an adequate overview of regional and large-scale patterns of precipitation trends, individual stations are invaluable in providing local details and geographical features associated with the observed trends.

The PSD dataset provides daily precipitation grids from 1938 to 2012, with 0.5° latitude/longitude resolution, and is based on precipitation observed at stations located over most of South America (Liebmann and Allured 2005). The dataset is composed of daily

Table 1.1 — Stations analyzed, their latitude, longitude, height, city where located, time range, percentage of missing, and source institution. The location of these stations is in Figure 1.1

ID	Station	Lat (°S)	Lon (° W)	Height (m)	City	First Year	Last Year	Missing (%)	Operated by
1	02041001	-20.77	-41.68	576	Guaçui, ES	1939	2013	1.18	ANA[a]/CPRM[b]
2	02041002	-20.61	-41.20	107	Castelo, ES	1939	2013	1.35	ANA/CPRM
3	02141003	-21.49	-41.61	20	Campos dos Goytacazes, RJ	1939	2013	0.16	ANA/CPRM
4	02141014	-21.21	-41.46	59	Mimoso do Sul, ES	1937	2013	0.31	ANA/CPRM
5	02141044	-21.75	-41.33	25	Campos dos Goytacazes, RJ	1912	2009	2.66	INMET[c]
6	02141045	-21.20	-41.90	124	Itaperuna, RJ	1922	2009	1.60	INMET
7	02142002	-21.15	-42.22	177	Patrocínio do Muriaé, MG	1935	2013	0.17	ANA/CPRM
8	02142022	-21.95	-42.36	376	Cantagalo, RJ	1939	2013	0.40	ANA/CPRM
9	02143000	-21.31	-43.20	512	Rio Pomba, MG	1935	2013	2.19	ANA/CPRM
10	02242027	-22.20	-42.90	650	Teresópolis, RJ	1936	2013	0.12	ANA/CPRM
11	02243010	-22.49	-43.15	1085	Petrópolis, RJ	1938	2013	0.23	ANA/CPRM
12	02243011	-22.44	-43.17	704	Petrópolis, RJ	1938	2013	0.43	ANA/CPRM
13	02243015	-22.13	-43.15	270	Três Rios, RJ	1936	2013	0.26	ANA/CPRM
14	02244004	-22.58	-44.97	520	Cruzeiro, SP	1929	2004	1.21	LIGHT[d]
15	02244010	-22.69	-44.98	550	Cachoeira Paulista, SP	1935	2013	1.90	ANA/CPRM
16	02244035	-22.15	-44.09	530	S. Rita de Jacutinga, MG	1935	2013	1.33	ANA/CPRM
17	02244036	-22.24	-44.26	550	Passa Vinte, MG	1935	2013	0.80	ANA/CPRM
18	02244047	-22.33	-44.54	1030	Resende, RJ	1937	2013	1.17	ANA/CPRM
19	02244092	-22.48	-44.45	440	Resende, RJ	1925	2009	3.17	INMET
20	02244097	-22.77	-44.09	500	Pinheiral, RJ	1915	2004	0.28	LIGHT
21	02244133	-22.68	-44.32	460	Bananal, SP	1937	2013	3.26	FURNAS[e]
22	02245032	-22.81	-45.18	519	Guaratinguetá, SP	1930	2012	0.49	FURNAS
23	02245048	-22.91	-45.47	524	Pindamonhangaba, SP	1932	2012	1.76	ANA/CPRM
24	02245055	-23.00	-45.04	790	Cunha, SP	1935	2013	0.74	ANA/CPRM
25	02345047	-23.53	-45.85	770	Salesópolis, SP	1927	2004	1.17	FCTH[f]/DAEE[g]
26	02345048	-23.57	-45.83	790	Salesópolis, SP	1928	2004	0.22	FCTH/DAEE
27	02345063	-23.08	-45.71	545	Caçapava, SP	1929	2013	2.94	ANA/CPRM
28	02345065	-23.22	-45.32	760	S. L. do Paraitinga , SP	1935	2013	1.43	ANA/CPRM
29	02345067	-23.33	-45.14	888	S. L. do Paraitinga, SP	1936	2013	1.02	ANA/CPRM
30	02346045	-23.53	-46.63	730	São Paulo, SP	1888	1999	2.13	FCTH/DAEE
31	02346059	-23.65	-46.63	780	São Paulo, SP	1933	2004	0.01	FCTH/DAEE
32	02346099	-23.42	-46.02	567	Guararema, SP	1929	2003	0.97	ANA
33	02348033	-23.56	-48.39	580	Angatuba, SP	1938	2013	3.54	ANA/COHIDRO[h]
34	02447043	-24.25	-47.38	18	Miracatu, SP	1939	2013	1.25	ANA/COHIDRO
35	02447045	-24.29	-47.18	42	Itariri, SP	1937	2013	2.31	ANA/COHIDRO
36	02447046	-24.32	-47.62	15	Juquiá, SP	1937	2006	2.70	ANA/COHIDRO

[a] ANA – Agência Nacional de Águas
[b] CPRM – Serviço Geológico Brasileiro
[c] INMET – Instituto Nacional de Meteorologia
[d] LIGHT – Light Energia SA
[e] FURNAS Centrais Hidrelétricas
[f] FCTH – Fundação Centro Tecnológico de Hidráulica
[g] DAEE – Departamento de Águas e Energia Elátrica
[h] COHIDRO Consultoria, Estudos e Projetos

averages over all valid stations located within a sample radius of 0.5° from the center of the grid point. This assures the inclusion of all stations in at least one grid point. The disadvantage of this method is that a few stations may be included in up to four different grid points, causing additional smoothing of the data and masking out extreme precipitation with a spatial scale smaller than the grid resolution (Liebmann and Allured 2005). This dataset exhibits variable station density (Figure 1.2b) and data availability in space and time (Figure 1.2c). To avoid examining areas with relatively short time series that could misrepresent the extent of actual trends, we consider only grid points with less than 40% of days missing over the entire period (Figure 1.2a) and only years with more than 95% of valid days along the season. With these criteria, all PSD grid points have at least 30 years of data, although the majority has more than 60 years (Figure 1.2c).

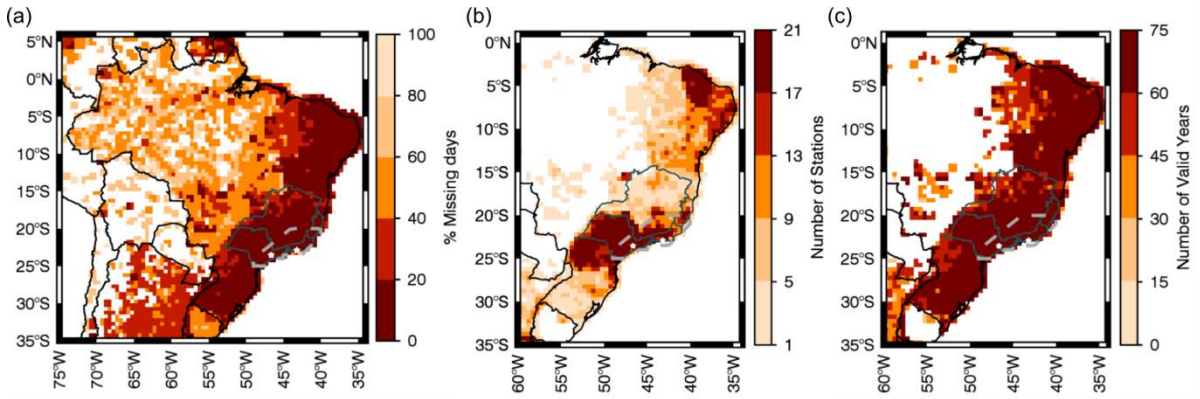

Figure 1.2 — PSD gridded dataset: (a) % of missing days; (b) average number of stations; and (c) number of valid years. (b) and (c): only grid points with less than 40% missing data. Gray dashed: study area; dark gray line: states of SE Brazil; white stars: cities of Sao Paulo (23.6°S, 46.6°W) and Rio de Janeiro (22.9°S, 43.2°W)

To further characterize the trends during intense precipitation events and their spatial variation over a topographically complex and highly urbanized area of SE Brazil, we also analyzed daily precipitation obtained from 36 rain gauges located on the coast of São Paulo

(SP), Rio de Janeiro (RJ), and Espírito Santo (ES), and southeastern Minas Gerais (MG) states (Figure 1.1). These stations are operated by different Brazilian agencies (Table 1.1) and are available from the Brazilian National Water Agency website (Agência Nacional de Águas — ANA*;* http://hidroweb.ana.gov.br/). All these stations have at least 70 years of observations and less than 5% missing days (Table 1.1). The quality control test carried out in this study checks for outliers based on neighboring stations, evaluates station metadata to detect changes in station location and days without readings, and adopts the Rodionov test (Rodionov, 2006) to detect steps and discontinuities in the time series.

Even though these stations are included in the gridded dataset, individual stations are useful to identify local variations in trends, particularly near complex terrain and urban centers. Urban areas (Figure 1.1, cross hatching) are delimited using the Global Rural–Urban Mapping Project Version 1 (GRUMPv1, http://sedac.ciesin.columbia.edu/data/collection/grump-v1; Balk et al., 2006). This data set considers night light observations collected by a series of US Department of Defense meteorological satellites as one of the variables in the definition of the urban-extent grid. The major topographic feature of coastal SE is the Coastal Range, with average elevation below 1000m and some peaks above 2000m in RJ state (Figure 1.1, shades).

This study focuses on the wet season (October to March) and thus most extreme precipitation events are related to the SACZ activity (Liebmann et al. 2001; Carvalho et al. 2002, 2004; Cavalcanti 2012). Mechanisms related to the observed trends are a subject of our current research but are not explored in this manuscript.

1.4. Detection and characterization of trends

Trends in precipitation can be described as changes in intensity and/or frequency of

rainfall events that may or not alter the total annual or the mean daily precipitation. To identify these changes, we derive various indices, based on daily precipitation observations for the wet season (October to March) from both gridded and station data, as described in Table 1.2: total precipitation (TotPR), daily average (DayPR), percentage of rainy days (%PRDay), number of light rainy days (NumbLightPR), maximum seasonal precipitation (MaxPR), 95th percentile of daily precipitation (95%), frequency of extreme events (NumbEx) and intensity of extreme events (IntEx).

Table 1.2 — Precipitation indices, acronyms, their definition and mean value for the wet season (based on the gridded data averaged over coastal SE Brazil — 49ºW to 40ºW and 25ºS to 20ºS)

INDEX	ACRONYM	DEFINITION	SE AVERAGE
Total precipitation	TotPR	Total precipitation accumulated during the wet season	1122.7 mm
Daily average	DayPR	Average daily precipitation for the wet season, considering only days with precipitation above 1mm.	9.7 mm/day
Percentage of rainy days	%PRDay	Number of days with precipitation above 1mm, divided by the total number of days in the season (182 for the wet season)	63.1%
Number of light rainy days	NumbLightPR	Number of days with precipitation between 1 and 5 mm	47.4 days
Maximum precipitation	MaxPR	Maximum daily precipitation for each season	52.3 mm/day
95th percentile	95%	Value of the 95th percentile of daily precipitation for each season.	29.1mm/day
Frequency of extreme events	NumbEx	Number of events with daily precipitation above the monthly 95th percentile, per season	7.1 events/year
Intensity of extreme events	IntEx	Exceedance precipitation above the 95th percentile threshold, accumulated during the season	92.6mm

We define extreme events as days with precipitation equal or greater than the 95th percentile, calculated for each station (and grid point) and month separately and using all years of record. The intensity of the events is defined as the amount of rainfall exceeding the 95th percentile monthly climatological value, accumulated over the season. The frequency of extremes is estimated as the number of days per season that precipitation exceeds the

monthly 95th percentile. If the extremes occur in two or more consecutive days this sequence is considered as a single event.

For each derived index, we investigate the presence and magnitude of trends by applying the Mann-Kendall trend test (Wilks 2011) and the Sen's slope test (Sen 1968; Gocic and Trajkovic 2013). The Mann-Kendall test identifies whether or not the index exhibits a trend whereas the Sen's slope test estimates the slope of the trend. Both are nonparametric tests and have been largely used in studies of tendencies in atmospheric and hydrological variables (Dufek and Ambrizzi 2008; Marengo et al. 2010; Ghosh et al. 2012; Gocic and Trajkovic 2013). The Mann-Kendal statistic *S* is estimated as (Wilks 2011):

$$S = \sum_{i=1}^{n-1} \sum_{j=i+1}^{n} sgn(x_j - x_i) \qquad \text{(Eq 1.1)}$$

where n is the number of data points; x is each of the measurements at different time steps i and j, with $i \neq j$; and $sgn(.)$ is defined as:

$$sgn = \begin{cases} 1, & if\ (x_j - x_i) > 0 \\ 0, & if\ (x_j - x_i) = 0 \\ -1, & if\ (x_j - x_i) < 0 \end{cases} \qquad \text{(Eq 1.2)}$$

The Mann-Kendall trend test checks the null hypothesis of no trend against the alternative hypothesis of the presence of a trend (Jain and Kumar 2012); positive (negative) *S* indicates an increasing (decreasing) trend. If $n > 10$, the *S* statistics follows a Gaussian distribution with $E[S] = 0$ and

$$Var[S] = \frac{n(n-1)(2n+5) - \sum_{i=1}^{m} t_i(t_i-1)(2t_i+5)}{18} \qquad \text{(Eq 1.1)}$$

where m is the number of tied groups (zero difference between compared values) and t_i is the number of data points in each tied group (Wilks 2011). The significance of this trend can

be found using *z*-scores, estimated as:

$$z = \begin{cases} \frac{S-1}{\sqrt{Var(S)}}, S > 0 \\ \frac{S+1}{\sqrt{Var(S)}}, S < 0 \end{cases} \quad \text{(Eq 1.2)}$$

If $|z| > z_{\alpha/2}$, the null hypothesis can be rejected at α level of significance in a two-sided test (Jain and Kumar 2012).

The Sen's slope estimator test (Gocic and Trajkovic 2013; Adarsh and Janga Reddy 2014), which considers the slopes between all data pairs in the time series, was also applied:

$$Q_i = \frac{x_j - x_k}{j - k} \; for \; i = 1,2, \dots, N \quad \text{(Eq 1.3)}$$

where N is the number of different pairs of observations so that $N = \frac{n(n-1)}{2}$; x_j and x_k are data values at time j and k, with $j > k$. The slope estimator is computed by considering the median value of all ranked $Q_{(i)}$:

$$Q_{med} = \begin{cases} Q_{[(N+1)/2]} & , if \; N \; is \; odd \\ \frac{Q_{(N/2)} + Q_{[(N+2)/2]}}{2} & , if \; N \; is \; even \end{cases} \quad \text{(Eq 1.4)}$$

where Q_{med} represents the steepness of the trend, with positive (negative) values representing positive (negative) trends. The confidence interval for this test is estimated by $C_\alpha = Z_{1-\alpha/2}\sqrt{Var[S]}$, where $Var[S]$ is estimated by Eq. 1.3, and $Z_{1-\alpha/2}$ is defined from the standard normal distribution. The confidence interval is:

$$Q_{min} = Q_{(M_1)} \; and \; Q_{max} = Q_{(M_2+1)} \quad \text{(Eq 1.5)}$$

$$M_1 = \frac{N - C_\alpha}{2} \; and \; M_2 = \frac{N + C_\alpha}{2} \quad \text{(Eq 1.6)}$$

where Q_{min} and Q_{max} are the lower and upper limits of the confidence interval. The slope Q_{med} is statistically different from zero when both limits (Q_{min} and Q_{max}) have the same

sign.

Before applying these tests, we also check the autocorrelation of each time series. Whenever the significance level of the lag-1 autocorrelation coefficient (r_1) is above 0.95, the Mann-Kendall variance is adjusted by $Var^*[S] = Var[S]\frac{1+r_1}{1-r_1}$, as suggested by Wilks (2011).

Here, the intensity of the trends is determined by the median Sen Slope (Eq 1.6). The trends are considered statistically significant based on the statistic *S* for the Mann-Kendall test (Eq 1.1) at 10% significance level. The confidence interval for the Sen's slope is also 10%.

1.5. Results

1.5.1. Climatology of the indices

We first calculate the climatology of all indices evaluated in this paper (Figure 1.3) at those grid points with less than 40% missing data (Figure 1.2a), effectively restricting the analysis to eastern Brazil. Table 1.2 summarizes the indices investigated in this study and shows the average for each index over all grid points between 49ºW to 40ºW and 25ºS to 20ºS, representing SE Brazil. During the wet season, the average TotPR in SE Brazil is 1122.7mm (Figure 1.3a), with DayPR above 9mm/day (Figure 1.3b). %PRDay and NumbLightPR (Figures 1.3c and d) emphasize the large number of rainy days per season, with more than 60% of the days with precipitation above 1mm and 47.4 days (out of 182 days) with precipitation between 1 and 5 mm.

The MaxPR and 95% (Figures 1.3e and f) are also large over SE Brazil and both have a spatial distribution similar to the DayPR spatial pattern, with all three consistent with the climatological position of the SACZ. Over SE Brazil, MaxPR is, on average, 52mm/day and

95% is 29.1mm/day. The average NumbEx is 7 events per season (Figure 1.3g), with IntEx larger than 90mm/season (Figure 1.3h).

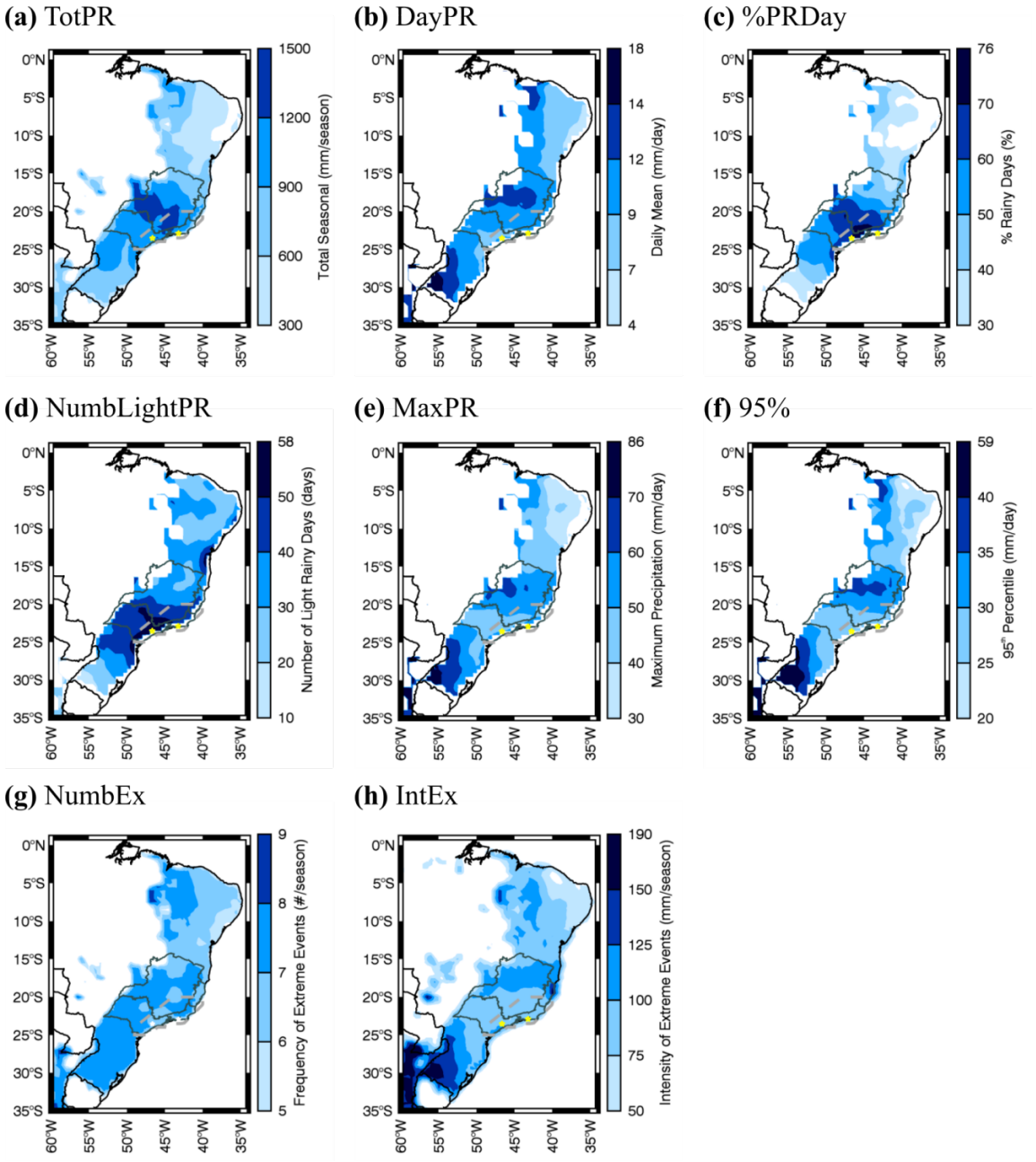

Figure 1.3 — Wet season climatology for gridded data: (a) TotPR; (b) DayPR; (c) %PRDay; (d) NumbLightPR; (e) MaxPR; (f) 95%; (g) NumbEx; (h) IntEx. Light gray dashed: study area; dark gray line: states of SE Brazil; white stars: Sao Paulo (23.6°S, 46.6°W) and Rio de Janeiro (22.9°S, 43.2°W)

Large DayPR, MaxPR, 95% and IntEx (Figures 1.3b, e, f, and i) are also observed over Southern Brazil. Intense precipitation in this region results from the interplay of phenomena on a broad range of spatiotemporal scales and this discussion is beyond the scope of the present article.

1.5.2. Trends in gridded dataset

The gridded dataset indicates a significant increase ($p<0.1$) in TotPR over SP and South Brazil (Figure 1.4a). Over SP, positive trends in TotPR are collocated with positive significant trends ($p<0.1$) in DayPR, MaxPR 95%, NumbEx, and IntEx (Figures 1.4b, e-h). Conversely, there are significant negative trends ($p<0.1$) in %PRDay and NumbLightPR (Figures 1.4c and d) in the state. These results suggest that precipitation events are becoming more intense and more frequent while rainy days are becoming less frequent, in agreement with previous studies (Xavier et al. 1994; Haylock et al. 2006; Dufek and Ambrizzi 2008; Sugahara et al. 2009; Marengo et al. 2010; Teixeira and Satyamurty 2011; Silva Dias et al. 2013; Skansi et al. 2013; Raimundo et al. 2014).

Interestingly, the area with positive trends in TotPR, DayPR, MaxPR, and 95%, over SP is located south of the area of climatological maximum for each index (compare Figures 1.3 and 1.4). The climatological maximum for these indices is collocated with the average position of the SACZ (Figure 1.3), indicating that trends observed in the indices could be related to a progressive southwestward displacement of the SACZ. Previous studies that investigated multimodel projections of climate change in the wet season precipitation regimes using the Coupled Model Intercomparison Project (CMIP) phase-3 (Seth et al. 2010), and more recently CMIP phase-5 dataset (Jones and Carvalho 2013), have indicated similar displacement of the SACZ. These results suggest that the observed trends could be

the signal of a regional response in precipitation caused by the radiative forcing due to global warming.

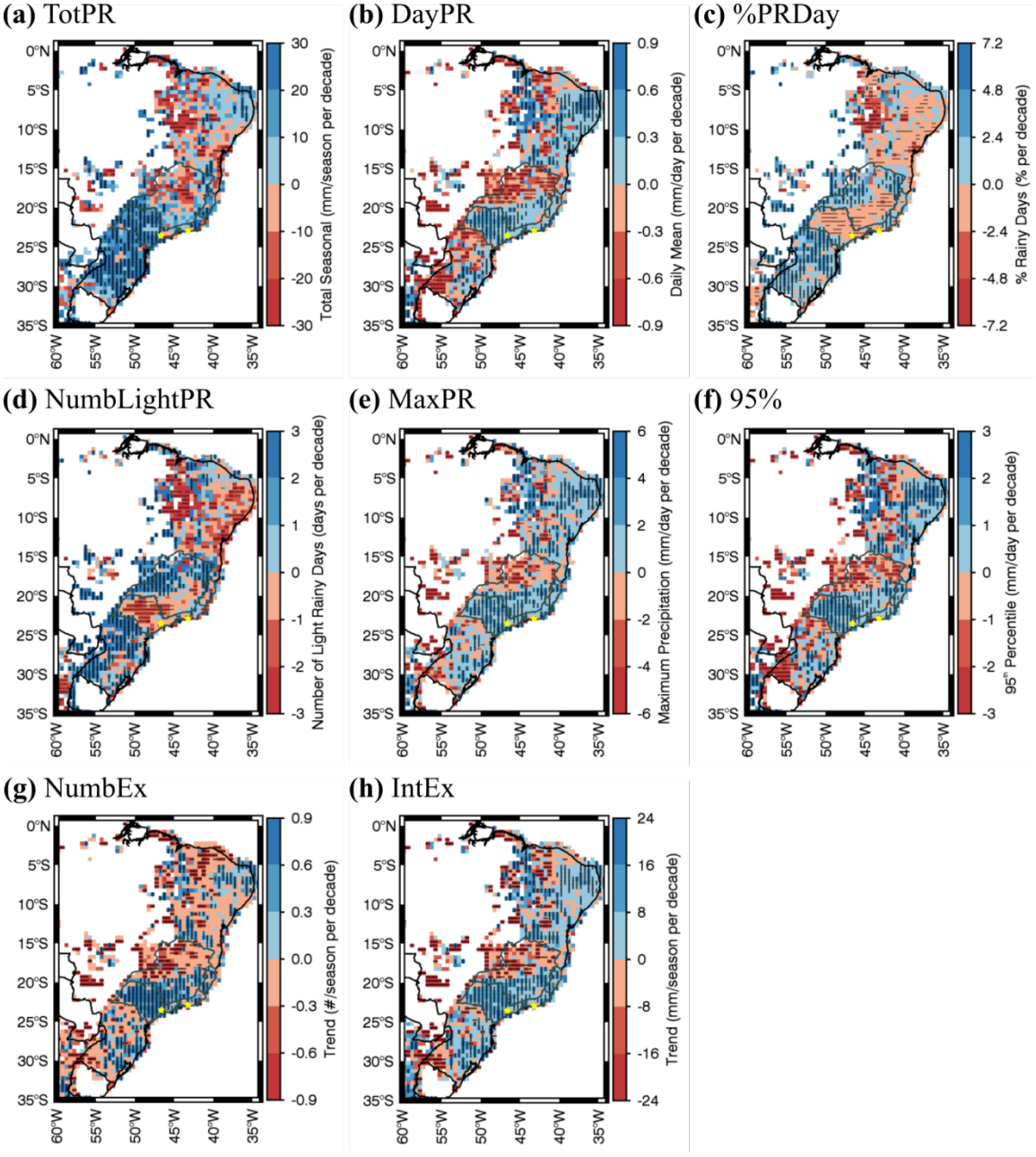

Figure 1.4 — Trends in gridded dataset for wet season: (a) TotPR; (b) DayPR; (c) %PRDay; (d) NumbLightPR; (e) MaxPR; (f) 95%; (g) NumbEx; and (h) IntEx. Red (blue) areas: positive (negative) trends (Sen's slope); vertical (horizontal) hatching: areas with significant trends ($p<0.1$). Gray contour: states of SE Brazil. Stars: cities São Paulo (23.6°S, 46.6°W) and Rio de Janeiro (22.9°S, 43.2°W)

Over northern SE Brazil, negative trends in TotPR, DayPR, MaxPR, 95%, NumbEx and IntEx (Figures 1.4a, b, e-h) and positive trends in %PRDay and NumbLightPR (Figures 1.4c and d) are opposite to the observed trends over SP. We speculate that this drying tendency, which is associated with decrease in the intensity and frequency of extreme events, could be a consequence of a southwestward displacement of the SACZ.

We also observe the presence of significant ($p<0.1$) trends over RJ for TotPR, %PRDay, MaxPR, 95%, NumbEx, and IntEx (Figures 1.4a, c, e-h). The DayPR and NumbLightPR (Figures 1.4b and d) also show positive but non-significant trends. These trends are observed over the northern portion of the state and indicate that the extreme events are becoming more frequent and intense without impacting average daily precipitation. Dereczynski et al. (2013) identified similar trends; however, their study focused only on the city of RJ. Our analysis, based on gridded data with longer time series, detected that these trends are broader and extend over the northern portion of RJ.

1.5.3. Trends at individual stations

To detail the spatial variability of trends over coastal areas of SE Brazil, we examined precipitation data from 36 individual stations (Figure 1.1). Positive significant trends ($p<0.1$) in TotPR are identified in 5 stations whereas only 2 stations showed negative and significant ($p<0.1$) trends (Figure 1.5a). The DayPR also exhibits similar spatial variability of trends: 22 stations indicate positive trends, with 8 stations significant ($p<0.1$; Figure 1.5b). These trends in DayPR occur mostly in RJ, where the %PRDay and NumbLightPR (Figures 1.5c and d) show negative significant trends, indicating a tendency for fewer but more intense precipitation events over that area.

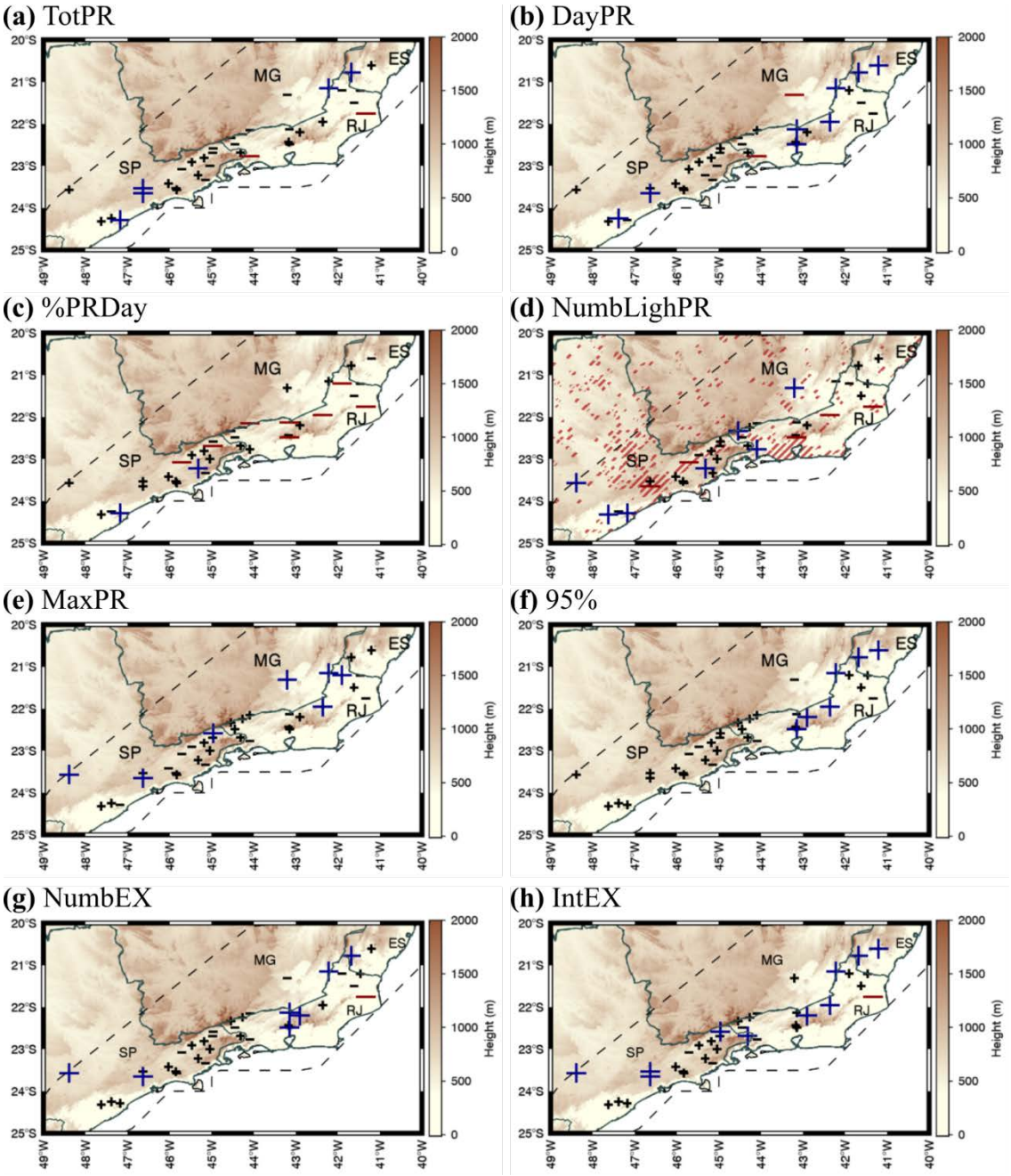

Figure 1.5 — Trends in station data for wet season: (a) TotPR; (b) DayPR; (c) %PRDay; (d) NumbLightPR; (e) MaxPR; (f) 95%; (g) NumbEx; (h) IntEx. "+" ("–"): positive (negative) trends; larger blue (red) symbols: positive (negative) significant trends, with significance level at the lower right corner; shades: local topography; dashed line: study area. In (d) red cross-hatching: urban areas (source: GRUMPv1 dataset, Balk et al. 2006)

Further south, over SP, positive trends in TotPR and DayPR (Figures 1.5a and b) are observed along with positive trends in %PRDay (Figure 1.5c), in agreement with previous

investigations based on individual stations (Dufek and Ambrizzi 2008; Teixeira and Satyamurty 2011). Trends in NumbLightPR (Figure 1.5d) are more complex, with negative significant trends observed over urbanized areas around the city of São Paulo as indicated in Xavier et al. (1994) and Marengo et al. (2013). Stations over rural areas show positive significant trends for the number of light rainy days, as observed by Raimundo et al. (2014).

Trends in intense precipitation events are examined based on 4 indices: MaxPR, 95%, NumbEx and IntEx (Figures 1.5e-h). Positive trends in all four indices are observed in at least 24 out of the 36 stations for each index and were statistically significant ($p<0.1$) in at least 6 of them. The majority of stations with significant trends are located over RJ and over urban areas of SP. These results reinforce that the increase in DayPR over RJ (Figure 1.5b) is related to more intense (Figure 1.5e, f, and h) and more frequent (Figure 1.5g) heavy precipitation days, with a decrease in %PRDay and NumbLightPR (Figure 1.5c and d).

To compare our results with previous studies, we focus our analysis on two stations located in the Metropolitan Area of São Paulo (stations 30 and 31 in Figure 1.1 and Table 1.1). The precipitation records from station 31 have been investigated in many previous studies due to its proximity to a large urban center, long records and excellent quality control of the data (e.g., Xavier et al. 1994; Sugahara et al. 2009; Silva Dias et al. 2013; Marengo et al. 2013; Raimundo et al. 2014). Our analyses indicate positive significant trends in TotPR, DayPR, MaxPR, NumbEx, and IntEx (Figures 1.5a, b, e, g, and h), and a negative trend in NumbLightPR (Figure 1.5d), in agreement with those previous studies.

1.5.4. Comparison between gridded data and individual station trends

Overall, trends observed for the gridded dataset are similar to those for individual stations. This is not completely surprising as all stations used in this study were averaged in

the gridded data. However, some local discrepancies do exist. The most noticeable differences are observed for %PRDay and NumbLightPR over RJ. Gridded data indicate positive trends for both indices, significant for %PRDay over the north of the state (Figures 1.4c and d) while most stations over this area show a negative significant trend (Figures 1.5c and d). These discrepancies are likely related to the averaging method utilized in the gridded dataset. In regions with complex topography, precipitation exhibits large spatial variability, with large amounts concentrated in small areas where orographic lifting may increase the probability of convective rainfall relative to neighboring stations. However, when averaging precipitation records into a 0.5° grid, these few stations may contribute to the relative increase in the average number of rainy days. In these cases, individual stations provide a more realistic characterization of spatial variability of rainfall trends.

Over SP, trends in NumbLightPR are also different, with the gridded dataset indicating a negative trend over the entire state (statistically significant over central SP; Figure 1.4d) while stations indicate negative trends only in two stations located in urbanized areas (Figure 1.5d). Other stations located in rural areas of SP show positive trends, indicating that 0.5° grid is not sufficient to resolve the difference between urban and rural areas.

The analysis of both datasets also reveals a spatial pattern of trends over SP to RJ. While over SP there is an increase in total precipitation and daily rates (TotPR and DayPR, Figures 1.4a, b, and 1.5a, b) caused by more intense and frequent extreme precipitation events (MaxPR, 95%, NumbEx, and IntEx; Figures 1.4e–h and 1.5e–h), over RJ the intense events are becoming stronger and more frequent (MaxPR, 95%, NumbEx and IntEx; Figures 1.4e–h and 1.5e–h), but the number of days with precipitation is decreasing (NumbLightPR and %PRDay, Figures 1.4c, d, and 1.5c, d).

1.6. Discussions and Conclusion

Previous studies have shown compelling evidence that precipitation and its extremes have changed in the last decades in SE Brazil. These studies, however, were based on spatially averaged precipitation with relatively coarse resolution (Liebmann et al. 2004; Teixeira and Satyamurty, 2011), or based on a few stations located in SP (Haylock et al. 2006; Dufek and Ambrizzi 2008; Sugahara et al. 2009; Marengo et al. 2010, 2013; Silva Dias et al. 2013). The present study develops a comprehensive analysis of rainfall and its extremes using the most up to date and longest gauged rainfall records available in SP, RJ, ES, and MG. Our major objective is to properly characterize patterns of changes in intensity and frequency of both light and extreme rainfall events. The trends detected using these observational precipitation datasets provide additional evidence that the projected changes for future scenarios of climate change are already occurring.

Although the two datasets used are not independent, trend analysis using gridded precipitation identified regional patterns of changes in rainfall whereas station records improved the identification of local variations in these patterns, particularly near complex terrain and major urban centers. Mapping trends in SE Brazil have significant economic and social impacts for the country. High urban population density, the inappropriate occupation of risk areas in RJ, SP, and MG, and positive trends in extreme precipitation suggests an increasing exposure to rain-related disasters in the region.

Table 1.3 summarizes the main results observed in this study. Over SP, the analysis of both datasets indicates an increase in total seasonal and average daily precipitation and suggests that these changes are related to an increase in the frequency and intensity of extreme events, consistent with previous studies. Additionally, the gridded dataset indicates a large continuous area with significant trends for these indices, located southwestward their

climatological maximum. Since SACZ is the most important climatological phenomenon modulating precipitation in the region, a plausible explanation for the positive trend in total precipitation over SP is a southwestward displacement of the SACZ in recent decades, as speculated by Liebmann et al. (2004) and suggested in coupled climate model simulations of future scenarios of climate change in South America discussed in Seth et al (2010) and Jones and Carvalho (2013).

Farther north, in RJ and ES, both datasets indicate positive trends in daily average related to trends in intensity and frequency of extreme precipitation days (Table 1.3). Individual stations in this region also reveal negative trends in the percentage of rainy days and in the number of light rainy days. These trends, not evident in the gridded dataset, indicate changes in the frequency and intensity of precipitation events, with larger accumulation occurring during fewer rainy days. Dereczynski et al. (2013) identified similar trends in future scenarios of climate change for the city of Rio de Janeiro. Our results confirm that these trends are already detectable in historical data and show that these trends actually extend to larger areas north of the state.

Table 1.3 — Trends in each index considering both dataset, for the states of RJ and ES, SP, and the Metropolitan Area of São Paulo (MASP). Symbols: positive (↗), negative (↘) or no significant (▬) trends

INDEX	RJ AND ES	SP	MASP
TotPR	▬	↗	↗
DayPR	↗	↗	↗
%PRDay	↘	▬	▬
NumbLightPR	↘	▬	↘
MaxPR	↗	↗	↗
95%	↗	↗	▬
NumbEx	↗	↗	↗
IntEx	↗	↗	↗

Therefore, while over SP there is an increase in the number of rainy days and in the frequency and intensity of extreme events, over RJ and ES we observe a negative trend in the frequency of rainy days, with precipitation concentrated in fewer and more intense events. These results are consistent with the hypothesis of the southwestward displacement of the SACZ.

Tropical South America has undergone a rapid warming in the last five decades, a trend that is expected to continue and increase by the end of the 21st century (Carvalho and Jones 2013). Recent studies argue that the reduction in the frequency of rainy days along the margin of the convective zones, such as the SACZ, is one of the consequences of the changes in moisture spatial variability in a warmer atmosphere (Chou and Neelin 2004; Held and Soden 2006; Lintner and Neelin 2010; Ma et al. 2011). According to these authors, warmer temperatures would increase the saturation vapor pressure, increasing the moisture necessary to reach saturation. In the core of convective regions, there is always enough moisture to meet this higher threshold for precipitation. However, along the convective margins, the moisture available might not be enough, since these areas receive most of their influx from more stable areas, in this case the ocean. In addition, the moisture in convective margins is also exported to the region of strong convection, reducing even more the moisture available and, consequently, increasing stability and decreasing the precipitation events in these regions. We speculate that the observed reduction in the number of rainy events over RJ and ES could be related to the warming and consequent changes in saturation water vapor along the northern margin of the SACZ. The observed positive trends in extreme daily precipitation could be related to thermodynamic effects such as an increase in convective instability. Nevertheless, many other dynamic and thermodynamic mechanisms, combined with

environmental changes such as the effect of rapid urbanization and land-use and change, could also have played a significant role in the observed trends in precipitation. Therefore, further investigation is necessary to properly recognize the underlying dynamical and physical mechanisms responsible for the observed trends in precipitation over SE Brazil.

1.7. Acknowledgements

GPCP Precipitation data was provided by the NOAA/OAR/ESRL PSD, Boulder, Colorado, USA, from their Web site at http://www.esrl.noaa.gov/psd/. NOAA High Resolution SST data was provided by the NOAA/OAR/ESRL PSD, Boulder, Colorado, USA, from their Web site at http://www.esrl.noaa.gov/psd/. M. Zilli acknowledges the Brazilian National Council for Scientific and Technological Development (CNPq) for the financial support through the Science without Borders Program (202691/2011-0). L. Carvalho acknowledges the São Paulo Research Foundation (FAPESP) Proc. 2008/58101-9. L. Carvalho and B. Lintner acknowledge the support of NSF-AGS-1505198.

1.8. References

Adarsh S, Janga Reddy M (2014) Trend analysis of rainfall in four meteorological subdivisions of southern India using nonparametric methods and discrete wavelet analysis, Int J Climatol 35:1107-1124. doi: 10.1002/joc.4042

Balk DL, Deichmann U, Yetman G, Pozzi F, Hay SI, Nelson A (2006) Determining global population distribution: methods, applications, and data. Adv Parasitol 62:119-156. doi: 10.1016/S0065-308X(05)62004-0

Carvalho LMV, Jones C (2013) CMIP5 simulations of low-level tropospheric temperature and moisture over tropical Americas. J Clim 26:6257-6286. doi: 10.1175/JCLI-D-12-00532.1

Carvalho LMV, Jones C, Liebmann B (2002) Extreme precipitation events in southeastern South America and large-scale convective patterns in the South Atlantic Convergence Zone. J Clim 15:2377-2394

Carvalho LMV, Jones C, Liebmann B (2004) The South Atlantic Convergence Zone: intensity, form, persistence, and relationships with intraseasonal to interannual activity and

extreme rainfall. J Clim 17:88-108

Cavalcanti IFA (2012) Large scale and synoptic features associated with extreme precipitation over South America: a review and case studies for the first decade of the 21st century. Atmos Res 118:27-40. doi: 10.1016/j.atmosres.2012.06.012

Chou C, Neelin JD (2004) Mechanisms of global warming impacts on regional tropical precipitation. J Clim 17:2688-2701

Dereczynski CP, Luiz Silva W, Marengo JA (2013) Detection and projections of climate change in Rio de Janeiro, Brazil. Am J Clim Change 2: 25–33, doi: 10.4236/ajcc.2013.21003

Dufek AS, Ambrizzi T (2008) Precipitation variability in São Paulo state, Brazil. Theor Appl Climatol 93:167-178. doi: 10.1007/s00704-007-0348-7

Ghosh S, Das D, Kao SC, Ganguly AR (2012) Lack of uniform trends but increasing spatial variability in observed Indian rainfall extremes. Nat Clim Change 2:86-91. doi: 10.1038/NCLIMATE1327

Gocic M, Trajkovic S (2013) Analysis of changes in meteorological variables using Mann-Kendall and Sen's slope estimator statistical test in Serbia. Glob Planet Change 100:172-182. doi: 10.1016/j.gloplacha.2012.10.014

Hartmann DL et al (2013) Observations: atmosphere and surface. In: Stocker TF et al (Eds.), Climate change 2013: the physical science basis. Contribution of working group I to the fifth assessment report of the Intergovernmental Panel on Climate Change, Chapter 2. Cambridge University Press, New York, pp 159-254

Haylock MR et al (2006) Trends in total and extremes South American rainfall in 1960-2000 and links with sea surface temperature. J Clim 19:1490-1512. doi: 10.1175/JCLI3695.1

Held IM, Soden BJ (2006) Robust response of the hydrological cycle to global warming. J Clim 19:5686-5699

IBGE (2012) Contas regionais do Brasil 2012. Contas Nacionais número 42. ftp://ftp.ibge.gov.br/Contas_Regionais/2012/pdf/. Accessed Jul 17th 2017 (originally in Portuguese)

Jain SK, Kumar V (2012) Trend analysis of rainfall and temperature data for India. Curr Sci 102:37-49

Jones C, Carvalho LMV (2013): Climate change in the South American Monsoon System: present climate and CMIP5 projections. J Clim 26:6660–6678. doi: 10.1175/JCLI-D-12-00412.1

Kodama Y-M (1992) Large-scale common features of subtropical precipitation zones (the Baiu Frontal Zone, the SPCZ and the SACZ) part I: Characteristics of subtropical frontal zones. J Meteorol Soc Jpn 70:813-835

Kodama YM (1993) Large-scale common features of subtropical convergence zones (the Baiu Frontal Zone, the SPCZ and the SACZ). Part II: conditions of the circulations for generating the STCZs. J Meteorol Soc Jpn 75:581-610

Liebmann B, Allured D (2005) Daily precipitation grids for South America. Bull Am Meteorol Soc 86:1567-1570

Liebmann B, Jones C, Carvalho LMV (2001) Interannual variability of daily extreme precipitation events in the state of São Paulo, Brazil. J Clim 14:208-218

Liebmann B, Vera CS, Carvalho LMV, Camilloni A, Hoerling MP, Allured D, Barros VR, Baez J, Bidegain M (2004) An observed trend in central South American precipitation. J Clim 17:4357-4367

Lintner BR, Neelin JD (2010) Tropical South America-Atlantic sector convective margins and their relationship to low-level inflow. J Clim 23:2671-2685. doi:10.1175/2009JCLI3301.1

Ma H-Y, Ji X, Neelin JD, Mechoso CR (2011) Mechanisms for precipitation variability of the eastern Brazil/SACZ convective margin. J Clim 24:3445-3456. doi: 10.1175/2011JCLI4070.1

Marengo JA, Rusticucci M, Penalba O, Renom M (2010) An intercomparison of observed and simulated extreme rainfall and temperature events during the last half of the twentieth century: part 2: historical trends. Clim Change 98:509-529. doi: 10.1007/s10584-009-9743-7

Marengo JA, Valverde MC, Obregon GO (2013) Observed and projected changes in rainfall extremes in the Metropolitan Area of São Paulo. Clim Res 57:61-72. doi: 10.3354/cr01160.

Muza MN, Carvalho LMV, Jones C, Liebmann B (2009) Intraseasonal and interannual variability of extreme dry and wet events over southeastern South America and the subtropical Atlantic during austral summer. J Clim 22:1682-1699. doi: 10.1175/2008JCLI2257.1

Raimundo CC, Sansigolo CA, Molion LCB (2014) Trends of rainfall classes in the metropolitan region of São Paulo. Rev Bras Meteorol 29:397-408. doi: 10.1590/s0102-778620130655 (in Portuguese)

Rodionov S (2006) Use of prewhitening in climate regime shift detection. Geophys Res Lett 33: L12707, doi: 10.1029/2006GL025904.

Sen PK (1968) Estimates of the regression coefficient based on Kendall's Tau. J Am Statist Assoc 63:1379-1389

Seth A, Rojas M, Rauscher SA (2010) CMIP3 projected changes in the annual cycle of the South American Monsoon. Clim Change 98:331–357. doi: 10.1007/s10584-009-9736-6

Silva Dias MAF, Dias J, Carvalho LMV, Freitas ED, Silva Dias PL (2013) Changes in extreme daily rainfall for São Paulo, Brazil. Clim Change 116:705-722. doi:

10.1007/s10584-012-0504-7

Skansi MM et al (2013) Warming and wetting signals emerging from analysis of changes in climate extreme indices over South America. Glob Planet Change 100:295-307. doi: 10.1016/j.gloplacha.2012.11.004

Sugahara S, Rocha RP, Silveira R (2009) Non-stationary frequency analysis of extreme daily rainfall in São Paulo, Brazil. Int J Climatol 29:1339-1349. doi: 10.1002/joc.1760

Teixeira MS, Satyamurty P (2011) Trends in the frequency of intense precipitation events in Southern and Southeastern Brazil during 1960-2004. J Clim 24:1913-1921. doi: 10.1175/2011JCLI3511.1

USGS (2004) Shuttle Radar Topography Mission, 30 Arc Second, Global Land Cover Facility, University of Maryland, College Park, Maryland, February 2000

Wilks DS (2011) Statistical methods in the atmospheric sciences. Vol. 100. Academic Press: San Diego, CA

Xavier TMBS, Xavier AFS, Silva Dias MAF (1994) Evolução da precipitação diária num ambiente urbano: o caso da cidade de São Paulo. Rev Bras Meteorol 9:44-53 (in Portuguese)

Zhou J, Lau K-M (2001) Principal modes of interannual and decadal variability of summer rainfall over South America. Int J Climatol 21:1623-1644. doi: 10.1002/joc.700

Chapter 2: The Poleward Shift of South Atlantic Convergence Zone in Recent Decades

Marcia T.Zilli[1], Leila M. V. Carvalho[1,2], Benjamin R. Lintner[3]

[1] Department of Geography, University of California, Santa Barbara, CA, USA.

[2] Earth Research Institute, University of California, Santa Barbara, CA, USA

[3] Department of Environmental Sciences, Rutgers, The State University of New Jersey, NJ, USA

2.1. Abstract

During austral summer (December to February), intense precipitation over Eastern Brazil is modulated by the South American Monsoon System and the South Atlantic Convergence Zone (SACZ). Previous studies identified spatial variability in precipitation trends over this region, suggestive of a poleward shift of the SACZ. To identify underlying mechanisms associated with changes in the precipitation intensity and position of the SACZ, decadal averages of observed precipitation and mean state of the atmosphere and ocean during three different periods from 1979 to 2014 are compared. The results provide evidence of decreasing (increasing) average daily precipitation along the equatorward (poleward) margin of the climatological SACZ, likely related to a poleward shift of the convergence zone. This behavior is associated with weakening of the poleward winds along the eastern Brazilian coast and a drying of low-to-mid troposphere (700hPa) over the tropical Atlantic. Variations in precipitation along the SACZ's margins were partially related to climatic modes, but these relationships were not systematic throughout the entire period. We suggest that changes in SACZ could be related to the combination of the increase in diabatic heating over the continent and the positioning and strength of the South Atlantic Subtropical High.

2.2. Introduction

Persistent and intense precipitation characterizes the summer season (December-February, DJF) in Eastern and Southeastern Brazil (SE Brazil), with summertime rainfall accounting for more than 50% of the annual total there (Barros et al. 2000; Liebmann et al. 2001; Vera et al. 2006). Precipitation in these regions is influenced by both the South American Monsoon System (SAMS) and the South Atlantic Convergence Zone (SACZ; Zhou and Lau 1998; Barros et al. 2000; Zhou and Lau 2001; Carvalho et al. 2004, 2011; Vera et al. 2006; Muza et al. 2009).

The onset of the wet phase of the SAMS typically occurs between mid-September and mid-October (Silva and Carvalho 2007; Carvalho et al. 2011), when deep convection over the Amazon warms the troposphere and contributes to the formation of the upper tropospheric Bolivian High over the Andes Altiplano (Lenters and Cook, 1997). At lower levels, deep convection and surface heating strengthen the continental thermal low, increasing the land-ocean pressure gradient and accelerating the trade winds over the equatorial Atlantic Ocean toward South America (SA), contributing to the onset of the rainy season (Zhou and Lau 1998; Wang and Fu 2003). During the peak of the monsoon season (DJF), the deep convective heating over tropical SA intensifies the poleward flow along the eastern flank of the Andes through the Sverdrup balance, closing the anticyclonic circulation around the South Atlantic Subtropical High (SASH; Rodwell and Hoskins 2001; Liu et al. 2004; Wu et al. 2009). As the flow approaches the Chaco Low, which is a thermal low over central SA, it is deflected southeastward, thereby transporting moisture toward Southeastern SA. Episodes of intense northerly winds east of the Andes are referred to as Low Level Jet (LLJ) and are associated with deepening of the Chaco Low and increasing southward moisture transport (Liebmann et al. 2004).

The South Atlantic Convergence Zone (SACZ), which is one of the main features of the SAMS (Kodama 1992, 1993; Zhou and Lau 1998; Liebmann et al. 2001; Carvalho et al. 2002, 2004; Marengo et al. 2012), comprises a diagonally-oriented band of deep convection extending from tropical SA southeastward toward SE Brazil and subtropical South Atlantic Ocean. Kodama (1992, 1993) described the SACZ as a baroclinic structure located to the east of a trough in the subtropical jet. It is formed by moisture converging from two different regions: low-level northerly inflow originating along the western periphery of the SASH; and westerly flows along the convergence zone, increasing in intensity with height and forming part of the subtropical jet in upper levels. These two components are thought to be essential for the development and strengthening of the SACZ through frontogenesis and convective instability generation (Kodama 1993).

The spatial variability of the DJF precipitation over SA is dominated by a dipole-like pattern of opposing anomalies over Eastern Brazil and Southeastern SA occurring across multiple time scales (Zhou and Lau 1998; Nogués-Paegle et al. 2000; Carvalho et al. 2002, 2011; Grimm and Zilli 2009; Grimm and Saboia 2015). Grimm and Saboia (2015) showed that this dipole is observed on decadal time scales and is partially influenced by large scale climatic modes of variability, such as the Interdecadal Pacific Oscillation (IPO) and the Atlantic Multidecadal Oscillation (AMO). On intraseasonal time-scales, phenomena such as the Madden-Julien Oscillation (MJO) and modes of variability such as the Pacific South America (PSA) pattern, also modulate circulation and convective activity over Eastern Brazil and the SACZ (Mo and Nogués-Paegle 2001; Carvalho et al. 2004, 2011; Cunningham and Cavalcanti 2006).

The position and intensity of the SACZ have been associated with variations in sea

surface temperatures (SSTs) in the Atlantic and Pacific on interannual time-scales. Bombardi et al. (2013) showed that negative (positive) SST anomalies over tropical (subtropical) South Atlantic, associated with the South Atlantic Dipole (SAD), are related to the enhancement of the westerly winds over Eastern Brazil, with the associated increase of cyclonic moisture transport enhancing precipitation over this region. The positive phase of the El Niño/Southern Oscillation (ENSO) has been related to above average precipitation in January over Eastern Brazil (e.g., Grimm 2003; Drumond and Ambrizzi 2006; Grimm et al. 2007; Krishnamurthy and Misra 2010) and a persistent oceanic SACZ (Carvalho et al. 2004), which increases the probability of extreme rainfall events over coastal SE Brazil (Liebmann et al. 2001; Carvalho et al. 2002). On interannual to decadal time scales, positive (negative) phases of the Pacific Decadal Oscillation (PDO) are associated with positive (negative) precipitation anomalies over Eastern Brazil (Krishnamurthy and Misra 2011), intensifying the effects of ENSO when both oscillations are in phase (Kayano and Andreoli 2007).

A warmer and more humid troposphere has been projected in future scenarios of climate change. These conditions are expected to enhance precipitation due to increased moisture availability (Held and Soden 2006). However, the dynamical responses to global warming are spatially variable and may offset thermodynamic factors affecting precipitation, particularly in regions influenced by advective transports of temperature and moisture (Schneider et al. 2010, Cherchi et al. 2011, Kitoh et al. 2013). Over SA, studies based on coupled climate model simulations (historical scenarios) and on reanalyses suggest that the tropospheric warming of recent years, which is larger over central-north Brazil than other areas (Carvalho and Jones 2013; de Barros Soares et al. 2017), cannot be explained by natural climate variability alone (de Barros Soares et al. 2017). Observations have shown that

the global monsoon precipitation has increased in the last three decades due to global warming (Hsu et al. 2011). Multiple coupled climate model simulations project a poleward expansion of the areal extent of the SAMS, increasing extreme precipitation, and weakening of the monsoon circulation (Hsu et al. 2013; Kitoh et al. 2013). Moreover, changes in convective heating over the Amazon could influence the position and intensity of the SASH with possible impacts on the SACZ (Seth et al. 2010, Li et al. 2013).

One possible consequence of the southward expansion of the SAMS and intensification of the SASH is the poleward displacement of the SACZ. A few studies evaluated the consequences of a warmer atmosphere on the formation and intensity of the SACZ (Seth et al. 2010, Lintner and Neelin 2010, Ma et al. 2011, Carvalho and Jones 2013). Changes in the SASH can affect the intensity of advection of relatively stable (low moist static energy) air masses from the tropical and subtropical South Atlantic into the northeastern margin of SACZ, thereby inducing thermodynamic conditions less favorable to deep convection (Lintner and Neelin, 2010, Ma et al. 2011). Zilli et al. (2017) identified an increase in total precipitation during the rainy season over the southern portion of SE Brazil resulting from more rainy days (days with precipitation above 1mm/day) and more frequent and intense extreme events. Further north, Zilli et al. (2017) showed that extreme events are also becoming more intense and frequent, although the number of rainy days is decreasing. That study suggested that the spatial variability of trends in extreme precipitation over coastal SE Brazil could be explained by the poleward shift of the SACZ. Such spatial pattern of changes in precipitation have not been accurately reproduced in climate model projections based on historical scenarios (e.g. Carvalho and Jones 2013; Jones and Carvalho 2013; Kitoh et al. 2013), most likely because of model's misrepresentation of precipitation variability,

especially over the monsoon region during summer (de Barros Soares et al. 2017).

The present study investigates the poleward shift of the SACZ and accompanying changes in the mean basic state of the atmosphere in the recent decades. This study focuses on decadal changes in the circulation features related to the position and intensity of the SACZ that could influence dynamical and thermodynamical processes related to convection and precipitation over Eastern Brazil. This study also examines possible mechanisms by which the tropospheric warming is influencing circulation. The discussion is organized as follows: dataset and methodology are described in Section 2.3. Changes in the decadal mean state of the atmosphere during DJF, including changes in precipitation, circulation, and temperature, are presented in Section 2.4. Section 2.5 discusses the implications of large scale changes in regional precipitation, while in Section 2.6 we summarize the results and present conclusions.

2.3. Data and methods

2.3.1. Data

The precipitation dataset used in this study is the monthly gridded data from the Global Precipitation Climatology Project Version 2.2 (GPCP; Huffman et al. 2009), with 2.5° lon/lat horizontal resolution and spanning 1979 to 2015. This dataset combines rain gauge and satellite precipitation estimates and is utilized to investigate the interdecadal variability of SACZ. Changes in the basic state of the atmosphere are evaluated with the National Center for Environmental Prediction (NCEP) Climate Forecast System Reanalysis (CFSR; Saha et al. 2010), at a spatial resolution of 0.5° lon/lat and daily temporal resolution, from 1979 to 2015. The atmospheric fields investigated are: geopotential height at 200hPa (Z200), vertical velocity at 500hPa (ω500), specific humidity at 700hPa (Q700) and 850 (Q850), wind at

850hPa (Wind850), temperature at 850hPa (T850), and sea level pressure (SLP). Sea surface temperatures (SSTs) are derived from the National Oceanic and Atmospheric Administration (NOAA) Optimum Interpolation (OI) SST Version 2 High Resolution dataset (Reynolds at al. 2007), with daily data since 1981 at a spatial resolution of 0.25° lon/lat. Indices of low-frequency climate variability, including the unsmoothed Atlantic Multidecadal Oscillation (AMO; Enfield et al. 2001), unfiltered Interdecadal Pacific Oscillation (IPO; Henley et al. 2015), and Pacific Decadal Oscillation (PDO; Mantua et al. 1997), are obtained from the NOAA Physical Science Division (PSD), with monthly data from 1979 to 2014.

2.3.2. Methods

Changes in the mean DJF precipitation rate and in the basic state of other atmospheric fields over South America were estimated by comparing the austral summer averages for three 10-year periods. Since ENSO is the most important coupled mode of variability influencing precipitation in SA (e.g. Grimm 2003; Grimm et al. 2007), the 10-year periods were determined after excluding strong ENSO events. These events were identified when the absolute values of Oceanic Niño Index (ONI, available at http://www.cpc.ncep.noaa.gov/products/analysis_monitoring/ensostuff/ensoyears.shtml) were greater than 1.4°C for at least three consecutive 3-month running means, as long as these conditions were satisfied in at least one month in DFJ. Thus, the resultant periods were: 1979-1991 (excluding 1982-83 El Niño, 1988-89 La Niña, and 1991-92 El Niño); 1992-2004 (excluding 1997-98 El Niño, 1998-99 and 1999-2000- both La Niña); and 2005-2014 (no strong ENSO events). Because the SST dataset begins in 1981, the first period considered when investigating changes in the mean SST conditions in this analysis spans 1981-1992 and the second period 1993-2004, excluding the same ENSO years. The years considered in each period and dataset, as well as

the years excluded due to ENSO events, are summarized in Table 2.1. Notice that the DJF average of a variable for a specific year is calculated using December of that year and January and February of the next year.

Table 2.1 — First year, last year, number of years (#Yr), and years excluded due to strong ENSO events (EN – El Niño; LN – La Niña) on each period considered for each dataset (GPCP, CFSR, and NOAA OI SST V2)

PERIODS	**DATASETS**						**EXCLUDING**
	GPCP and CFSR			**NOAA OI SST V2**			
	First Year	Last Year	#Yr	First Year	Last Year	#Yr	
1979-91	1979	1991	10	1981	1992	9	1982-83 (EN) 1988-89 (LN) 1991-92 (EN)
1992-04	1992	2004	10	1993	2004	9	1997-98 (EN) 1998-99 (LN) 1999-2000 (LN)
2005-14	2005	2014	10	2005	2014	10	-

To identify decadal changes in the mean basic state of the atmosphere during DJF, we compared the decadal average for the period 1979-1991 with those for 2005-2014. Since we used all daily values for each period (900 days), the null hypothesis of the averages over two periods being equal was tested using a *z*-test considering two independent samples, at 5% significance level, according to a Student's t-distribution (Wilks 2011). The degrees of freedom were assessed based on the effective sample size of each grid point, after accounting for serial autocorrelation (Wilks 2011). The correlation between precipitation and the climatic modes was calculated using Spearman rank correlation (Wilks 2011) and trends in precipitation anomalies were estimated using the Mann Kendall test (Wilks 2011; Zilli et al. 2017)

Changes in SLP were based on the zonally asymmetric SLP (ZA_SLP), estimated as the DJF average SLP at each grid point. Upper level (200hPa) divergence (Div200) and the

700hPa and 850hPa saturation deficits ($Q700_d$ and $Q850_d$, respectively) were also calculated using CFSR. The latter quantifies how far the atmosphere is from saturation, in terms of vapor mass (g/kg), and is defined for each level as the difference between the saturation specific humidity (Q_{sat}) and the ambient specific humidity (Q) at that level. The Q_{sat} was estimated as (Emanuel, 1994):

$$Q_{sat} = \frac{\epsilon e_{sat}}{p - e_{sat}(1 - \epsilon)} \quad \text{(Eq 2.1)}$$

where p is pressure, ϵ $(= 0.62220)$ is the ratio between the gas constant for dry air and for water vapor, and e_{sat} is the saturation vapor pressure at that level, estimated following (Bolton, 1980):

$$e_{sat} = 6.112exp\left[\frac{17.67 \times T}{T + 243.5}\right] \quad \text{(Eq 2.2)}$$

where T is the temperature at that level.

2.4. Decadal Changes in the Mean State

2.4.1. Precipitation

Both the SAMS and the SACZ are evident in the GPCP average DJF daily-mean precipitation rate (Figure 2.1a). Additionally, the seasonal average precipitation in Figure 2.1a also indicates the climatological position of the Intertropical Convergence Zone (ITCZ) over equatorial Atlantic and Pacific oceans, as well as the South African Summer Monsoon and the South Pacific Convergence Zone (SPCZ) over central South Pacific.

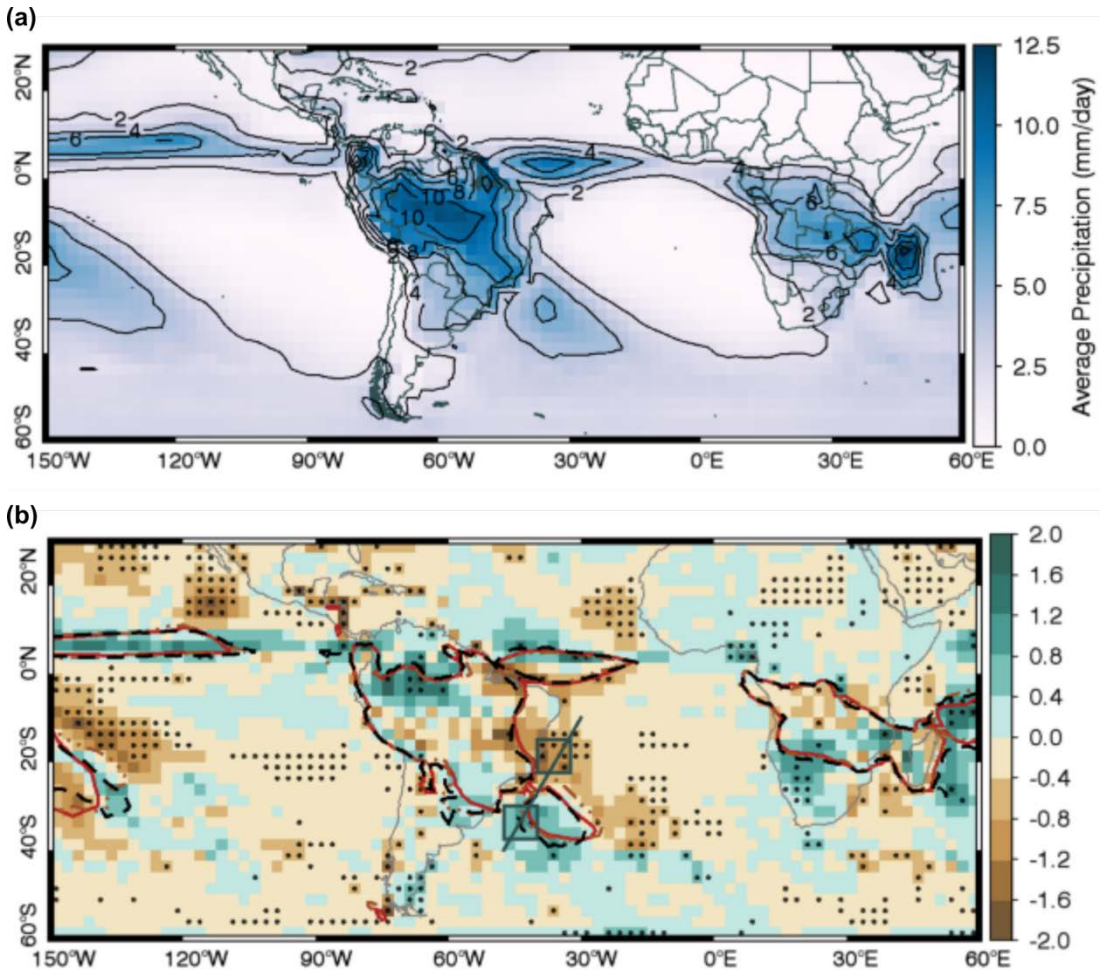

Figure 2.1 — GPCP DJF precipitation rate (mm/day): (a) Climatology for 1979-2014 (contours each 2mm/day); (b) Difference between the first (1979-91) and last (2005-14) periods, with positive (negative) differences in green (brown) and significant difference ($p<0.05$) stippled. Contours at the 5mm/day isohyet for each period (1979-91, solid red; 1992-04, dot-dashed brown; and 2005-14, dashed black, excluding strong ENSO years). Bold gray line: location of the oceanic SACZ cross-section. Gray boxes: location of the areas over the equatorward (40°W, 22.5°S to 32.5°W, 15°S) and poleward (47.5°W, 37.5°S to 40°W, 30°S) margins of the SACZ

The difference between DJF precipitation averaged during the first (1979-91) and last (2005-14) considered periods (Figure 2.1b) indicates an area of reduced (increased) precipitation along the equatorward (poleward) margin of the climatological SACZ that extends from SA into the subtropical Atlantic ocean. For reference, we have included in Figure 2.1b the 5mm/day isohyet for each 10-yr period (1979-91, solid red; 1992-04, dot-dashed brown; and 2005-14, dashed black), to indicate the climatological location of the

SACZ. A similar drying/wetting pattern is observed along the Atlantic ITCZ and over southern Africa, while the South Pacific Convergence Zone (SPCZ) exhibits a drying trend along both its poleward and equatorward margins. Additionally, there is an increase in precipitation over equatorial western Amazon, at the northern margin of the SAMS. These spatial patterns were not significantly affected by the inclusion of ENSO years (Figure not shown).

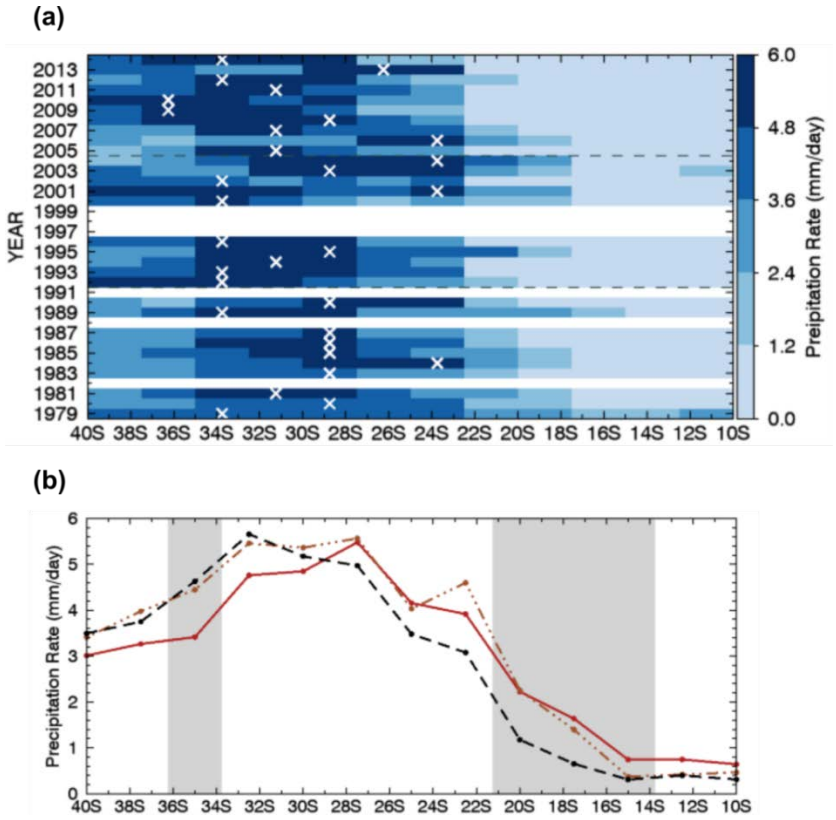

Figure 2.2 — GPCP DJF precipitation rate (mm/day) along the oceanic SACZ cross-section (bold gray line in Figure 2.1b): (a) Hovmöller diagram, with averages of all grid points along the cross-section and white "x" symbols indicating the latitude of maximum precipitation per season; gray dashed lines separate each period considered. (b) Average for each of the three periods (1979-91, solid red; 1992-04, dot-dashed brown; and 2005-14, dashed black). Gray shades show grid points with statistically significant ($p<0.05$) differences in precipitation average between first and last periods. ENSO years are excluded from this analysis (see text for details)

To demonstrate the shift in precipitation at the poleward and equatorward margins of

the SACZ, we defined a cross-section perpendicular to the NW-SE orientation of the SACZ (between 40°S, 47.5°W and 10°S, 30°W) and across the regions with the largest changes in precipitation (Figure 2.1b). The Hovmöller diagram in Figure 2.2a represents the DJF average precipitation for each season along this cross-section and the plot in Figure 2.2b shows the DJF averages for each of the three consecutive periods. Along the cross-section, the wetting tendency over the poleward margin of the SACZ (south of 30°S) is noticeable as early as 1992 (Figure 2.2a). Figure 2.2b clearly shows these differences and illustrates the poleward shift of the convergence zone during the second period (1992-04) compared to the first period (1979-91; compare the solid red line with the dot-dashed brown line in Figure 2.2b). At the equatorward margin of the section (north of 30°S), the drying tendency begins after 2007 (Figure 2.2a), affecting the average over the last period (2005-14) and shifting precipitation poleward (Figure 2.2b, dashed black line).

The average position of maximum precipitation along this cross-section has also been displaced southward by as much as 4° since 1979 (Figure 2.2b), albeit with significant interannual variability, particularly after 2000 ("x" symbols, Figure 2.2a). The low-frequency evolution of precipitation, more evident after the mid-2000s, indicates that the drying tendency along the SACZ equatorward margin is not simply the effect of the intense drought that affected SE Brazil in 2014/2015 (Otto et al. 2015; Coelho et al. 2016a, b; Nobre et al. 2016). These changes are further consistent with the drying tendency observed since 1998 in the region as documented in Coelho et al. (2016a).

The temporal variation of the DJF precipitation anomalies along each margin of the SACZ (boxes in Figure 2.1b and Figure 2.3, left) supports the hypothesis of a poleward shift of the SACZ over time. Areas along the equatorward margin of the SACZ, and to the north

(40°W, 22.5°S to 32.5°W, 15°S), exhibited precipitation anomalies that were predominantly positive during the 1980s and over 2000-2007, and negative in the 1990s and over 2008-2014 (Figure 2.3a and b, left), with a negative precipitation trend of -0.46 mm/day/decade, significant at 5% level.

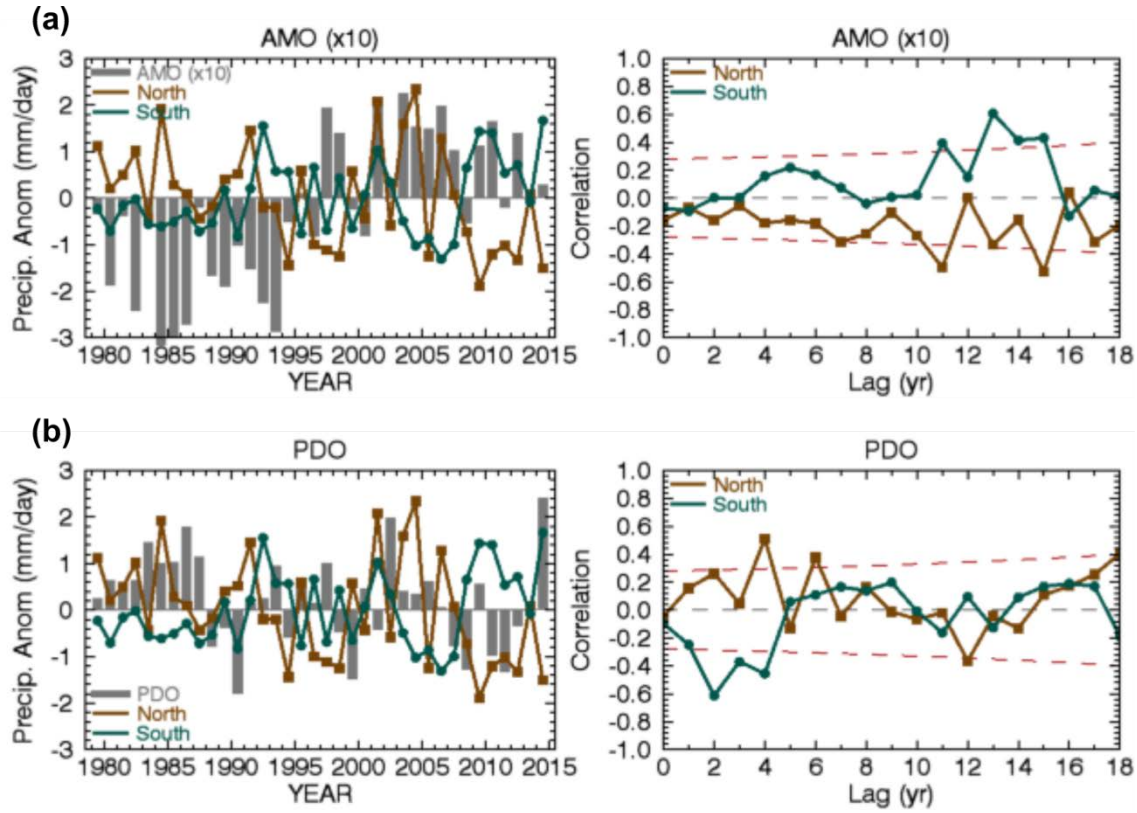

Figure 2.3 — Left: DJF average for climatic mode index (gray bar) and DJF precipitation anomalies (lines) over areas to the north (brown) and south (green) of the SACZ. See boxes in Figure 2.1b for the location of these areas. Right: Lagged Spearman rank correlation between climatic mode index and DJF precipitation anomalies for areas to the north (brown) and south (green) of the SACZ. Dashed red lines represent the 5% significance level for the correlation. Climatic indices: (a) AMO (index multiplied by 10) and (b) PDO. Note that ENSO years are included in these analyses

On the other hand, precipitation anomalies along the SACZ poleward margin, and to the south (47.5°W, 37.5°S to 40°W, 30°S), are generally antiphased, with Spearman rank correlation between the two domains approximately -0.54, significant at 1% level. The precipitation trend for the southern margin is positive, but not statistically significant. For

both areas, the largest fluctuations in precipitation anomalies occur after 2000.

The spatial pattern of precipitation anomalies observed here (Figures 2.1 and 2.3) resembles the dipole pattern often associated with variations in the SACZ over Southeastern SA on multiple scales (e.g., Zhou and Lau 1998; Carvalho et al. 2002, 2011; Grimm and Zilli 2009; Grimm and Saboia 2015). On decadal timescales, Grimm and Saboia (2015) identified correlations between the dipole and the AMO, IPO, and PDO. To evaluate the influence of these climatic modes on our results, we calculated the Spearman rank correlation between DJF averages of these indices and DJF precipitation anomalies observed at the north and south margins of the SACZ (boxes in Figure 2.1b).

The rank correlations between AMO and precipitation anomalies for the northern and southern areas are, respectively, negative and positive and statistically significant ($p<0.05$) when precipitation lags AMO by more than 11 years (Figure 2.3a, right). Conversely, lag-rank-correlations between the PDO index and precipitation anomalies over the northern (southern) area are positive (negative) and statistically significant ($p<0.05$) for precipitation lagging PDO by 4 and 6 (2 to 4) years (Figure 2.3b, right). The lag-rank-correlation between IPO and precipitation anomalies at each area is not significant, even when considering a lag between the index and precipitation (Figure not shown). These results indicate that the PDO and AMO, and their respective changes in the mean state of the atmosphere, can play a role in modulating precipitation along the margins of the SACZ, consistent with previous studies (Krishnamurthy and Misra 2011; Grimm and Saboia 2015). However, Figure 2.3 also indicates that these relationships are not systematic throughout the period: the PDO seems to be more relevant after 2002 while the shift in AMO phase in 1997 seems to have played a role in modulating precipitation anomalies after 2008. Therefore, fluctuations in the PDO and

AMO are not sufficient to explain precipitation trends observed along the two margins of the SACZ. None of these results were affected by the inclusion or exclusion of ENSO years or by the positioning of the areas along the opposite margins of the SACZ, even when they were placed over the continent (Figure not shown). The next section investigates changes in dynamic and thermodynamic aspects of the regional environment and circulation to better understand the observed shift.

2.4.2. Temperature and Specific Humidity

The SAMS circulation is mainly driven by the differential heating between land and ocean and resulting land-ocean pressure gradient (Zhou and Lau 1998). Over the period analyzed here, the average temperature at 850hPa (T850) in DJF has increased over tropical SA and adjacent oceans, whereas subtropical and mid-latitude regions have cooled (Figure 2.4a). Over the tropics, the largest warming has occurred over the equatorial Pacific and equatorial and subtropical North Atlantic Ocean basins. Moreover, SSTs have increased over the tropical North Atlantic Ocean, as seen by the northward shift of the 27°C isotherm along the northern SA coast during the three consecutive periods (Figure 2.4b). Although the increase in SST in the subtropics resembles the positive phase of SAD, the equatorial counterpart of this mode is not consistent with the observed decadal changes in low latitudes (Bombardi et al. 2013).

Over the continent, T850 increased over the Amazon and northeastern Brazil and the progressive warming since the 1990s can be illustrated by the behavior of the 18°C isotherm in Figure 2.4a. At 850hPa, summertime temperature is largely controlled by cloudiness and precipitation in the tropics and subtropics (e.g., McGregor and Nieuwolt 1998). The warming

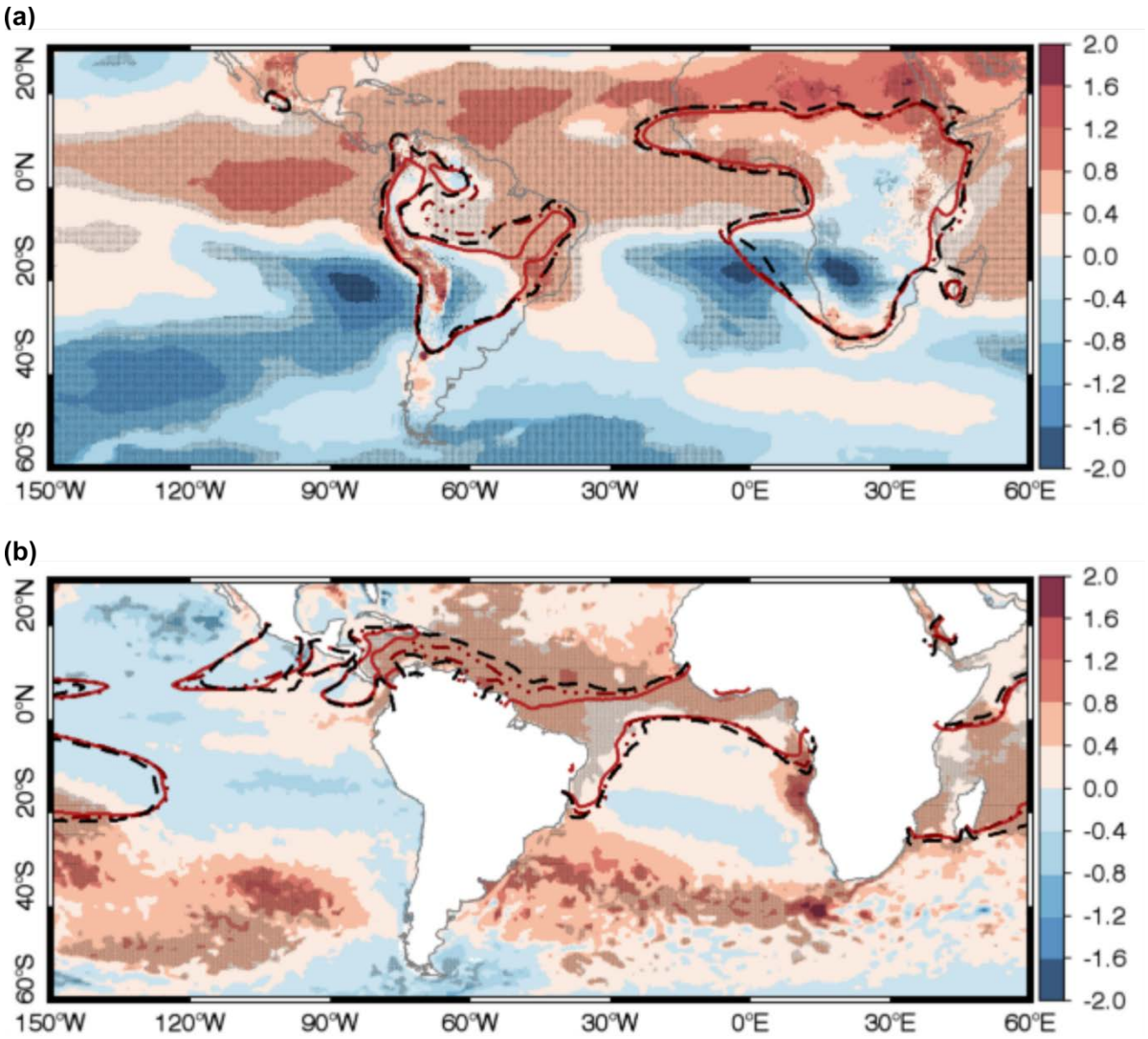

Figure 2.4 — Difference in DJF average between first (1979-91) and last (2005-14) periods (shades), with positive (negative) differences in red (blue) and significant differences ($p<0.05$) stippled, and DJF average (contours) for each period (1979-91, solid red; 1992-04, dot-dashed brown; and 2005-14, dashed black): (a) T850 (in °C), contours at 18°C; and (b) SST (in °C), contour at 27°C

over tropical SA is consistent with Carvalho and Jones (2013). By contrast, significant cooling at 850hPa (Figure 2.4a) is observed in the subtropics, coinciding with the climatological position of the semi-permanent anticyclones of the southeastern Pacific and Atlantic oceans. Cooling is also observed in the storm track over southeastern Pacific and southwestern Atlantic, and over northwestern Argentina. The cooling over these regions is

restricted to levels below 500hPa (Figure not shown), which suggests the importance of the increase in cloudiness in these regions.

Consistent with the observed tropospheric warming and with Clausius-Clapeyron scaling of moisture saturation, specific humidity has also increased over the tropics. The tropospheric moistening is larger over the monsoonal regions of SA and Africa (Figure 2.5a for 850hPa and Figure 2.5b for 700hPa). Over the oceans, however, the moistening is not uniform with elevation. Interestingly, at 700hPa (Figure 2.5b), there is drying of the troposphere equatorward of the SACZ and extending eastward over the tropical South Atlantic; similarly, drying occurs over the tropical Central Pacific to the north of the SPCZ (Figure 2.5b). Both regions are characterized by subsidence (ω500, c.f. Figure 2.7b, contours) associated with persistent anticyclones in the southeast of each basin. It is worth noticing that over eastern Brazil the increase in specific humidity is not as pronounced, despite the strong warming observed over the region (compare Figures 2.4a, 2.5a and b). These results are further explored in Section 2.5.

2.4.3. Circulation and Geopotential

The warming trend of the tropical troposphere can be diagnosed by the vertical expansion of the troposphere and consequent increase in the 200hPa geopotential height (Z200). Figure 2.6a illustrates this by highlighting the mean 12400gpm isopleth for the three consecutive periods. During 1979-1991 (red solid contour), the 12400gpm isopleth is confined to the Bolivian Altiplano, near the center of the Bolivian High. During 1992-2004, (brown dot-dashed contour), this isopleth encompasses most of tropical SA, while during 2005-2014 (black dashed line) it extends over most of the tropics, between 20°N and 20°S. Similar behavior is observed for the upper level high over southern Africa. One possible

result of the vertical expansion of the troposphere is the widening of the Hadley cell and shifting poleward of the semi-permanent subtropical high pressure systems and the Southern Hemisphere storm track (Seidel and Randel 2007; Schneider et al. 2010).

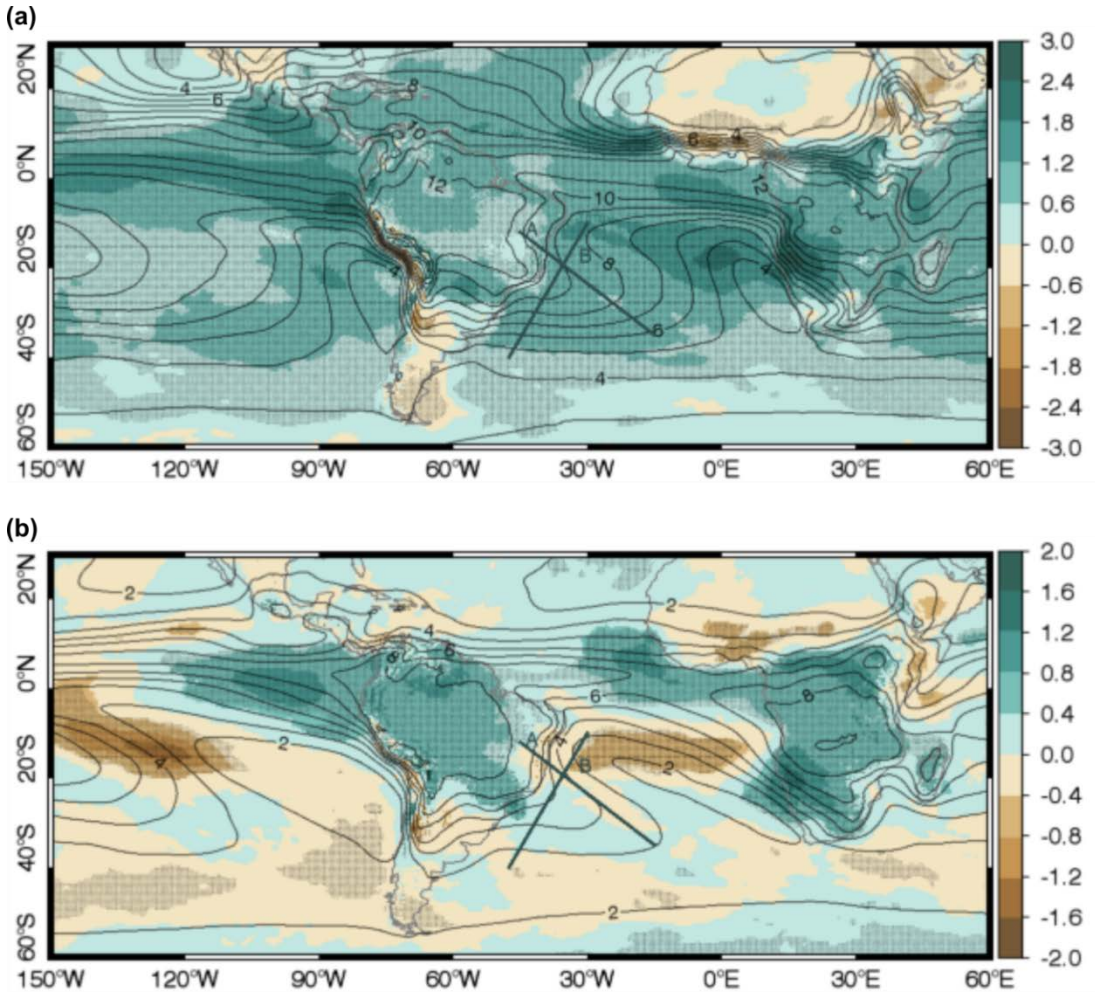

Figure 2.5 — Difference in DJF average between first (1979-91) and last (2005-14) periods (shades), with positive (negative) differences in green (brown) and significant differences ($p<0.05$) stippled, and climatology for 1979-2014 (contours each 1g/kg). Bold gray line: location of the cross-sections along the equatorward margin of the SACZ ("A") and across the oceanic SACZ ("B"). (a) Q850 (in g/kg); and (b) Q700 (in g/kg)

One consequence of the increase in SST and T850 over the equatorial and subtropical North Atlantic is the reduction of the cross-equatorial temperature gradient and weakening of the ZA_SLP off the north coast of SA (Figure 2.6b). The weakening of the cross-equatorial

pressure gradient is likely related to observed deceleration of the trade winds over the equatorial Atlantic, shown by the westerly anomalies at the equator in Figure 2.7a. Along the eastern flank of the Andes over northwestern Argentina, the ZA_SLP has increased in the recent period (Figure 2.6b), weakening the Chaco Low and the land-ocean ZA_SLP gradient.

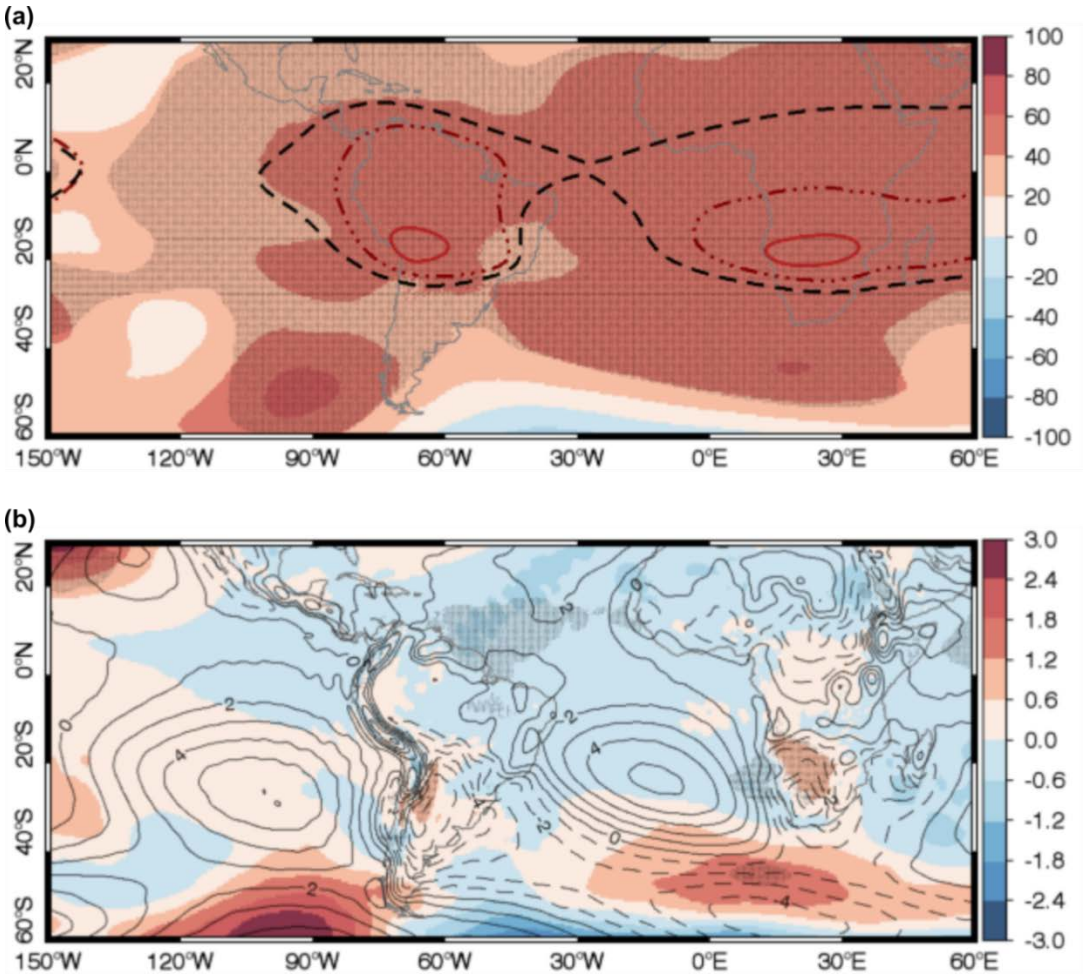

Figure 2.6 — Difference in DJF average between first (1979-91) and last (2005-14) periods (shades), with positive (negative) differences in red (blue) and significant differences ($p<0.05$) stippled. (a) Z200 (in gpm), contours at 12400gpm representing the DJF average for each period (1979-91, solid red; 1992-04, dot-dashed brown; and 2005-14, dashed black); (b) ZA_SLP (in hPa), with contours representing the DJF climatology (1979-2014; contours each 1hPa, with negative values dashed)

Changes in the Chaco Low affect the intensity of both the LLJ east of the Andes and the northerly winds along the eastern Brazilian coast, through the land-ocean pressure

gradient. In fact, the difference between the average summer wind at 850hPa between 1979-91 and 2005-14 shows a cyclonic anomaly over subtropical South Atlantic Ocean (Figure 2.7a), consistent with the weakening of the land-ocean ZA_SLP gradient. The anomalous southerly winds along the western flank of this anomalous circulation reduce the poleward flow over Eastern Brazil and adjacent tropical Atlantic (Figure 2.7a). Given that the northerlies in this region are related to the position and strength of the SACZ (Kodama, 1992, 1993), a weakening of the meridional wind component is potentially associated with reduced precipitation caused by the weakening of the low-level convergence and ascent (ω500; Figure 2.7b). This will be examined in more detail in Section 2.5.

Over western Amazon and along the eastern slopes of the Andes, the northerly winds accelerate (Figure 2.7a) and the ascending motion is intensified (Figure 2.7b). Together with the larger specific humidity (Figure 2.5) over the region, the increased low-level flow enhances the poleward moisture flux toward subtropical SA. Additionally, the weakening of the Chaco Low favors southeastward deflection of this flow from the Amazon toward the poleward margin of the SACZ. The anomalous westerlies along this margin form the northern flank of a cyclonic circulation anomaly centered at about 35^{o}S and 56^{o}W (Figure 2.7a), which is thus associated with the enhancement of ascending air (Figure 2.7b) and convection over the region (Figure 2.1b).

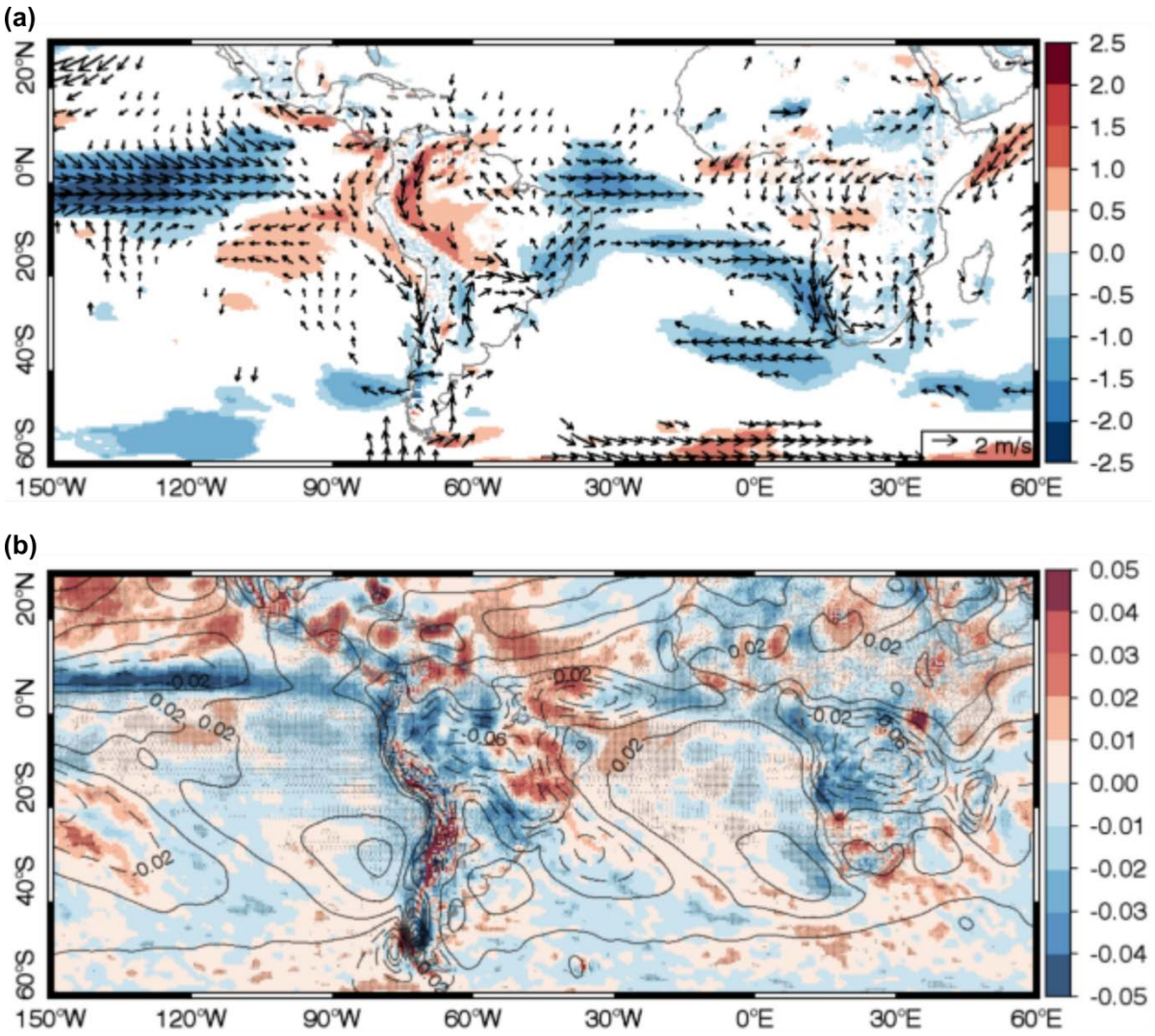

Figure 2.7 — Difference in DJF average between first (1979-91) and last (2005-14) periods (shades), with positive (negative) differences in red (blue) and significant differences ($p<0.05$) stippled: (a) Wind850 (in m/s): wind speed (shaded) and vectors (arrows); only areas with significant differences ($p<0.05$) for at least one component plotted. (b) ω500 (in Pa/s), with contours representing the DJF climatology (1979-2014; contours each 0.02Pa/s, with negative values dashed)

2.5. Impact of large scale changes on regional precipitation over Eastern Brazil

According to Kodama (1992, 1993), subtropical diagonal convective zones such as the SACZ are maintained by the convergence between the low-level poleward flow along the west flank of the subtropical anticyclone and the mid-to-upper level westerlies on the equatorward flank of the subtropical jet. On interannual time scales, above-average northerly

winds on the equatorward margin of the SACZ are related to intense precipitation events, both over the continent and the adjacent ocean (Muza et al. 2009). Furthermore, deep convective activity over the continent warms the mid-troposphere and increases the land-ocean temperature gradient, favoring northerly winds on the western flank of the SASH and increasing convergence and precipitation (Wu et al. 2009). Our results indicate a decadal weakening of the low-level poleward flow (Wind850, Figure 2.7a) along with a decrease in convection over eastern Brazil, as exemplified by reduced precipitation (Figure 2.1b) and ascent (Figure 2.7b), and increased tropospheric temperature (T850, Figure 2.4a).

A more detailed analysis of the difference in winds at 850hPa averaged over the first (1979-91) and last periods (2005-14) is presented in Figure 2.8a. The wind speed weakens along the western flank of the anticyclonic circulation, with the black arrows representing the average for the last period (2005-14) and red arrows the average for the first period (1979-91). The black arrows are systematically smaller than, and pointing to the right of, the red arrows. To further investigate the implications of weaker northerlies on precipitation over the equatorward margin of the SACZ, we defined a cross-section along the convective margin (between 12°S, 45°W and 35°S, 15°W, Figure 2.8a). The Hovmöller diagram obtained along the cross-section (Figure 2.8b) shows the DJF average of meridional wind at 850hPa from 1979 to 2014. Until 1995, the maximum wind speed along this cross-section used to occur between 41°W and 35°W. After 2000, the position of the maximum meridional wind has shifted southeastward, with reduced intensity after 2005. Figure 2.8c shows the meridional wind and precipitation along this cross-section, averaged over the three periods considered here. The reduction in the meridional wind during the last period

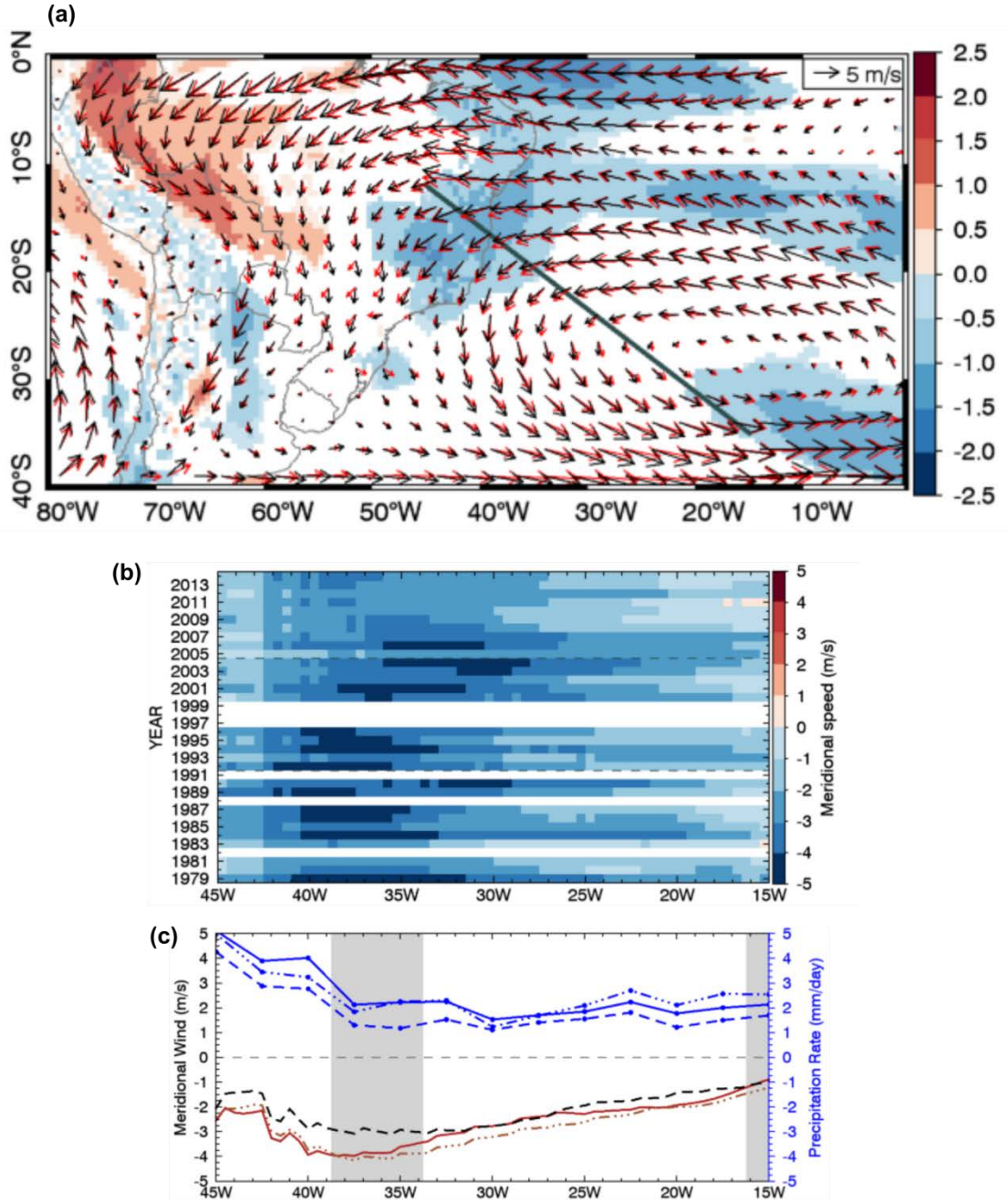

Figure 2.8 — Wind at 850hPa (in m/s): (a) Arrows: DJF average during the first (red, 1979-91) and last (black; 2005-14) periods; shades: positive (red) and in negative (blue) significant ($p<0.05$) differences between DJF average wind speed for the first (1979-91) and last (2005-14) periods. Bold gray line: location of the cross-section along the equatorward margin of the SACZ. (b) Hovmöller diagram of the average meridional wind for all grid points along the cross-section in (a) with positive (negative) differences in red (blue); gray dashed lines dividing each of the periods considered. (c) Average meridional wind (red, brown, and black lines) and precipitation (blue lines with circles marking the center of each grid point, right y-axis) for each period (1979-91, solid; 1992-04, dot-dashed; and 2005-14, dashed) along the cross-section in (a). Shaded areas: grid points with significant ($p<0.05$) difference between average precipitation for the first (1979-91) and last periods (2005-14)

(2005-14) between 39°W and 34°W along the convective margin is as large as 1m/s and corresponds to a decrease in average precipitation of about 1mm/day (Figure 2.8c).

The weakening of the northerly winds along the equatorward margin of the SACZ in recent decades is associated with weakened low-level convergence and consequently reduced ascent (Figure 2.7b), weakening the upper-level divergence (at 200hPa, Div200; Figure 2.9a). The cross-section along the convective margin is located where the climatology for the upper-level divergence changes from divergence to the south to convergence to the north (cross-section "A" in Figure 2.9a). Consequently, the divergence was close to zero along this cross-section until 1990, with a region of small positive values between 41°W and 36°W near the Eastern Brazilian coast (Figure 2.9b). After 1992, the divergence has become consistently negative near the coast, with more intense convergence occurring after 2005. From 2009 until 2014, upper-level convergence has dominated over the entire oceanic portion of the cross-section (east of 41°W, Figure 2.9b). The average Div200 during each of the three periods (Figure 2.9c) shows that the area of the cross-section with the largest decrease in divergence coincides with the region with a significant reduction in precipitation (Figure 2.9c).

Changes in Div200 along the equatorward margin of the SACZ suggest a poleward shift in the upper-level convergence-divergence boundary, evident in the DJF Div200 averaged across the oceanic portion of the SACZ, along the cross-section in Figure 2.1b (also cross-section "B" in Figure 2.9a). Until 2004, the transition from convergence to divergence was located near 19°S (Figure 2.9d). After 2005, the convergence-divergence boundary shifted southwestward, accompanying changes in precipitation. The DJF average over each of the periods manifests this shift in both precipitation and Div200 between 24°S

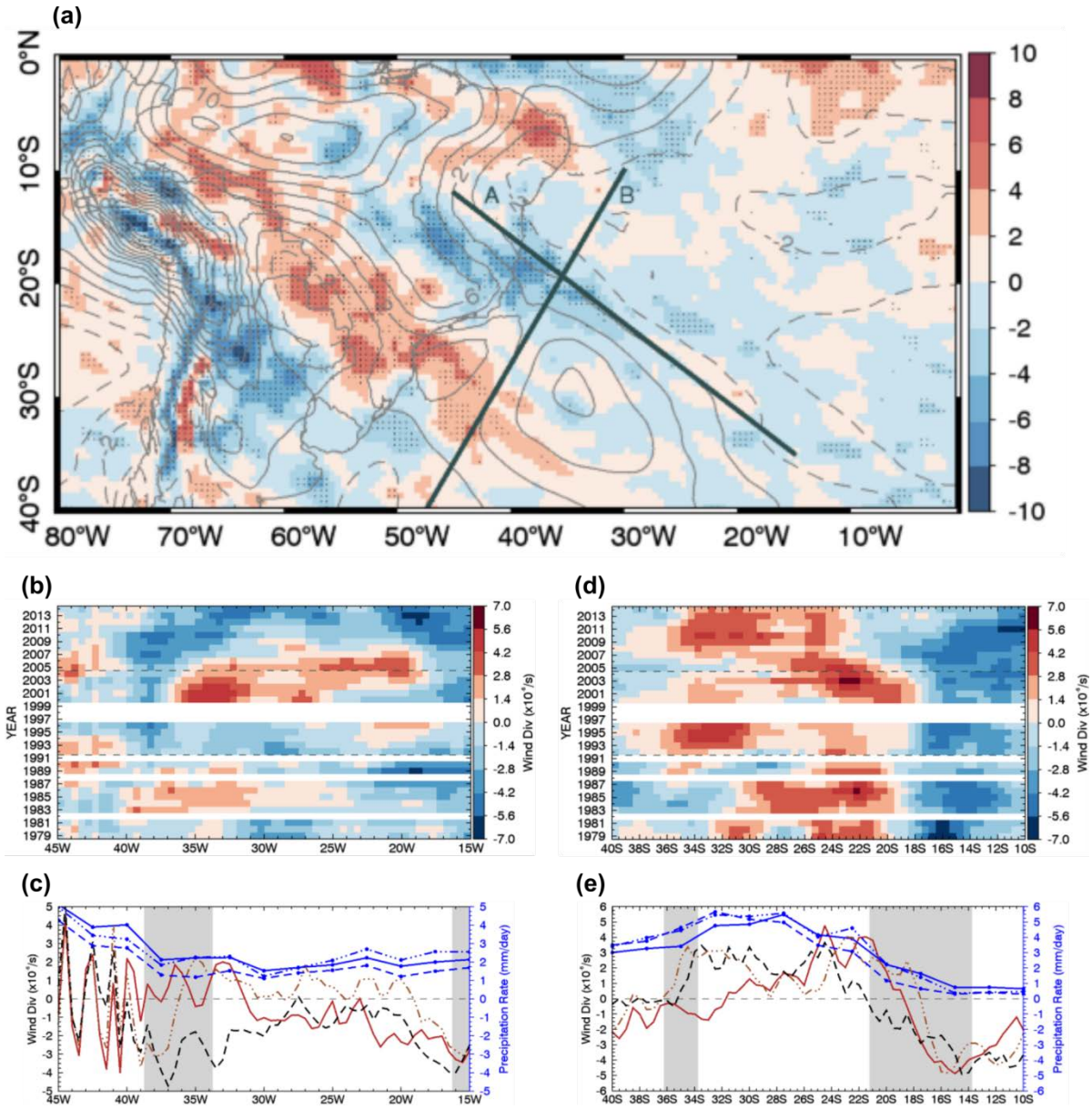

Figure 2.9 — Div200 (in x10^6/s): (a) As in Figure 2.7b (contours each 1x10^6/s with negative values dashed). Bold gray lines: location of the cross-sections along the equatorward margin of the SACZ ("A") and across the oceanic SACZ ("B"). (b-e) As in Figures 2.8b and c, along the cross-sections in (a): (b-c) averages for the cross-section along the equatorward margin of the SACZ ("A"); and (d-e) averages for the cross-section across the oceanic SACZ ("B")

and 18°S (Figure 2.9e). Over the poleward margin of the SACZ (south of ~32°S along the "B" cross-section), the upper-level divergence reversed from convergence to divergence in the beginning of the 1990s (Figure 2.9d and 2.9e), shifting the convergence-divergence boundary poleward. Consequently, precipitation increased along the poleward margin of the

SACZ (Figure 2.2 and 2.9e) following the pattern of increased upper-level divergence (Figure 2.9d and e). These results, particularly the changes observed along the equatorward margin of the SACZ, are strong evidence that the weakening of the winds in the lower troposphere over Eastern Brazil and adjacent ocean has reduced the dynamic support for convection in this region, decreasing precipitation and shifting convergence southward.

The weakening in the meridional component of the wind along the equatorward margin of the SACZ yields a more zonal orientation of the winds (Figure 2.8a). According to Lintner and Neelin (2010), a more zonal inflow into the continent could reduce precipitation due to advection of relatively low moist static energy (MSE) air from the tropical South Atlantic. The results presented here partially agree with this hypothesis, with more zonally distributed winds collocated with decreasing precipitation along the northern margin of the SACZ. However, our results also indicate an overall weakening of wind speed, which, according to the simple moisture budget prototype discussed in Lintner and Neelin (2010), should favor more precipitation because of decreased ventilation of the margin by low MSE air.

For further insight, we examined changes in the mean specific humidity between 1979-91 and 2005-14 periods for an atmospheric column along the convective margin (Figure 2.10). As noted earlier, the profile of changes in specific humidity in the lower troposphere is not uniform (compare Q850, Figure 2.5a, and Q700, Figure 2.5b). Considering the cross-section along the equatorward margin of the SACZ ("A" in Figure 2.5a), precipitation has decreased during the last period (2005-14) compared to the first period (1979-91) along the entire margin (Figure 2.10, bottom), despite the increase in moisture at 850hPa (Figure 2.10, top). In contrast, specific humidity at 700hPa has decreased along the same cross-section, especially between 43°W and 35°W (Figure 2.10, top), or coincident with the region of

largest precipitation decrease (Figure 2.10, bottom, and Figure 2.2).

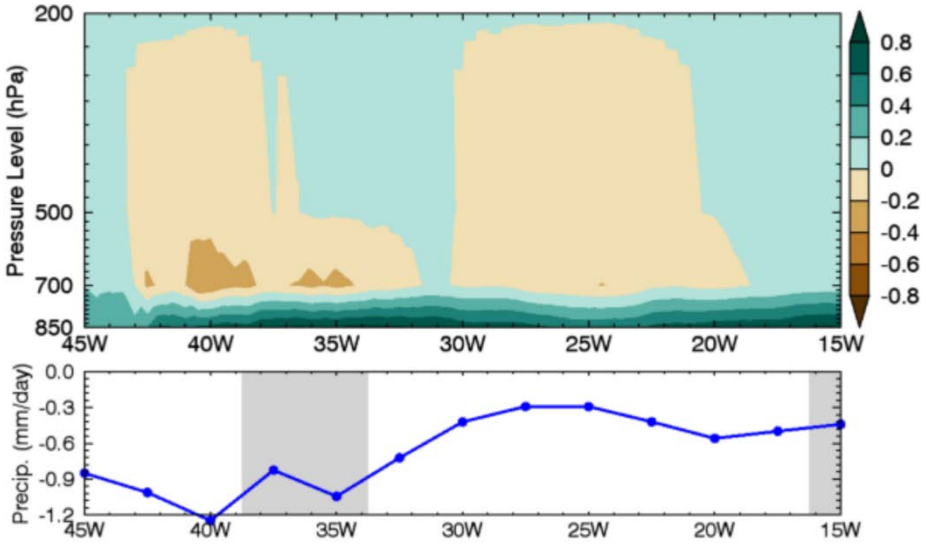

Figure 2.10 — Difference in DJF averages between first (1979-91) and last (2005-14) periods for all grid points along the equatorward margin of the SACZ (cross-section "A" in Figure 2.5). Top: vertical profile of specific humidity (in g/kg), with positive (negative) differences in green (brown). Bottom: Precipitation (in mm/day), with circles marking the center of each grid point and shaded areas where the difference is statistically significant ($p<0.05$)

To better characterize the relationships between ventilation at 700hPa and the observed precipitation changes, we estimated changes in the average saturation deficit ($Q700_d = Q700_{sat} - Q700$) from the first (1979-91) to the last period (2005-14; Figure 2.11). Large (small) values of $Q700_d$ are related to a relatively dry (humid) atmosphere. Therefore, positive (negative) differences between the two periods indicate that the atmosphere is moving away from (closer to) saturation.

Between 1979-91 and 2005-14, DJF average $Q700_d$ decreased over the southern Amazon and along the poleward margin of the continental SACZ and increased over the equatorward margin of the SACZ and over the tropical South Atlantic (Figure 2.11a). Drying at this level is stronger over the ocean, with larger $Q700_d$ during the last period (2005-14) along the entire cross-section at the poleward margin of the SACZ (Figure 2.11c).

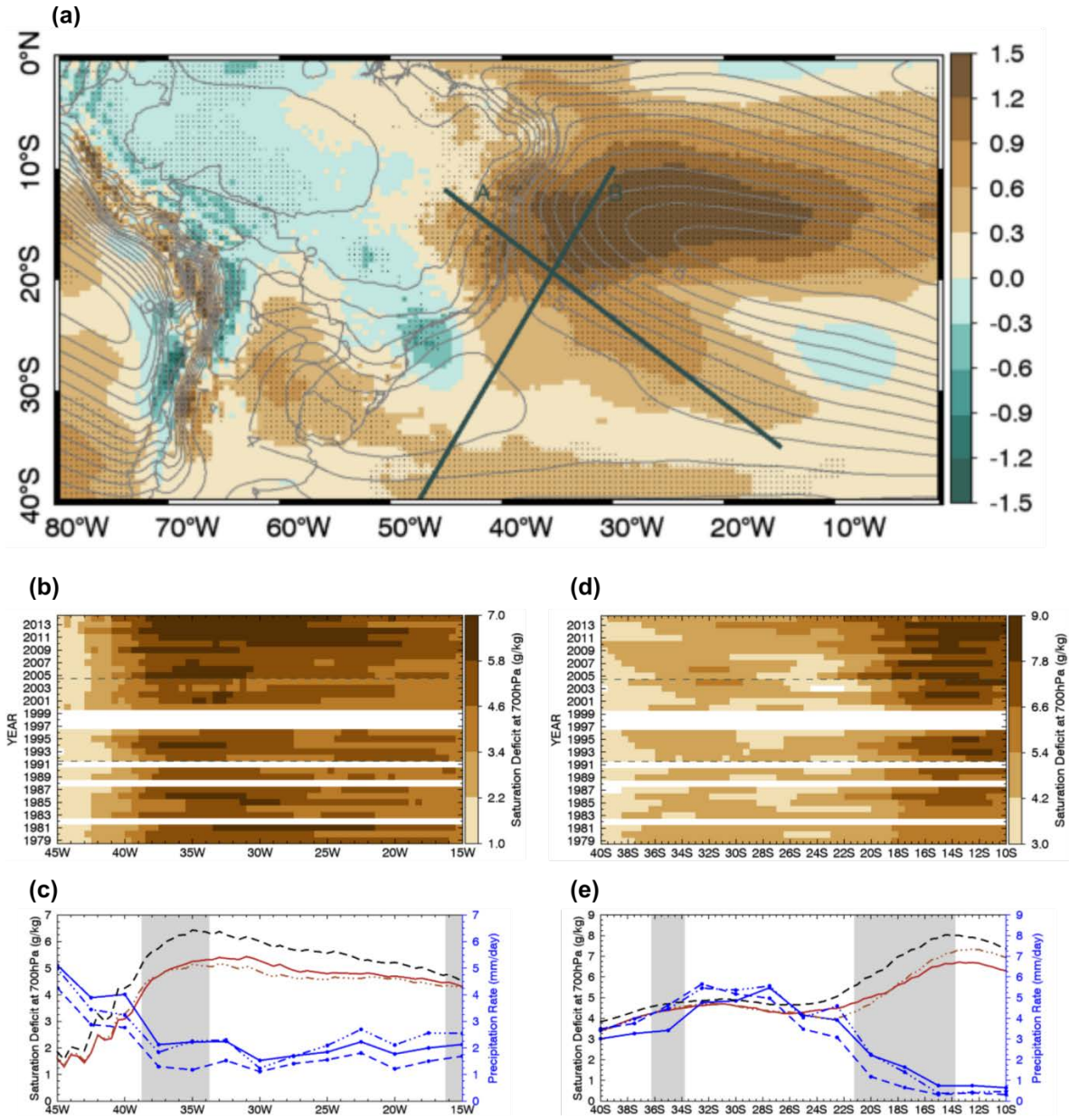

Figure 2.11 — Q700d (in g/kg): (a) Difference in DJF average between first (1979-91) and last (2005-14) periods (shades), with positive (negative) differences brown (green), significant differences ($p<0.05$) stippled, and contours representing the DJF climatology (1979-2014; contours each 1g/kg). Bold gray lines: location of the cross-sections along the equatorward margin of the SACZ ("A") and across the oceanic SACZ ("B"). (b-e) As in Figure 2.8b and c, along the cross-sections in (a): (b-c) averages for the cross-section along the equatorward margin of the SACZ ("A"); and (d-e) averages for the cross-section across the oceanic SACZ ("B")

The reduction in precipitation during the last period (2005-14) follows the increase in $Q700_d$, with larger changes between 39°W and 34°W (Figure 2.11c). Similar behavior is

observed on the equatorward side of the cross-section through the SACZ, where larger values of $Q700_d$ are collocated with a more pronounced reduction in precipitation (north of 22°S, Figure 2.11e). The Hovmöller diagrams along both cross-sections (Figure 2.11b and d) indicate that the drying along the equatorward margin of the SACZ is stronger after 2005 (Figure 2.11b), and it has been occurring since the beginning of the 1990s over tropical South Atlantic (north of 18°S, Figure 2.11d). However, on the poleward margin of the SACZ, represented by the poleward side of the cross-section across the oceanic SACZ (south of 28°S), precipitation has increased since 1992 but $Q700_d$ has not changed (Figure 2.11d and 2.11e). Similar analysis at 850hPa indicates moistening at this level, as represented by reduced $Q850_d$ along the oceanic portion of the convective margin (east of 39°W; Figure 2.12a) and across the oceanic SACZ (Figure 2.12b), both stronger after 2005.

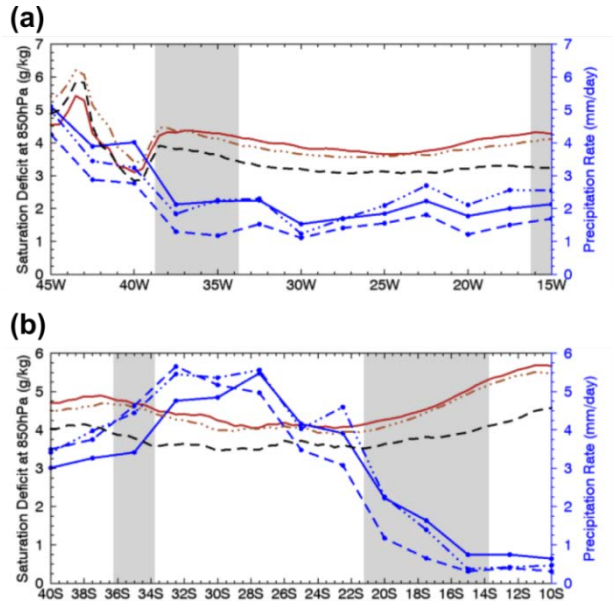

Figure 2.12 — DJF average for Q850d (in g/kg), as in Figure 2.8c, along the cross-sections in Figure 2.4a: (a) averages for the cross-section along the equatorward margin of the SACZ ("A"); and (b) averages for the cross-section across the oceanic SACZ ("B")

Hence, the reduction in precipitation over Eastern Brazil and adjacent Atlantic Ocean is

associated with weaker northerly winds, which reduce convergence and ascent over the region. The drying observed at 700hPa further contributes to reducing precipitation through the advection of relatively drier air toward the convective margin, which weakens or even inhibits convective activity due to increased stability.

2.6. Conclusions

During austral summer (DJF), intense precipitation in Eastern Brazil is modulated by the SAMS and by the SACZ. In prior work, Zilli et al. (2017) identified a trend toward increased average precipitation and intensity of extreme events over the southern portion of SE Brazil, while further north extreme events have intensified over time but the number of rainy days has decreased. This spatial variability in the low-frequency precipitation behavior suggests changes in the SACZ's positioning and intensity. To interpret these changes and identify underlying dynamic and thermodynamic mechanisms, we have examined here decadal changes in the mean state of the atmosphere and ocean, along with changes in precipitation at the margins of the SACZ.

By comparing GPCP average daily precipitation during DJF for the periods of 1979-1991 and 2005-2014 (excluding strong ENSO years) we identified a reduction in average daily precipitation along the equatorward margin of the SACZ, especially after 2007. Along the poleward margin, the difference in the average precipitation has increased since the earlier period. These results provide evidence of a recent poleward shift of the SACZ that partially explains the increase in average precipitation observed over the southern part of SE Brazil (Zilli et al. 2017). Over Eastern Brazil, the reduction in precipitation identified here could reflect the decreased number of rainy days described by Zilli et al. (2017).

Comparison of DJF averages of circulation and thermodynamic variables for the

periods of 1979-1991 and 2005-2014 reveals regional changes occurring over SA and adjacent South Atlantic Ocean that may have influenced the position and strength of the SACZ. The average circulation features associated with the SACZ, as well as the changes observed in this study, are schematically represented in Figure 2.13 (left and right, respectively). The spatial pattern of warming over the tropics has modified land-ocean temperature contrasts and sea level pressure gradient, the main drivers of the monsoonal circulation (Zhou and Lau 1998; Rodwell and Hoskins 2001). Consequently, winds around the SASH are decelerating, which implies cyclonic wind anomalies over tropical South Atlantic and weakening of the northerly winds over Eastern Brazil and adjacent ocean (represented in magenta in Figure 2.13). According to Kodama (1992, 1993), the presence of poleward flows on the west flank of a subtropical high is one of the necessary conditions for the establishment of convergence zones in the subtropics. This flow is responsible for advecting moisture and heat from lower latitudes into the convergence zone, increasing instability and convection. The observed weakening of the poleward flow over Eastern Brazil and adjacent Atlantic Ocean identified in this study is associated with reduced low-level convergence and ascending motion, consequently decreasing upper-level divergence along the SACZ convective margin. On the other hand, weakening of the Chaco Low and strengthening of cyclonic flow over Southeastern SA create favorable conditions for the enhancement of precipitation in the poleward margin of the SACZ. Together, these changes imply reduced (enhanced) dynamic support necessary for convection and precipitation along the equatorward (poleward) margin of the SACZ resulting in favorable conditions for the poleward shift of the convective zone.

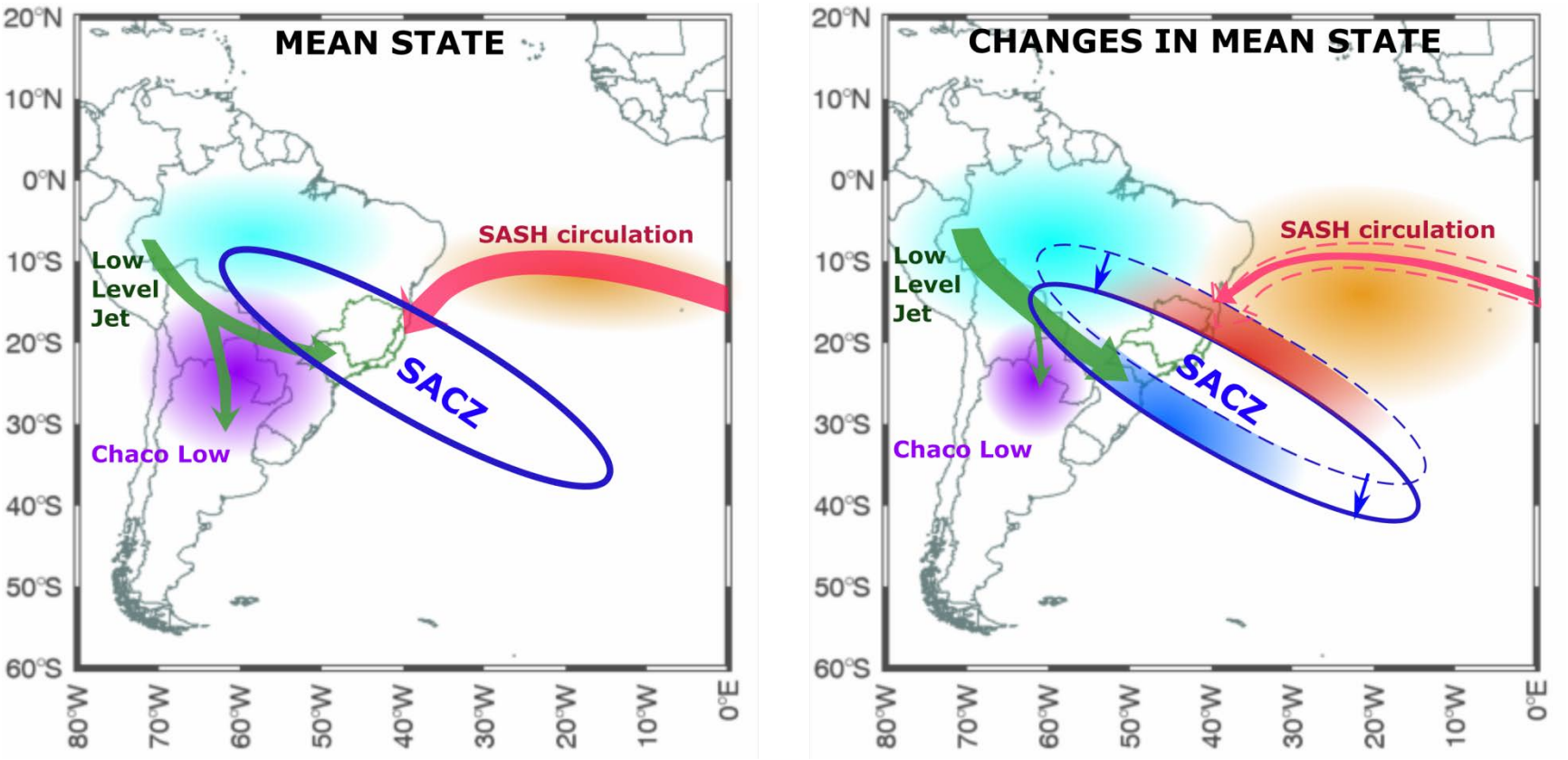

Figure 2.13 — Schematic main features related to the SACZ (left) and changes observed during the last period (2005-14, right). Changes in the thickness of the arrows represent relative intensity. Left: climatological position of the SACZ (blue) and poleward flow at the western flank of the SASH (magenta). Other features related to the convergence and precipitation at the SACZ: subsidence over tropical South Atlantic (brown) and the Chaco Low (purple), associated with the LLJ (green), which advects moisture from the Amazon (cyan). Right: changes in mean state of the atmosphere resulting in a poleward shift of the SACZ; long-dashed line represents the climatological position of the SACZ (blue) and of the flow around the SASH (magenta). Weakening of the circulation around the SASH (magenta) and a reduction of the specific humidity of tropical South Atlantic (brown) contribute to the poleward shift in the SACZ (blue) and the reduction of precipitation along its equatorward margin (red). Weakening of the Chaco low (purple), changes in the LLJ (green) and respective changes in precipitation in the poleward margin of the SACZ (blue)

Changes in specific humidity over Eastern Brazil and adjacent ocean are further consistent with a reduction in the average precipitation there. Even though the atmosphere has become more humid at 850hPa, it has dried at 700ha and 500hPa (brown area in Figure 2.13). The reduction in specific humidity at 700hPa and the increase in the saturation deficit could be indicative of an increase in subsidence along the northern flank of the SASH. As shown by Lintner and Neelin (2010), the flow into the equatorward margin of the SACZ originates mainly from the tropical South Atlantic, a region of relatively high stability. We speculate that drying of the 700hPa layer, which is more pronounced over the source region of flow toward the SACZ, reduces moisture transport into the convective margin, increasing the local saturation deficit and contributing to the reduction in precipitation. Of course, the presence of a drier layer atop of a moist layer may increase convective instability. Therefore, whenever atmospheric conditions are strong enough to force ascending motion, the presence of a dry layer at about 700hPa could increase convective instability, supporting the occurrence of deep convection and extreme precipitation. Indeed, this may account for the increasing intensity of extreme events observed in Zilli et al. (2017). A more detailed investigation of the air parcels trajectory toward the SACZ and changes in local thermodynamics is necessary to assess the role of drying at 700hPa.

Overall, the results presented here provide evidence that precipitation changes along the equatorward margin of the SACZ (including eastern Brazil) are likely related to the poleward shift of the convergence zone, caused primarily by the weakening of the northerly winds along the western flank of the SASH, drying of low-to-mid troposphere (700hPa) and enhanced low MSE ventilation along the equatorward margin of the SACZ (Figure 2.13, right). Based on these results, we suggest that changes in the SACZ could be related to the

combination of the increase in diabatic heating over the continent and the positioning and strength of the SASH. However, a more detailed analysis of changes in heating sources and the impacts of the changes in the regional circulation are necessary to test these hypotheses. Although previous studies have indicated that variations in the dipolar structure of the SACZ can be modulated by coupled modes on decadal to multi-decadal time-scales (e.g., Grimm and Saboia 2015) our study suggests that these relationships may not be consistent throughout time. Nonetheless, the relatively short length of records (36 years) restricts the ability of this study to investigate the influence of low-frequency climatic modes, such as the PDO and AMO, or attribute these observed changes to anthropogenic forcing. Also relevant, circulation and precipitation changes diagnosed here are consistent with coupled climate model projections under scenarios of climate change (e.g., Seth et al. 2010; Carvalho and Jones 2013; Li et al. 2013). Therefore, these changes, whether attributed to anthropogenic forcing, modulated by coupled climate modes or resulting from a combination of both, need to be further investigated to increase preparedness and assist with decision-making.

2.7. Acknowledgements

GPCP Precipitation data was provided by the NOAA/OAR/ESRL PSD, Boulder, Colorado, USA, from their Web site at http://www.esrl.noaa.gov/psd/. NOAA High Resolution SST data was provided by the NOAA/OAR/ESRL PSD, Boulder, Colorado, USA, from their Web site at http://www.esrl.noaa.gov/psd/. M. Zilli acknowledges the Brazilian National Council for Scientific and Technological Development (CNPq) for the financial support through the Science without Borders Program (202691/2011-0). L. Carvalho acknowledges the São Paulo Research Foundation (FAPESP) Proc. 2008/58101-9. L. Carvalho and B. Lintner acknowledge the support of NSF-AGS-1505198.

2.8. References

Barros V, Gonzalez M, Liebmann B, Camilloni I (2000) Influence of the South Atlantic Convergence Zone and South Atlantic sea surface temperature on interannual summer rainfall variability in Southeastern South America. Theor Appl Climatol 67:123-133

Bolton D (1980) Computation of equivalent potential temperature. Mon Weather Rev, 108:1046-1053

Bombardi R, Carvalho LMV, Jones C (2013) Precipitation over eastern South America and the South Atlantic Sea surface temperature during neutral ENSO periods. Clim Dyn 42:1553-1568. doi: 10.1007/s00382-013-1832-7

Carvalho LMV, Jones C (2013) CMIP5 simulations of low-level tropospheric temperature and moisture over tropical Americas. J Clim 26:6257-6286. doi: 10.1175/JCLI-D-12-00532.1

Carvalho LMV, Jones C, Liebmann B (2002) Extreme precipitation events in Southeastern South America and large-scale convective patterns in the South Atlantic Convergence Zone. J Clim 15:2377-2394

Carvalho LMV, Jones C, Liebmann B (2004) The South Atlantic Convergence Zone: intensity, form, persistence, and relationships with intraseasonal to interannual activity and extreme rainfall. J Clim 17:88-108

Carvalho LMV, Silva AE, Jones C, Liebmann B, Silva Dias PL, Rocha HR (2011) Moisture transport and intraseasonal variability in the South America Monsoon System. Clim Dyn 36:1865-1880. doi: 10.1007/s00382-010-0806-2

Cherchi A, Alessandri A, Masina S, Navarra A (2011) Effects of increased CO_2 level on monsoons. Clim Dyn 37:83-101. doi: 10.1007/s00382-010-0801-7

Coelho CAS, Cardoso DHF, Firpo MAF (2016a): Precipitation diagnostics of an exceptionally dry event in São Paulo, Brazil. Theor Appl Climatol 125:769-784. doi: 10.1007/s00704-015-1540-9

Coelho CAS, Oliveira CP, Ambrizzi T, Reboita MS, Carpenedo CB, Campos JLPS, Tomaziello ACN, Pampuch LA, Custódio MS, Dutra LMM, Rocha RP, Rehbein A (2016b) The 2014 Southeast Brazil austral summer drought: regional scale mechanisms and teleconnections. Clim Dyn 46:3737-3752. doi: 10.1007/s00382-015-2800-1

Cunningham CAC, Cavalcanti IFA (2006) Intraseasonal modes of variability affecting the South Atlantic Convergence Zone. Int J Climatol 26:1165-1180. doi: 10.1002/joc.1309

de Barros Soares D, Lee H, Loikith PC, Barkhordarian A, Mechoso CR (2017) Can significant trends be detected in surface air temperature and precipitation over South America in recent decades? Int J Climatol 37:1483–1493. doi:10.1002/joc.4792

Drumond ARM, Ambrizzi T (2006) Inter-ENSO variability and its influence over the South American Monsoon System. Adv Geosci 6:167-171.

Emanuel KA (1994) Atmospheric Convection. Oxford University Press, New York.

Enfield DB, Mestas-Nunez AM, Trimble PJ (2001) The Atlantic Multidecadal Oscillation and its relationship to rainfall and river flows in the continental U.S. Geophys Res Lett 28:2077-2080

Grimm AM (2003) The El Niño impact on the summer monsoon in Brazil: regional processes versus remote influences. J Clim 16: 263-280

Grimm AM, Pal JS, Giorgi F (2007) Connection between spring conditions and peak summer monsoon rainfall in South America: role of soil moisture, surface temperature and topography in eastern Brazil. J Clim 20:5929-5945. doi: 10.1175/2007JCLI1684.1

Grimm AM, Saboia J (2015) Interdecadal variability of the South American precipitation in the monsoon season. J Clim 28:755-775. doi: 10.1175/JCLI-D-14-00046.1

Grimm AM, Zilli MT (2009) Interannual variability and seasonal evolution of summer monsoon rainfall in South America. J Clim 22:2257-2275. doi: 10.1175/2008JCLI2345.1

Held IM, Soden BJ (2006) Robust response of the hydrological cycle to global warming. J Clim 19:5686-5699. doi: 10.1175/JCLI3990.1

Henley BJ, Gergis J, Karoly DJ, Power SB, Kennedy J, Folland CK (2015) A Tripole Index for the Interdecadal Pacific Oscillation. Clim Dyn 45:3077-3090. doi:10.1007/s00382-015-2525-1

Hsu PC, Li T, Murakami H, Kitoh A (2013) Future change of the global monsoon revealed from 19 CMIP5 models. J Geophys Res - Atmos 118:1247-1260. doi: 10.1002/jgrd.50145

Hsu PC, Li T, Wang B (2011) Trends in global monsoon area and precipitation over the past 30 years. Geophys Res Lett 38:L08701. doi: 10.1029/2011GL046893

Huffman GJ, Adler RF, Bolvin DT, Gu G (2009) Improving the global precipitation record: GPCP Version 2.1. Geophys Res Lett 36:L17808. doi:10.1029/2009GL040000.

Jones C, Carvalho LMV (2013) Climate change in the South American Monsoon System: present climate and CMIP5 projections. J Clim 26:6660-6678. doi: 10.1175/JCLI-D-12-00412.1

Kayano MT, Andreoli RV (2007) Relations of South American summer rainfall interannual variations with the Pacific Decadal Oscillation. Int J Climatol 27:531-540. doi: 10.1002/joc.1417

Kitoh A, Endo H, Kumar K, Cavalcanti I, Goswami P, Zhou T (2013) Monsoons in a changing world: a regional perspective in a global context. J Geophys Res - Atmos 118:3053-3065. doi: 10.1002/jgrd.50258

Kodama YM (1992) Large-scale common features of subtropical precipitation zones (the Baiu Frontal Zone, the SPCZ and the SACZ) Part I: characteristics of subtropical frontal zones. J Meteorol Soc Jpn 70:813-835

Kodama YM (1993) Large-scale common features of subtropical convergence zones (the Baiu Frontal Zone, the SPCZ and the SACZ). Part II: conditions of the circulations for generating the STCZs. J Meteorol Soc Jpn 75:581-610

Krishnamurthy V, Misra V (2010) Observed ENSO teleconnection with the South American Monsoon System. Atmos Sci Lett 11:7-12. doi: 10.1002/asl.245

Krishnamurthy V, Misra V (2011) Daily atmospheric variability in the South American Monsoon System. Clim Dyn 37:803-819. doi: 10.1007/s00382-010-0881-4

Lenters JD, Cook DR (1997) On the origin of the Bolivian High and related circulation features of the South American climate. J Atmos Sci 54:656-677

Li W, Li L, Ting M, Deng Y, Kushnir Y, Liu Y, Lu Y, Wang C, Zhang P (2013) Intensification of the Southern Hemisphere summertime subtropical anticyclones in a warming climate. Geophys Res Lett 40:5959-5964. doi: 10.1002/2013GL058124

Liebmann B, Jones C, Carvalho LMV (2001) Interannual variability of daily extreme precipitation events in the state of São Paulo, Brazil. J Clim 14:208-218

Liebmann B, Kiladis GN, Vera CS, Saulo C, Carvalho LMV (2004) Subseasonal variations of rainfall in South America in the vicinity of the low-level jet east of the Andes and comparison to those in the South Atlantic Convergence Zone. J Clim 17:3829-3842

Lintner BR, Neelin JD (2010) Tropical South America-Atlantic sector convective margins and their relationship to low-level inflow. J Clim 23:2671-2685. doi: 10.1175/2009JCLI3301.1

Liu YM, Wu GX, Ren R (2004) Relationship between the subtropical anticyclone and diabatic heating. J Clim 17:682–698

Ma HY, Ji X, Neelin J, Mechoso C (2011) Mechanisms for precipitation variability of the eastern Brazil/SACZ convective margin. J Clim 24:3445-3456. doi: 10.1175/2011JCLI4070.1

Mantua NJ, Hare SR, Zhang Y, Wallace JM, Francis RC (1997) A Pacific interdecadal climate oscillation with impacts on salmon production. Bull Am Meteorol Soc 78:1069-1079

Marengo JA, Liebmann B, Grimm AM, Misra V, Silva Dias PL, Cavalcanti I, Carvalho LM, Berbery E, Ambrizzi, T, Vera C, Saulo A, Nogués-Paegle J, Zipser E, Seth A, Alves L (2012) Review: recent developments on the South American Monsoon System. Int J Climatol 32:1-21. doi: 10.1002/joc.2254

McGregor GR, Nieuwolt S (1998) Tropical Climatology: An Introduction to the Climates of

the Low Latitudes, 2nd ed. Wiley, New York, NY.

Mo K, Nogués-Paegle J (2001) The Pacific-South American modes and their downstream effects. Int J Climatol 21:1211-1229. doi: 10.1002/joc.685

Muza MN, Carvalho LMV, Jones C, Liebmann B (2009) Intraseasonal and interannual variability of extreme dry and wet events over Southeastern South America and the Subtropical Atlantic during austral summer. J Clim 22:1682-1699. doi: 10.1175/2008JCLI2257.1

Nobre CA, Marengo JA, Seluchi ME, Cuartas LA, Alves LM (2016) Some characteristics and impacts of the drought and water crisis in Southeastern Brazil during 2014 and 2015. J Water Resour Prot 8:252-262. doi: 10.4236/jwarp.2016.82022

Nogués-Paegle J, Byerle LA, Mo KC (2000) Intraseasonal modulation of South American summer precipitation. Mon Weather Rev 128:837-850

Otto FEL, Coelho CAS, King A, Coughlan de Perez E, Wada Y, van Oldenborgh GJ, Haarsma R, Haustein K, Uhe P, van Aalst M, Aravequia JA, Almeida W, Cullen H (2015) Factors other than climate change, main drivers of 2014/15 water shortage in Southeast Brazil. Bull Am Meteorol Soc 96:S35-S40. doi:10.1175/BAMS-EEE_2014_ch8.1

Reynolds RW, Smith TM, Liu C, Chelton DB, Casey KS, Schlax MG (2007) Daily high-resolution-blended analyses for sea surface temperature. J Clim 20:5473-5496. doi: 10.1175/2007JCLI1824.1

Rodwell MJ, Hoskins BJ (2001) Subtropical anticyclones and summer monsoons. J Clim 14:3192-3211

Saha S, Moorthi S, Pan HL, et al. (2010) The NCEP Climate Forecast System Reanalysis. Bull Am Meteorol Soc 91:1015-1057. doi: 10.1175/2010BAMS3001.1

Schneider T, O'Gorman PA, Levine XJ (2010) Water vapor and the dynamics of climate changes. Rev Geophys 48:RG3001. doi:10.1029/2009RG000302

Seidel DJ, Randel WJ (2007) Recent widening of the tropical belt: Evidence from tropopause observations. J Geophys Res 112:D20113. doi:10.1029/2007JD008861

Seth A, Rojas M, Rauscher SA (2010) CMIP3 project changes in the annual cycle of the South American Monsoon. Clim Change 98:331-357. doi: 10.1007/s10584-009-9736-6

Silva AE, Carvalho LMV (2007) Large-scale Index for South America Monsoon (LISAM). Atmos Sci Lett 8:51-57. doi: 10.1002/asl.150

Vera C, Higgins W, Amador J, Ambrizzi T, Garreaud R, Gochis D, Gutzler D, Letternmater D, Marengo JA, Mechoso CR, Nogués-Paegle J, Silva Dias PL, Zhang C (2006) Toward a unified view of the American Monsoon System. J Clim 19:4977-5000. doi: 10.1175/JCLI3896.1

Wang H, Fu R (2002) Cross-Equatorial Flow and Seasonal Cycle of Precipitation over South America. J Clim 15:1591-1608

Wilks DS. 2011. Statistical Methods in the Atmospheric Sciences, Vol. 100. Academic Press: San Diego, CA.

Wu GX, Liu Y, Zhu X, Li W, Ren R, Duan A, Liang X (2009) Multi-scale forcing and the formation of subtropical desert and monsoon. Ann Geophys 27:3631-3644. doi: 10.5194/angeo-27-3631-2009

Zhou J, Lau KM (1998) Does a monsoon climate exist over South America? J Clim 11:1020-1040

Zhou J, Lau KM (2001) Principal modes of interannual and decadal variability of summer rainfall over South America. Int J Climatol 21:1623-1644. doi: 10.1002/joc.700

Zilli MT, Carvalho LMV, Liebmann B, Silva Dias MA (2017) A comprehensive analysis of trends in extreme precipitation over southeastern coast of Brazil. Int J Climatol. 37:2269-2279. doi: 10.1002/joc.4840

Chapter 3: Detection and Attribution of Causes of the Poleward Shift of the South Atlantic Convergence Zone in CMIP-5 simulations

Marcia T Zilli[1], Leila M. V. Carvalho[1,2], Benjamin R. Lintner[3], Qinghua Ding[1,2]

[1] Department of Geography, University of California, Santa Barbara, CA, USA.

[2] Earth Research Institute, University of California, Santa Barbara, CA, USA

[3] Department of Environmental Sciences, Rutgers, The State University of New Jersey, NJ, USA

3.1. Abstract

Evidence of a poleward shift in the South Atlantic Convergence Zone (SACZ) has been identified in observational studies and historical and future scenarios of global climate models participating on the fifth phase of the Coupled Model Intercomparison Project (CMIP5), suggesting an increase (decrease) in the frequency of precipitation events over Southeastern South America (Eastern Brazil). The objective of this study is to evaluate the contribution of natural variability and anthropogenic-related forcings to precipitation trends over Eastern Brazil in the 20th century based on historical, natural, and pre-industrial simulations from CMIP5 models. Only CMIP5 models that accurately reproduced the observed precipitation climatology over the SACZ, as represented by the Global Precipitation Climatology Project Version 2.2 (GPCP), were considered. 4 of the 17 CMIP5 models considered in this study realistically simulate the precipitation rates over SACZ during summer (December to February) and only 3 of these models are able to correctly simulate the observed southwestward shift of the SACZ. Despite the large discrepancies in

the simulated precipitation trends, the similarity among the ensemble members provides compelling evidence of the poleward shift of the simulated SACZ. Over the northern (southern) margin of the SACZ, positive (negative) precipitation trends can be attributed to anthropogenic forcing, with the natural variability partially offsetting the simulated trends. Nevertheless, the large uncertainties on the simulated precipitation over the region suggest that the mechanisms related to the position and intensity of the SACZ events are not well captured by the CMIP5 models analyzed.

3.2. Introduction

Austral summer (DJF) precipitation over tropical South America (SA) is characterized by the South American Monsoon System (SAMS) and the South Atlantic Convergence Zone (SACZ; Zhou and Lau 1998; Barros et al. 2000; Zhou and Lau 2001; Carvalho et al. 2004, 2011; Vera et al. 2006a; Muza et al. 2009). The SACZ is a diagonal convergence zone extending from the Amazon toward the west South Atlantic Ocean and is responsible for advecting moisture to the subtropical SA (Kodama, 1992, 1993; Zhou and Lau 1998; Liebmann et al. 2001; Carvalho et al. 2002, 2004; Marengo et al. 2012). It is formed by flow converging from two different regions: low-level northerly inflow originating along the western periphery of the South Atlantic Subtropical High (SASH); and westerly flows along the convergence zone, increasing in intensity with height and forming part of the subtropical jet in upper levels (Kodama 1992, 1993).

The spatial variability of the SACZ is dominated by a dipole-like pattern of opposing precipitation anomalies over Eastern Brazil (EBr) and Southeastern South America (SESA), recurrent on timescales ranging from intraseasonal to decadal (Nogués-Paegle and Mo 1997; Zhou and Lau 1998; Nogués-Paegle et al. 2000; Carvalho et al. 2002, 2011; Grimm and Zilli

2009; Grimm and Saboia 2015). During the SACZ active phase, precipitation is enhanced (inhibited) over EBr (SESA); the opposite is observed during its inactive phase (Zhou and Lau 1998; Nogués-Paegle et al. 2000; Carvalho et al. 2002; Grimm and Zilli 2009). On intraseasonal time-scales, the SACZ circulation and convective activity are modulated by the Madden-Julian Oscillation (MJO) and the Pacific South America (PSA) mode (Mo and Nogués-Paegle 2001; Carvalho et al. 2004, 2011; Cunningham and Cavalcanti 2006). On decadal time-scales, the dipole is partially influenced by the Interdecadal Pacific Oscillation (IPO) and the Atlantic Multidecadal Oscillation (AMO; Grimm and Saboia 2015).

The increase in atmospheric temperature over the SA during the last decades of the 20^{th} century has been consistently shown by the global climate models (GCM) contributing to the fifth phase of the Coupled Model Intercomparison Project (CMIP5). Trends are larger over central Brazil (Carvalho and Jones 2013; de Barros Soares 2017) and cannot be explained by natural variability alone, suggesting that the contribution of anthropogenic-related forcings to the warming is already detectable (de Barros Soares 2017). As expected for a warmer troposphere, the water vapor content is also increasing, particularly over the regions with larger warming (Carvalho and Jones 2013) with implications for duration and amplitude of the SAMS (Jones and Carvalho 2013). Over the Amazon and central Brazil, the CMIP5 models capture well the total rainfall during the rainy season (December to May), even though there is an underestimation (overestimation) of large-scale (convective) rainfall (Yin et al. 2013).

Evidence of changes in the SACZ-related dipole have been identified in observational studies (Zilli et al. 2017a, b, in review) and historical and future scenarios of CMIP3 and CMIP5 models simulations (Seth et al 2010; Jones and Carvalho 2013; Diaz and Vera

2017), suggesting an increase (decrease) in the frequency of precipitation events related to the dipole over SESA (EBr) (Junquas et al. 2012; Diaz and Vera 2017). Using a Regional Climate Model (RCM) forced by changes in sea surface temperature (SST) Junquas et al. (2013) demonstrated that the positive (negative) precipitation trends over SESA (EBr) in future scenarios were caused by enhanced (weakened) convergence over the region as part of the propagation of a Rossby wave train formed by zonally asymmetric warming over the Indian and equatorial western Pacific oceans.

The increase in total precipitation over the SESA has been identified in observational studies and is mostly related to an increase in the number of intense events and a reduction in the number of consecutive dry days over the region (Haylock et al. 2006; Barros et al. 2008; Skansi et al. 2013). These trends, as well as the precipitation variability over the region, are correctly reproduced by historical scenarios of coupled GCMs and RCM models (Vera et al. 2006b; Chou et al. 2014; Diaz and Vera 2017) and have been attributed to anthropogenic-related increase in the concentration of well-mixed green-house gases (Zhang et al. 2016). Future scenarios of climate change indicate that the positive precipitation trends over SESA will persist in the 21st century (Junquas et al. 2012, 2013; Chou et al 2014a; Sanchez et al. 2015) in response to tropical warming.

In addition to the positive precipitation trends over the SESA, previous studies also detected negative trends in precipitation over EBr. However, there are significant discrepancies among the CMIP5 projections over the EBr, typically because the models do not accurately reproduce the precipitation variability related to the SACZ position, intensity and seasonal variability (Carvalho and Jones 2013; Diaz and Vera 2017; de Barros Soares et al. 2017). Furthermore, there are large uncertainties regarding the magnitude and the signal

of the observed precipitation trends over EBr. Zilli et al. (2017a) detected changes in the observed precipitation distribution over Southeastern Brazil, with fewer rainy days and more intense events observed in recent decades along the northern margin of the SACZ during the rainy season (October to March). Zilli et al. (2017b, in review) related the reduction in precipitation rate over EBr to the weakening of the northerly winds and decrease in the available moisture at the mid-to-lower troposphere (700hPa) co-located with the climatological position of the South Atlantic anti-cyclone. These changes in circulation and low-level moisture have reduced convergence and moisture advected to EBr. Using an Atmospheric Global Climate Model (AGCM), Talento and Barreiro (2017) found that the negative precipitation trends and related circulation changes over tropical Brazil were a response to extratropical warming over the northern hemisphere, similar to the atmospheric warming observed over the last decades. The hemispheric warming is associated with changes in the Hadley circulation, resulting in weakened trade winds along the equator and enhanced SASH, increasing subsidence over the northern margin of the SACZ. Together with the well-documented positive precipitation trends over SESA, these results suggest a poleward shift in the SACZ position.

The objective of this study is to evaluate the contribution of natural variability and anthropogenic-related forcings to precipitation trends over EBr in the 20th century based on CMIP5 models. The attribution analysis is conducted using a subset of CMIP5 models that correctly reproduced the observed precipitation variability and trends over SACZ. Attribution studies based on climate change scenarios have some challenges due to the large uncertainties related to the climate system internal variability and to the model's representation of the climate system. We account for these uncertainties by evaluating

multiple CMIP5 ensemble members and by focusing on those models that best represent the observed variability. The discussion is organized as follows: dataset and methodology are described in Section 3.3. The observed and simulated average DJF precipitation over the SACZ are presented in Section 3.4. Section 3.5 discusses the trends in recent decades, emphasizing the role of natural and internal variability on the simulated trends, while in Section 3.6 we summarize the results and present conclusions.

3.3. Data and Methods

3.3.1. Data

This study compares precipitation trends reproduced by CMIP5 climate models with those identified in an observed dataset. The observational dataset is from the Global Precipitation Climatology Project Version 2.2 (GPCP; Huffman et al. 2009), a monthly dataset with 2.5° lon/lat horizontal resolution and spanning 1979 to 2015. GPCP merges directly observed precipitation from rain gauge data with indirect satellite measurements (Huffman et al. 2009), accurately reproducing the spatial and temporal precipitation variability related to the SAMS (Carvalho et al. 2012).

The simulated precipitation is from various GCMs participating in the fifth phase of the Coupled Model Intercomparison Project (CMIP5; Taylor et al. 2012). These multi-model simulations are available to the scientific community by the Program Climate Model Diagnosis and Intercomparison (PCMDI). For the first part of the analysis, this study examines the first ensemble member (r1i1p1) of the historical scenario simulation from 17 models with daily data at various spatial resolutions (Table 3.1). The historical scenario includes all forcings, both natural (incoming solar radiation and stratospheric aerosol related to volcanic activity) and anthropogenic (changes in greenhouse gases concentration, dust,

aerosol, land use and land cover change), reproducing the current climate.

Table 3.1 — CMIP5 models, institutes, resolution, and references

MODEL	INSTITUTE AND COUNTRY	RESOLUTION	REFERENCE
ACCESS1-3	Centre for Australian Weather and Climate Research (CAWCR), Australia	1.875°x1.25° (N96)	Bi et al. (2013)
CanESM2	Canadian Centre for Climate Modelling and Analysis (CCCMA), Canada	2.8°x2.8° (T63L35)	Arora et al. (2011)
CCSM4	National Center for Atmospheric Research (NCAR), USA	1.25°x0.9° (F09G16)	Gent et al. (2011)
CNRM-CM5	Centre National de Recherches Météorologiques (CNRM) and Centre Européen de Recherche et de Formation Avancée) (CERFACS), France	1.4°x1.4° (TL127L31)	Voldoire et al. (2013)
CSIRO_Mk3.6.0	Centre for Australian Weather and Climate Research (CSIRO) and Queensland Climate Change Centre of Excellence, Australia	1.875°x1.875° (T63)	Jeffrey et al. (2013)
GFDL-ESM2M	Geophysical Fluid Dynamics Laboratory, National Oceanic and Atmospheric Administration (GFDL/NOAA), USA	2.5°x2° (M45L24)	Dunne et al. (2012)
GISS-E2H	Goddard Institute for Space Studies, National Aeronautics and Space Administration (GISS/NASA), USA	2.5°x2.0°	Schmidt et al. (2014)
HadCM3	Met Office Hadley Centre, UK	3.75°x2.5° (N48L19)	Collins et al. (2001)
HadGEM2-CC	Met Office Hadley Centre, UK	1.875°x1.25° (N96L60)	Collins et al. (2011) Martin et al. (2011)
HadGEM2-ES	Met Office Hadley Centre, UK	1.875°x1.25° (N96L38)	Collins et al. (2011) Jones et al. (2011)
INMCM4	Institute for Numerical Mathematics (INM), Russia	2.0°x1.5°	Volodin et al. (2010)
IPSL-CM5A-LR	Institut Pierre Simon Laplace (IPSL), France	3.75°x1.875°	Dufresne et al. (2013)
MIROC4h	Atmosphere and Ocean Research Institute (AORI) of the University of Tokyo, National Institute for Environmental Studies (NIES), and Japan Agency for Marine-Earth Science and Technology (JAMSTEC), Japan	0.5625°x0.5625° (T213L56)	Sakamoto et al. (2011)
MIROC-ESM	Atmosphere and Ocean Research Institute (The University of Tokyo), National Institute for Environmental Research, and Japan Agency for Marine-Earth Science and Technology, Japan	2.8125°x2.8125° (T42L80)	Watanabe et al. (2011)
MPI-ESM-LR	Max Planck Institute for Meteorology (MPI-M), Germany	1.875°x1.875° (T63L47)	Giorgetta et al. (2013)
MRI-CGCM3	Meteorological Research Institute, Japan	1.125°x1.125° (TL159L48)	Yukimoto et al. (2011)
NorESM1-M	Norwegian Climate Centre (NorClim), Norway	2.5°x1.875° (F19L26)	Bentsen et al. (2013)

In order to attribute statistically significant trends in summer precipitation over South America to natural variability or to anthropogenic forcing, we examine the historical,

natural, and pre-industrial scenarios of those CMIP5 models that best represent the summer average precipitation and standard deviation (Table 3.2). Therefore, we assume that trends detected in the historical scenario (HIST) result from the combination of natural forcings (incoming solar radiation and stratospheric aerosol related to volcanic activity), internal variability (e.g. ENSO, PDO, NAO, AMO), and anthropogenic forcings (emission of greenhouse gases, aerosol, dust, and land-use changes). In the natural scenario (NAT), the atmospheric composition is kept constant at pre-industrial levels and forcings are only due to incoming solar radiation and changes in stratospheric volcanic aerosol; thus trends in this scenario are related to natural variability. The difference between HIST and NAT scenarios can be considered as anthropogenic (ANTHROP). The pre-industrial scenario (PICONTROL) is the control experiment with all forcings kept constant at pre-industrial levels, including incoming solar radiation, and there are no volcanic eruptions. Thus, trends detected in this scenario are related to climatic internal variability and model's uncertainties. A more in-depth discussion of these scenarios can be found in Taylor et al. (2012). The list of models, specificities and details about the integration aspects of each model and scenario can be found in the references listed in Table 3.1.

For this attribution analysis, we consider all ensemble members available for each model and scenario (Table 3.2). For each model, experiments with the same member are initialized with pre-industrial conditions from the same parent experiment. For example: the r1i1p1 member for both the natural and historical experiments from HadGEM2-ES have initial conditions derived from the first day of the pre-industrial experiment, while the r2i1p1 member is initialized with conditions from the pre-industrial scenario at the year 50. The difference between trends in the HIST and NAT are only calculated when both

experiments have the same initial conditions.

Table 3.2 — Selected models, description of the forcings related to each scenario, the ensemble members, and the number of years available for each member and scenario

MODEL	SCENARIO	FORCINGS	MEMBERS	# YEARS
CCSM4	PICONTROL	Incoming solar radiation (SI), greenhouse gases (GHG), sea salt (SS) dust (Ds), direct effects of anthropogenic sulfate aerosol (SD), black carbon (BC), mineral dust (MD), organic carbon (OC), tropospheric and stratospheric ozone (OZ), and anthropogenic aerosol (AA) fixed at 1850 values.	r2p1i1	156
	HIST	Time varying Sl, GHG, volcanic aerosol (Vl), SS, Ds, SD, BC, MD, OC, Oz, AA, and land use change (LU).	r1i1p1, r2i1p1, r6i1p1	156 (1850-2005)
	NAT	Time varying Sl, Vl; GHG, LU, SS, Ds, SD, BC, MD, OC, Oz, and AA fixed or cycled over 1850 values.	r1i1p1, r2i1p1, r6i1p1	156 (1850-2005)
CanESM2	PICONTROL	GHG (CO_2, CH_4, N_2O, CFC11, and effective CFC12), SA, Oz, LU, Sl, Vl, BC and OC fixed at 1850 levels.	r1i1p1	1096
	HIST	Time varying GHG (CO_2, CH_4, N_2O, CFC11, and effective CFC12), SA, Oz, LU, Sl, Vl, BC and OC.	r1i1p1, r2i1p1, r3p1i1, r4i1p1, r5i1p1	156 (1850-2005)
	NAT	Time varying Sl and Vl; GHG (CO_2, CH_4, N_2O, CFC11, and effective CFC12), SA, Oz, LU, MD, BC and OC fixed at 1850 levels	r1i1p1, r2i1p1, r3p1i1, r4i1p1, r5i1p1	163 (1850-2012)
GFDL-ESM2M	PICONTROL	GHG (CO_2, CH_4, N_2O), Oz, tropospheric sulfates, BC, OC, Ds, SS, SI all fixed at 1860 levels.	r1i1p1	500
	HIST	Time varying GHG (CO_2, CH_4, N_2O, CFC11, CFC12, HCFC22, CFC113), SD, Oz, LU, Sl, Vl, SS, BC, MD, OC.	r1i1p1	145 (1861-2005)
	NAT	Time varying Sl and Vl; GHG (CO_2, CH_4, N_2O), Oz, SS, BC, OC, Ds, SD fixed or cycled over 1860 values.	r1i1p1	145 (1861-2005)
HadGEM2-ES	PICONTROL	GHG (CO_2, CH_4, N_2O, and halocarbons), Oz, aerosols, Sl, Vl, and LU fixed at 1860 levels.	r1i1p1	577
	HIST	Time varying GHG (CO2, N2O, CH4, halocarbons), anthropogenic sulfate aerosol direct and indirect effects (SA), Oz, LU, Sl, Vl, BC, and OC.	r1i1p1, r2i1p1, r3p1i1, r4i1p1	147 (1859-2005)
	NAT	Time varying Sl and Vl; GHG, SA, Oz, BC, OC, and LU fixed or cycled over 1860 values.	r1i1p1, r2i1p1, r3p1i1, r4i1p1	161 (1859-2019)

3.3.2. Precipitation variability

With the objective of selecting CMIP5 models (listed in Table 3.1) that best reproduce the observed SACZ precipitation variability during austral summer (December-January-February, DJF), we first compared the seasonal average precipitation daily rate and standard deviation from GPCP with all 17 CMIP5 models. For CMIP5 models with daily data, we first calculated monthly averages. The seasonal average and standard deviation for the GPCP were calculated from 1979-2014. Since ENSO is the most important coupled mode on interannual time-scale influencing precipitation in SA (e.g. Grimm, 2003; Grimm et al. 2007), we excluded strong ENSO events, identified as the years with absolute values of Oceanic Niño Index (ONI, available at http://www.cpc.ncep.noaa.gov/products/analysis_monitoring/ensostuff/ensoyears.shtml) greater than 1.4°C for at least three consecutive 3-month running means, as long as these conditions were satisfied in at least one month during the DJF. Using this criterion, we excluded the years 1982-83 (El Niño), 1988-89 (La Niña), 1991-92 (El Niño), 1997-98 (El Niño), 1998-99 (La Niña), and 1999-2000 (La Niña), resulting in 30-year average. Notice that the DJF average precipitation rate of a specific year is calculated using December of that year and January and February of the next year. All CMIP5 historical simulations are available until 2005 and the seasonal average and standard deviation is calculated for the austral summer of the last 30 years, 1975-2004.

To compare CMIP5 datasets with GPCP, all CMIP5 models were interpolated to GPCP 2.5° resolution. The interpolation was performed using a kriging method, considering a spherical model. Kriging is an interpolation method based on prior knowledge of the degree of spatial dependence on the data. In essence, it is equivalent to a weighted moving

average, with the weights determined by the data's spatial variogram (Fortin and Dale 2005). Here, a spherical variogram model was adopted. The results obtained with the interpolated models are similar to those with in their original resolution. Thus, all maps are shown with their original resolution to keep the level of details.

The main goal of this study is to investigate rainfall trends over EBr and equatorward margin of the SACZ. Therefore, models selected for this analysis are the ones that exhibited the smallest Root Mean Square Error (RMSE) obtained with respect to GPCP over the climatological SACZ position (black boxes in Figure 3.1). The RMSE was calculated according to Taylor et al. (2001):

$$RMSE = \sqrt{\sigma_o^2 + \sigma_e^2 - 2\sigma_o\sigma_e\rho} \quad \text{(Eq 3.1)}$$

where σ_o and σ_e are the spatial standard deviation of the GPCP (observed) and CMIP5 average precipitation (estimated), respectively; and ρ is the spatial correlation between the observed and the estimated datasets. The spatial standard deviation is calculated as:

$$\sigma = \sqrt{\frac{NP}{NP-1}\sum_{i=1}^{NP} W_i(PP_i - \overline{PP})^2} \quad \text{(Eq 3.2)}$$

where PP_i is the average precipitation rate (in mm/day) at each one of the NP grid points in the considered area; $\overline{PP}$ is the spatial average of the precipitation over the area; and W_i is the spatial weight, calculated as $1/\cos\varphi$, where φ is the latitude. The areal average of the precipitation $\overline{PP}$ is:

$$\overline{PP} = \sum_{i=1}^{NP} W_i\, PP_i \quad \text{(Eq 3.3)}$$

3.3.3. Precipitation Trends

To investigate whether the poleward shift in the SACZ is related to natural variability or to anthropogenic forcing, we selected the CMIP5 models that best reproduced the DJF precipitation average and standard deviation. For these models, we investigate trends in the HIST, NAT, and ANTHROP scenarios. Trends in all datasets and scenarios are estimated based on Mann Kendall (Wilks 2011) and the Sen's Slope (Sen 1968) tests, as described in Zilli et al. (2017a). The Sen's slope measures the magnitude of the trend in all datasets and the Mann Kendall test indicates the areas where the trends were significant ($p<0.1$).

In addition to the Mann-Kendall significance test, we also performed another test based on trends calculated using the PICONTROL dataset. Since in this scenario all forcings are kept constant at pre-industrial levels, all simulated precipitation variability is related to interactions between the different components of the climate system (Taylor et al. 2012) and are referred to as the model's internal variability. The Sen's slope was calculated for every consecutive 30-year period and for each grid point in the PICONTROL of all selected model. The probability distribution of 30-year trends in the PICONTROL (based on Sen's slopes) was then estimated. To account for the model's drift, the average trend estimated with the PICONTROL was removed from all scenarios. Thus, after the correction, trends in other scenarios that were above (below) the 95^{th} (5^{th}) percentile of the PICONTROL trend distribution were considered significant.

3.4. Climatology

The GPCP climatology for DJF precipitation rate over SA (Figure 3.1a) is characterized by the Intertropical Convergence Zone (ITCZ) over equatorial Atlantic and Pacific oceans; the SAMS, with large seasonal averages over the central Amazon and central

Brazil; and the SACZ (black boxes in Figure 3.1). The precipitation standard deviation (contours in Figure 3.1a) indicates two maxima in precipitation variability along both margins of the SACZ and more evident over the ocean (Carvalho et al. 2002; 2004). Additionally, the DJF precipitation variability is also large over SESA, in association with the SACZ dipolar pattern on intraseasonal timescale (Liebmann et al. 1999).

Not all CMIP5 historical simulations accurately reproduce the DJF average and standard deviation precipitation over SA. Visual inspection of Figure 3.1 indicates that the largest uncertainties occur over the Amazon basin, with most of the selected models (CanESM2, CCSM4, CNRM-CM5, GFDL-ESM2M, HadCM3, INMCM4, MIROC-ESM, MIROC4h, MRI-CGCM3, and NorESM1-M) displacing the maximum precipitation eastward of the observed climatological position. Four models fail in reproducing the spatial characteristics of SAMS precipitation, as indicated by a zonal maximum precipitation band either over the equator (GISS-E2-H and MPI-ESM-LR) or over the subtropics (ACCESS1-3, CSIRO-Mk3-6-0), while five models are unable to reproduce the average precipitation variability associated with the SACZ (CNRM-CM5, GISS-E2-H, INMCM4, MPI-ESM-LR, and MRI-CGCM3). In fact, these models have the largest RMSE when compared to GPCP average precipitation over the SACZ (calculated after interpolating all models to 2.5° resolution; not shown). Conversely, CCSM4, GFDL-ESM2M, CanESM2, HadGEM2-ES, HadGEM2-CC, MIROC4h, and MIROC-ESM more accurately simulate the SACZ mean position and standard deviation and have the smallest RMSE (Table 3.3).

Over the northern margin of the SACZ (black boxes in Figure 3.1), CCSM4 and GFDL-ESM2M exhibit the smallest RMSE and spatial correlation equal to 0.92 (Table 3.3). On the other hand, all models underestimate the average precipitation and overestimate the

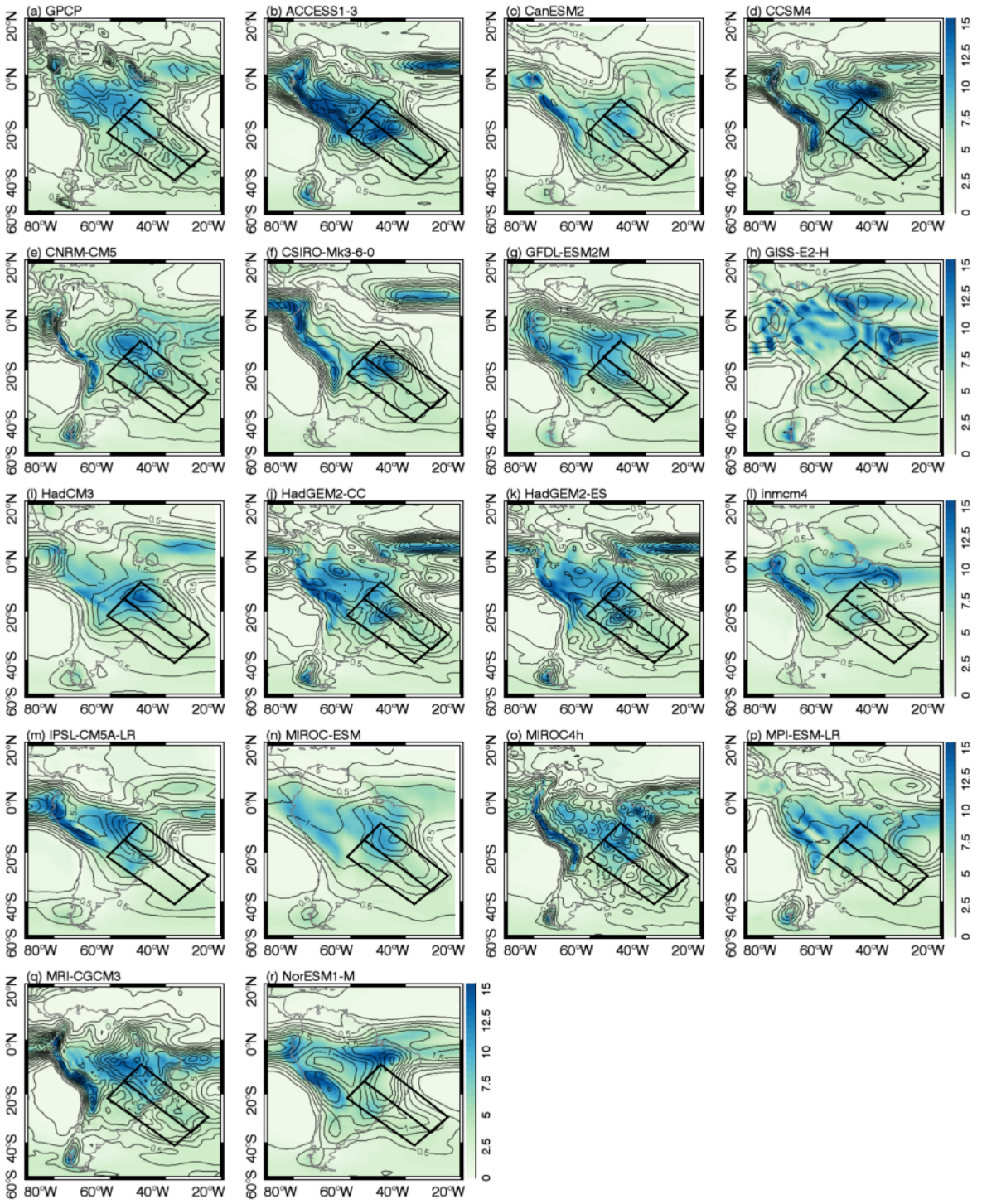

Figure 3.1 — DJF precipitation rate average (in mm.day^{-1}; shades) and standard deviation (contours, interval each 0.25mm.day^{-1}) for (a) GPCP, (b)-(r) CMIP5 HIST models on their original resolution (as in Table 1). Black boxes represent the climatological location of the SACZ and its northern and southern margins.

Table 3.3 — Spatial average ($\overline{PP}$) and standard deviation (σ) of each dataset (CMIP5 models are interpolated to 2.5^{o} degrees GPCP spatial resolution), spatial correlation (ρ) and RMSE (Eqs 3.1-3.3), with respect to GPCP calculated over the entire SACZ region and its northern and southern margins (black boxes, Figure 3.1). Only selected models that best represent the SACZ precipitation are shown

MODELS	$\overline{PP}$	σ	ρ	**RMSE**
	SACZ			
GPCP	5.51	2.02	1.00	-
CFSR	5.90	2.64	0.74	0.88
CCSM4	5.12	1.99	0.90	0.44
GFDL-ESM2M	5.08	2.43	0.93	0.47
CanESM2	4.99	2.15	0.87	0.54
HadGEM2-ES	5.99	2.23	0.83	0.62
HadGEM2-CC	5.89	2.18	0.80	0.66
MIROC4h	5.48	2.54	0.81	0.73
MIROC-ESM	5.27	2.33	0.68	0.99
	SACZ Northern Margin			
GPCP	4.69	2.17	1.00	-
CFSR	6.25	3.17	0.91	0.70
CCSM4	4.67	2.38	0.94	0.38
GFDL-ESM2M	4.17	2.51	0.94	0.41
CanESM2	4.54	2.41	0.86	0.57
HadGEM2-ES	5.90	2.49	0.92	0.45
HadGEM2-CC	5.92	2.22	0.92	0.41
MIROC4h	5.36	2.92	0.84	0.74
MIROC-ESM	5.72	2.83	0.83	0.73
	SACZ Southern Margin			
GPCP	6.37	1.69	1.00	-
CFSR	5.76	2.23	0.81	0.77
CCSM4	5.71	1.75	0.87	0.51
GFDL-ESM2M	6.04	2.17	0.90	0.58
CanESM2	5.45	1.83	0.88	0.51
HadGEM2-ES	6.25	2.19	0.86	0.67
HadGEM2-CC	6.02	2.27	0.86	0.71
MIROC4h	5.74	2.27	0.91	0.60
MIROC-ESM	5.06	1.93	0.86	0.58

standard deviation over the southern margin of the SACZ (Table 3.3). CCSM4 and CanESM2 have the smallest RMSE over this region (0.51 for both) while MIROC4h and GFDL-ESM2M have the largest spatial correlation coefficient with GPCP (0.91 and 0.9, respectively). In addition to a realistic simulation of the standard deviation of precipitation, GFDL-ESM2M and MIROC4h models also correctly simulate the large-scale characteristics of the SAMS (Jones and Carvalho 2013). Accordingly, Jones and Carvalho (2013), using a

multivariate large-scale monsoon index (Silva and Carvalho 2007), identified that GFDL-ESM2M and MIROC4h realistically simulated large scale characteristics of SAMS (onset, withdrawal, and amplitude) whereas CanESM2 poorly represents SAMS features. CCSM4, HadGEM2-ES, HadGEM2-CC, and MIROC-ESM models were not included in Jones and Carvalho (2013) analysis. Gulizia and Camilloni (2015) also identified MIROC4h as the CMIP5 model that best reproduces the DJF precipitation rate over Southeastern Brazil and SESA.

In addition to correctly simulating the SACZ precipitation climatology, the models listed in Table 3.3 also accurately simulate the frequency distribution of DJF average daily precipitation rate over the SACZ (Figure 3.2). Over the northern margin, CCSM4 reproduces accurately the average, standard deviation, and skewness of the daily precipitation rate; HadGEM2-CC, HadGEM2-ES, MIROC-ES, and MIROC4h overestimate the average and the standard deviation, and exhibit a distribution skewed toward larger precipitation rates; GFDL-ESM2M and CanESM2 underestimate the average and have distributions skewed toward low daily precipitation rates. Over the southern margin, excluding ACCESS1-3, all 17 CMIP5 models underestimate the average precipitation rate and overestimate the standard deviation (Figure 3.2b). Among all models listed in Table 3.3, CCSM4, GFDL-ESM2M, MIROC-4h, and MIROC-ESM are the ones that best simulate the precipitation rate climatology along the southern margin of the SACZ.

Hence, among the 17 CMIP5 models analyzed (Table 3.1), those listed in Table 3.3 are the ones that more realistically reproduce the DJF precipitation average and spatial variability, as well as the climatological distribution of precipitation rates over the SACZ region. For this reason, the following analyses focuses on different scenarios obtained from

these models.

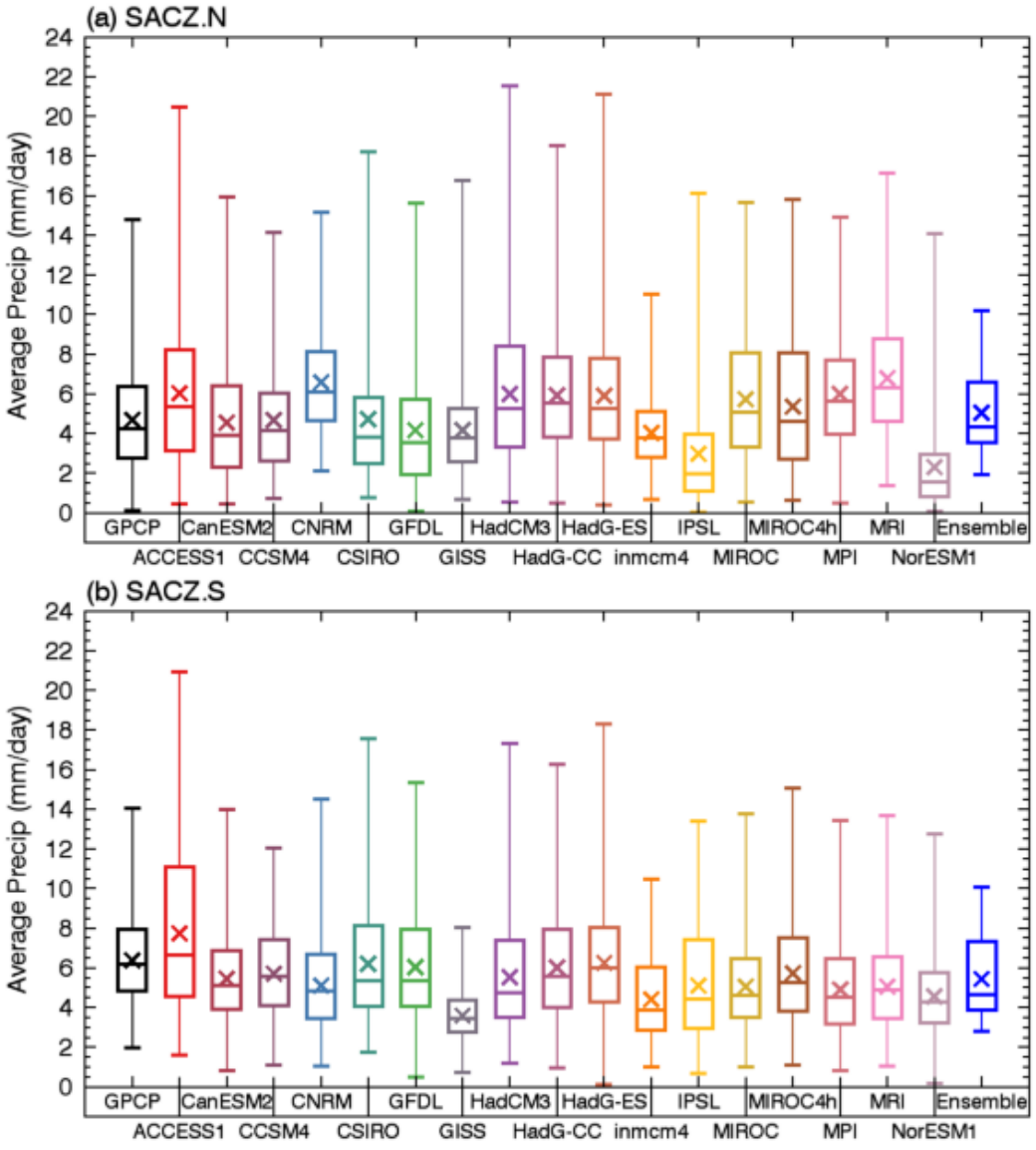

Figure 3.2 — Spatial statistics for the DJF precipitation rate calculated over the (a) northern and (b) southern margin of the SACZ (black boxes in Figure 3.1). Represented statistics: standard deviation (box), average (central line), median ("x" symbol), and 5th and 95th percentiles (whiskers) for the GPCP and CMIP5 models, and their ensemble (all dataset interpolated to 2.5° resolution)

3.5. Precipitation trend in recent decades

Previous studies (Zilli et al. 2017a) observed an overall drying trend in the equatorward portion of the climatological SACZ, associated with fewer but more intense

precipitation events while the poleward portion of the SACZ exhibited a positive trend in the frequency of both light and intense rainy days increasing (Zilli et al. 2017a, b, in review). To identify trends in the opposite margins of the SACZ and address the contribution of natural variability and anthropogenic forcing to the observed precipitation changes, we compared trends in GPCP with those in HIST, NAT, and ANTHROP scenarios of the CMIP5 models that best reproduce the SACZ variability (Table 3.3). Out of the 7 models listed in Table 3.3, HadCM3, HadGEM2-CC, and MIROC4h do not provide either natural or pre-industrial scenarios. Thus, we used CCSM4, CanESM2, GFDL-ESM2M, and HadGEM2-ES models for the attribution analysis. These are Earth System Models with a full representation of the carbon cycle, including fluxes of carbon between the ocean, atmosphere, and terrestrial reservoirs (Taylor et al. 2012).

Consistently with Zilli et al (2017a, b, in review), the trends in GPCP DJF mean precipitation rate (1979-2014, excluding ENSO years) exhibit a dipolar pattern along the margins of the SACZ (Figure 3.3). Over the northern margin (black boxes in Figure 3.3), and over the oceanic and continental SACZ (Carvalho et al. 2004), trends in the average DJF daily precipitation are negative and about $-0.24 mm.day^{-1}.10yr^{-1}$; along the southern margin, the average trend is negligible, despite some areas with small positive trends. Nonetheless, it is worth noticing that over the oceanic SACZ, trends are positive and statistically significant.

3.5.1. Simulated historical trends

This section investigates DJF daily precipitation trends in the SACZ region simulated by the four selected CMIP5 models (Table 3.2). To account for the uncertainties related to model's internal variability, we analyzed all members available in HIST for each model (Table 3.2). From the 13 members considered here, 8 have indication of reduced (increased)

DJF average precipitation rates along the northern (southern) margin of the SACZ during 1975-2004 (Figure 3.4). CCSM4 is the most consistent model, with all three ensemble members indicating negative and significant trends ($p<0.1$, considering the Mann-Kendall trend test) over the northern margin of the SACZ (Figure 3.4a-c), even though each member places the negative trends on different areas along the northern margin. Along the southern margin, 2 out of 3 members have positive precipitation trends either over the continent (Figure 3.4a) or along the entire SACZ (Figure 3.4c). Differences in location of trends could be related to differences in rain rate over the SACZ in each member. For instance, the second member of CCSM4 (r2i1p1; Figure 3.4b) has the largest average precipitation and the weakest trends over the northern margin of the SACZ. CCSM4 multi member mean trend correctly reproduces the spatial pattern observed in GPCP trends, and is the most accurate among the four models considered in this study (Figure 3.5a).

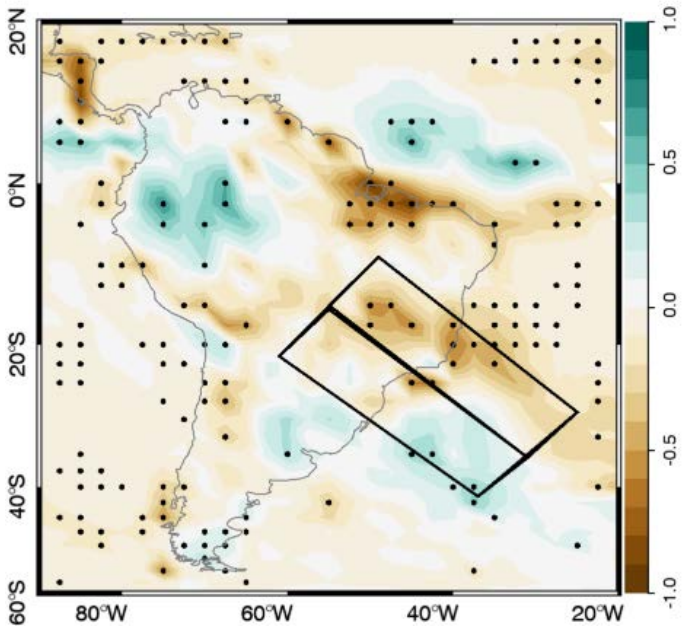

Figure 3.3 — GPCP DJF average precipitation rate (contours, each 2mm.day^{-1} starting in 1mm.day^{-1}), Sen's slope trends (shades, in mm.day^{-1}10yr^{-1}), and its significance ($p<0.1$, stippled), according to the Mann-Kendall trend test, for 30 years period (1979-2014, excluding ENSO years). Black boxes represent the climatological location of the SACZ and its northern and southern margins

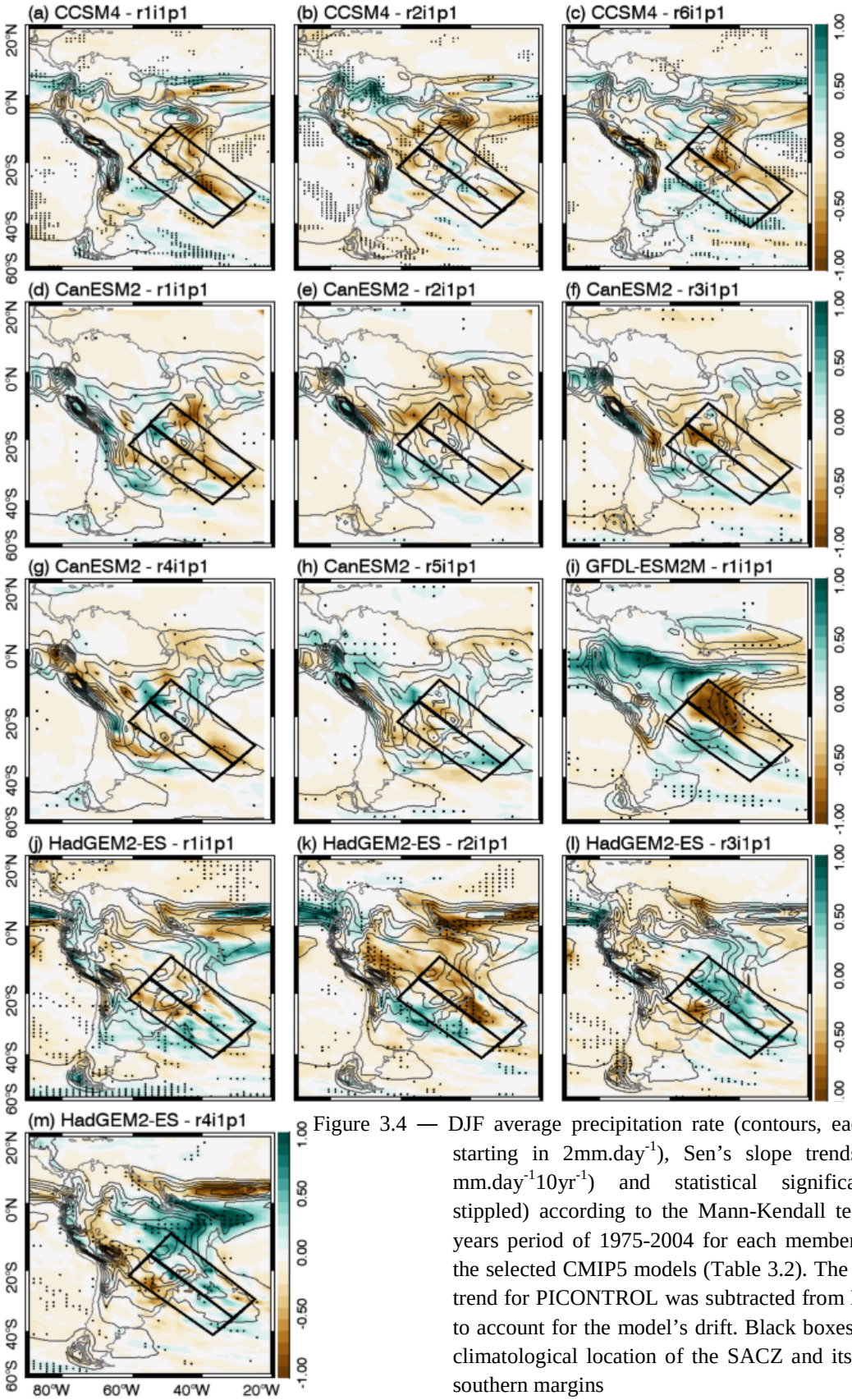

Figure 3.4 — DJF average precipitation rate (contours, each 2mm.day^{-1} starting in 2mm.day^{-1}), Sen's slope trends (shades, in mm.day^{-1}10yr^{-1}) and statistical significance ($p<0.1$, stippled) according to the Mann-Kendall test, for the 30 years period of 1975-2004 for each member of HIST for the selected CMIP5 models (Table 3.2). The 30-year mean trend for PICONTROL was subtracted from HIST's trends to account for the model's drift. Black boxes represent the climatological location of the SACZ and its northern and southern margins

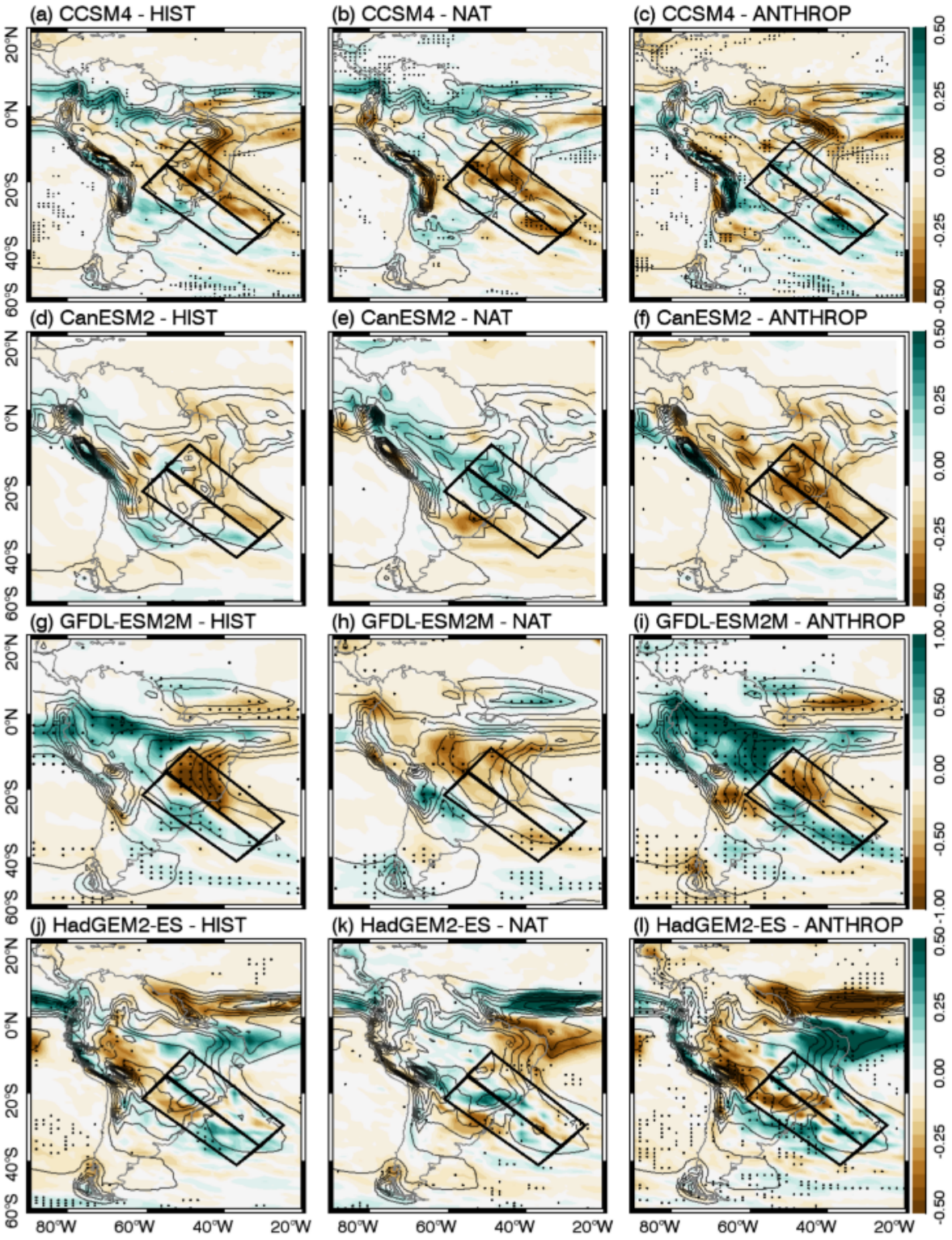

Figure 3.5 — Multi-member ensemble mean trends of DJF precipitation rate (each 2mm.day^{-1} starting in 2mm.day^{-1}) and Sen's slope trends (shades, in mm.day^{-1}10yr^{-1}) for 1975-2004 for HIST (first column), NAT (second column), and ANTHROP (HIST-NAT, third column) scenarios of (a-c) CCSM4; (d-f) CanESM2; (g-i) GFDL-ESM2M; and (j-l) HadGEM2-ES. Areas with

statistically significant trends in the multi-member ensemble mean are stippled. A positive (negative) trends is considered statistically significant if exceeds (is below) the 95th (5th) of the PICONTROL distribution, estimated using all consecutive 30-year period intervals. The trends are calculated for each individual member before averaging as a multi-member ensemble mean. Trends in multi-member ensemble mean are considered statistically significant when at least half of the individual members of the ensemble show significant trends at a specific grid point. The mean 30 years trend for PICONTROL was subtracted from each member before calculating the trends to account for the model's drift

For the CanEMS2 model, 3 out of 5 members simulated negative (positive) precipitation trends along the northern (southern) margin of the SACZ (r1i1p1, r2i1p1, and r3i1p1; Figure 3.4d-f), but trends are statistically significant ($p< 0.1$) only for the first member of the ensemble (r1i1p1; Figure 3.4d). For the other 2 members (r4i1p1 and r5i1p1; Figure 3.4g-h), the SACZ-related precipitation is larger along the southern margin, resulting in a SACZ displaced poleward of its observed position. The multi-member mean trend reflects the lack of agreement among the runs, with weak and non-statistically significant trends over both margins of the SACZ (Figure 3.5d). Despite having only one member, GFDL-ESM2M also simulates well observed trends along both margins of the SACZ, albeit with overestimated intensity (Figures 3.4i and 3.5g). Zhang et al (2016) found similar behavior when analyzing precipitation changes over SESA in the 20th century and attributed them to changes in the radiative forcing due to increasing concentration of well-mixed greenhouse gases. Their study was based on the GFDL-CM2.5 model, a coupled physical model successor of the CM2.1 version used as the base for the GFDL-ESM2M.

HadGEM2-ES exhibits the largest discrepancies in the spatial patterns of precipitation trends, with increased (reduced) precipitation along the northern (southern) margin of the SACZ for members r3i1p1 and r4i1p1 (Figures 3.4l-m). These members also exhibit relatively larger precipitation rate along the northern margin of the SACZ, when compared to the other members of the scenario. Precipitation trends in the r2i1p1 member (Figure

3.4k) shows opposite behavior, with negative (positive) trends along the northern (southern) margin of the SACZ, while for the first member (r1i1p1) only the positive precipitation trends over the southern margin of the SACZ are significant (Figure 3.4j). As for CanESM2, the lack of agreement among the HadGEM2-ES members also results in negligible trends along the northern margin (Figure 3.5j). For the southern margin, all members simulate positive precipitation trends along the oceanic portion of the SACZ while 3 members simulated negative precipitation trends over the continent (Figures 3.4j-m), resulting in positive (negative) trends over the oceanic (continental) part of the SACZ observed in the multi-member ensemble mean trend (Figure 3.5j). This is the only one among the four models selected for this study that simulates a positive precipitation trend over EBr, based on the multi-member ensemble mean. Similar trends were also detected in previous studies (Cavalcanti and Shimizu 2012).

The HIST multi member mean precipitation trend of each model show a dipolar spatial pattern along the SACZ's margins, with exception of HadGEM2-ES (Figures 3.5a, d, g, and j). This dipolar pattern is also evident when averaging precipitation trends over all HIST members of all models, in a multi model mean trend (Figure 3.6a). Note that in this case the ensemble members are averaged as independent simulations, i.e., without previously averaging over each model. Thus, even though the internal variability in the models is still large, the majority of the HIST (8 in 13) show precipitation trends over EBr and SESA, consistent with a poleward shift of the SACZ; 2 simulations have opposite sign, indicating a northward shift in the SACZ; and in 3 simulations the spatial pattern of the precipitation trends do not resemble the dipolar structure.

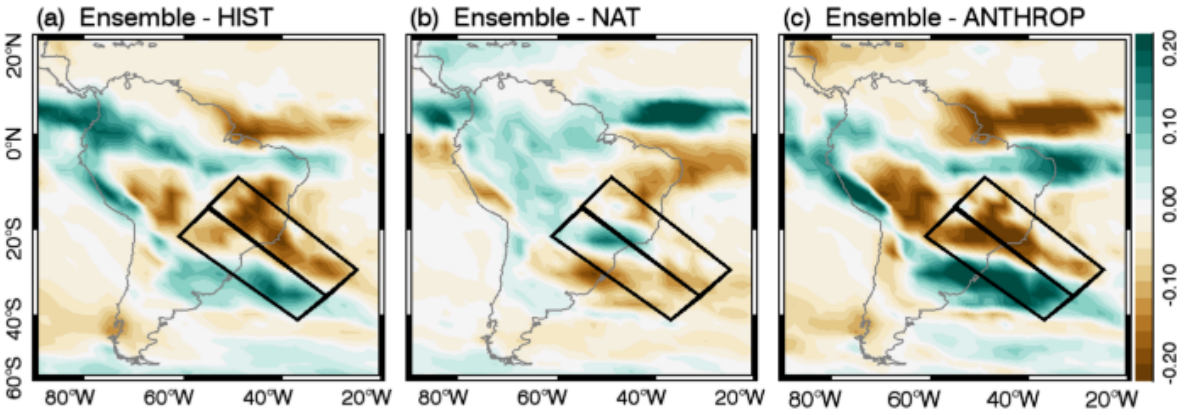

Figure 3.6 — Multi-model ensemble mean of the Sen's slope trend (shades, in mm.day^{-1}10yr^{-1}) for all members and models for (a) HIST; (b) NAT; and (c) ANTHROP scenarios. All members were interpolated (using a kriging method) to 2.5°lon/lat resolution before averaging them as independent simulations (i.e., without averaging over the members of each model first). Black boxes represent the climatological location of the SACZ and its northern and southern margin

3.5.2. Attribution to Anthropogenic Forcing

The objective of this section is to identify the contribution of anthropogenic forcing on patterns of trends in DJF daily rainfall rate over the SACZ (north and south margins) during the most recent 30-yr period of HIST simulations (1975-2004). Precipitation trends estimated from HIST can be related to both natural and/or anthropogenic forcing. To access the relative contribution of anthropogenic forcing on trends, we repeated the previous analysis for NAT and ANTHROP scenarios. Trends in ANTHROP (HIST–NAT) were calculated for each available ensemble member and then averaged for each model. To account for the internal variability of the model, the statistical significance of trends was assessed based on the distribution of trends estimated for all consecutive 30-year period available in the PICONTROL. That is, a positive (negative) trend is considered statistically significant if it exceeds (is below) the 95th (5th) percentile of the PICONTROL distribution obtained at a particular grid point. The trends are calculated for each individual member before averaging as a multi member mean. Trends in multi member mean are considered

statistically significant when at least half of the individual members of the ensemble show significant trends at a specific grid point. This approach results in patterns of statistically significant trends that are similar to the ones estimated with the Mann-Kendall test.

Both CCSM4 and GFDL-ESM2M show negative precipitation trends in NAT and HIST over the northern margin of the SACZ (Figures 3.5b and h), indicating that the natural variability may have played an important role in the 1975-2004 HIST trends over the SACZ. Nonetheless, over the northern (southern) margin of the SACZ, negative (positive) precipitation trends simulated in the GFDL-ESM2M NAT (Figure 3.5h) are smaller than those simulated in HIST (Figure 3.5g). This result suggests that the anthropogenic forcing may have enhanced dynamic and physical conditions responsible for the reduction (increase) in precipitation rate over the area (Figure 3.5i). Notice that GFDL-ESM2M NAT shows drying trends over most of tropical South America and ITCZ (with the caveat that most trends are not statistically significant), including the northern and southern margins of the SACZ. Conversely, the ANTHROP indicates a dipole pattern that largely explains the statistically significant drying (wetting) trends observed in HIST over the northern (southern) margins of the SACZ. Interestingly, positive precipitation trends over the southern margin of the SACZ and western and central Amazon is observed in HIST and ANTHROP only, suggesting that the wetting trends in tropical and subtropical South America are strongly linked to anthropogenic forcing in the GFDL-ESM2M simulations.

Conversely, negative trends in the northern margin of the SACZ simulated in CCSM4 multi-member ensemble HIST (Figure 3.5a) are largely explained by natural forcing (Figure 3.5b) as suggested by the nearly opposite (most not statistically significant) trends in the ANTHROP (Figure 3.5c). Over the southern margin of the SACZ, the precipitation trends in

ANTHROP are positive, particularly over the ocean (Figure 3.5c). All 3 members of the ensemble show similar pattern for both margins of the SACZ for both NAT and ANTHROP (Appendix A, Figures 3.A.1 and 3.A.2).

While CCSM4 and GFDL-ESM2M simulations indicate an important contribution of natural variability on the precipitation trends over the SACZ, the natural variability simulated by the CanESM2 model offsets the anthropogenic forcing, resulting in weaker trends in HIST (Figures 3.5d-f). For this model, the dipolar pattern of precipitation trends associated with the poleward shift of the SACZ is explained by changes in ANTHROP (Figure 3.5f) with the spatial pattern consistent throughout all five available ensemble members available (Appendix A, Figure 3.A.2). However, areas with significant trends in each member of this scenario are located in different positions along the margins of the SACZ, resulting in intense but non-significant trends in the multi-member mean (Figure 3.5f).

The ensemble members of the HadGEM2-ES NAT have a similar behavior as those in HIST, with each member simulating a different trend: the first member has a dipolar pattern with positive (negative) precipitation trends over the northern (southern) margin of the SACZ; in the second member, trends are positives over the oceanic portion of the southern margin and negative along the northern margin, extending over EBr; in the third member the trends are positive over the continental SACZ; and in the fourth member the trends are negative over the SACZ and over northeastern Brazil (Appendix A, Figures 3.A.1). Consequently, the ANTHROP members are also different from each other (Appendix A, Figures 3.A.2), even though the multi member mean trend indicate an increase in precipitation intensity over SESA and adjacent South Atlantic (Figure 3.5l).

In summary, three out of four models analyzed here simulate a poleward shift of the SACZ, which is caused mostly by anthropogenic forcing in two of the models (and half of the ensemble members). The uncertainties on the signal of the precipitation trend over the SACZ are larger when considering the NAT and ANTHROP individually than when considering them together in HIST. In the HIST multi-model ensemble mean, negative (positive) trends simulated over EBr (SESA) and along the northern (southern) margin of the SACZ (Figure 3.6a) are strongly related to anthropogenic forcing (Figure 3.6c) and partially offset by trends associated with natural variability (Figure 3.6b). Due to large uncertainties among the ensemble members, with statistically significant trends located in different regions of the study area, these trends are within the 5^{th}-95^{th} confidence interval derived from the PICONTROL and cannot be totally separated from the models' internal variability.

The presence of statistically significant trends in the last 30 years of NAT simulations reveals the importance of the models' decadal variability in modulating precipitation. This issue was further investigated by calculating 30-year moving trends of DJF mean precipitation rate averaged over each margin of the SACZ for HIST, NAT and ANTHROP simulations. Trends were calculated for the spatially averaged precipitation over each margin of the SACZ, considering each ensemble member separately before estimating the multi-member ensemble mean (Figures 3.7 and 3.8). The trend obtained with GPCP (1979-2014) is included for comparison. In fact, 30-year moving trends, calculated over the northern margin of the SACZ (Figure 3.7), oscillate with periods between 30 and 60 years in all models, with trends in HIST (black line) and NAT (green line) mostly in phase with each other in CCSM4 and GFDL-ESM2M models (Figures 3.7a and c, respectively). The long period of these oscillations may indicate the influence of coupled modes of variability in

modulating precipitation regimes in tropical South America on decadal-to-multidecadal timescales.

The 30-year moving trends calculated after 1981 (center of the 30-year period) are consistently negative for HIST (black line) and NAT (green line) simulations and for all models investigated here, except for HADGEM2-ES (Figure 3.6d). For CanESM2 and GFDL-ESM2M models, trends in recent decades in HIST (black line in Figures 3.6b and c, respectively) and ANTHROP (orange lines in Figure 3.6b and c, respectively) are below the 5^{th} percentile of the distribution. The influence of the anthropogenic forcing in these trends is evident in these two models. As discussed before, HadGEM2-ES and CCSM4 do not exhibit mean trends over the northern margin of the SACZ that can be considered statistically significant. One limitation in this analysis is that mean trends were estimated over a relatively large domain, which may include trends of opposite sign that could cancel each other (Figure 3.5). Nonetheless, the average precipitation trends obtained with GPCP for the same area shows reasonable agreement with CCSM4 HIS and NAT scenarios and with CanESM2 ANTHROP scenario.

It is worth noticing that other 30-year periods have exhibit trends that are above (below) the 95^{th} (5^{th}) percentiles of the model's distribution of the respective PICONTROL simulation. These periods are normally characterized by trends with opposite sign between natural forcing and anthropogenic forcing, which resulted in neutral trends in the HIST simulations. The uniqueness of the recent period (centered in 1981) relatively to other periods of the simulation, is mostly evident in HIST of GFDL-ESM2M and CANESM2.

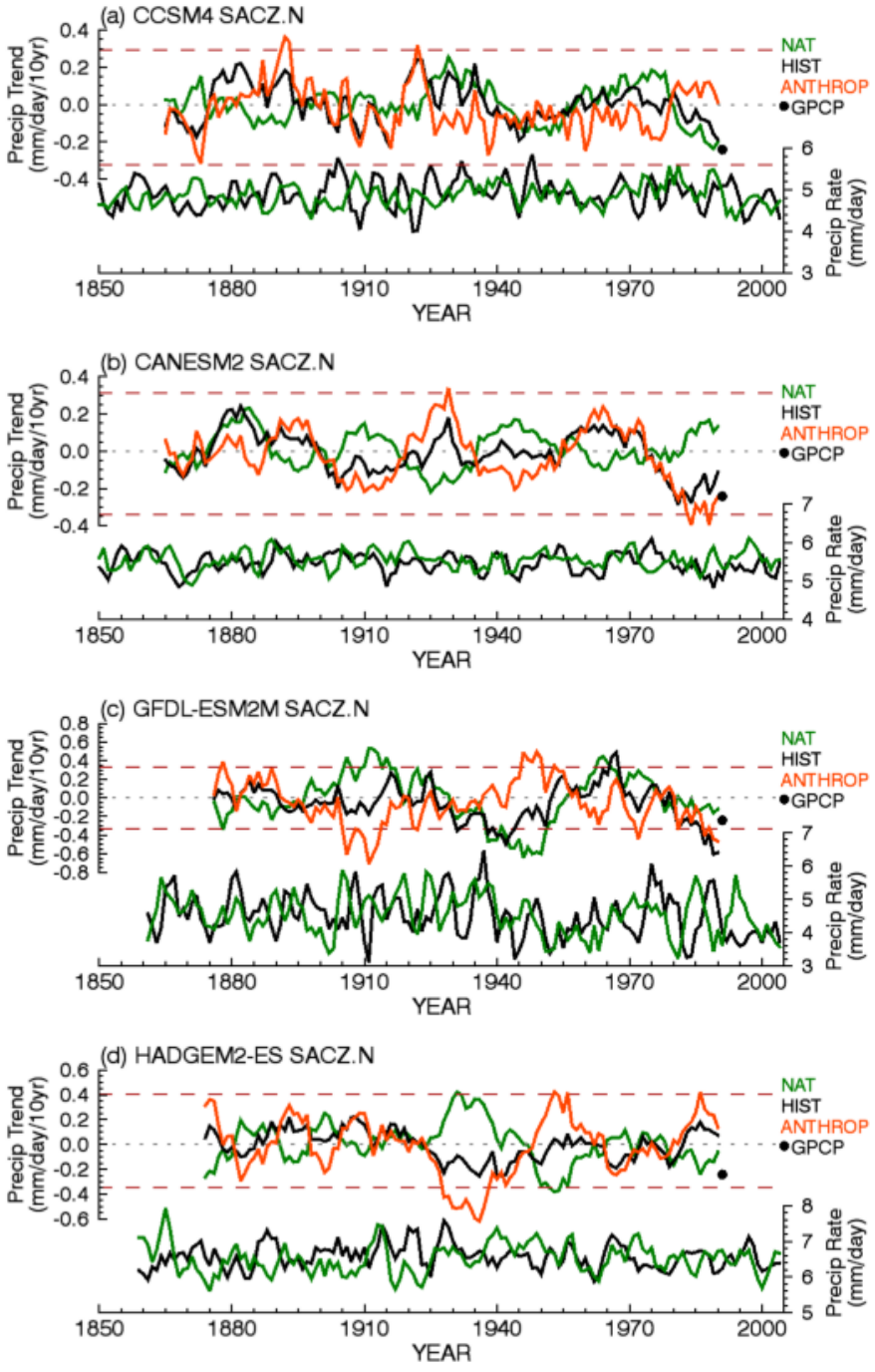

Figure 3.7 — Top: moving 30 years trends for HIST (black line), NAT (green line), and ANTHROP (HIST-NAT, orange line) for the average DJF precipitation rates over the northern margin of the SACZ (black box in Figure 3.4) for each model. Black circles indicate the average trends for the GPCP for the 30 years period (1979-2014, excluding ENSO years). Values plotted at the center of the 30 years interval. Dashed red lines indicate the 5th and 95th percentiles confidence interval of the trend distribution of PICONTROL, calculated using all consecutive 30 years for each model. Bottom: DJF precipitation rate (smoothed by a 3 years moving window), averaged over the northern margin of the SACZ for HIST (solid black line) and NAT (dashed green line) scenarios: (a) CCSM4; (b) CanESM2; (c) GFDL-ESM2M; and (d) HadGEM2-ES

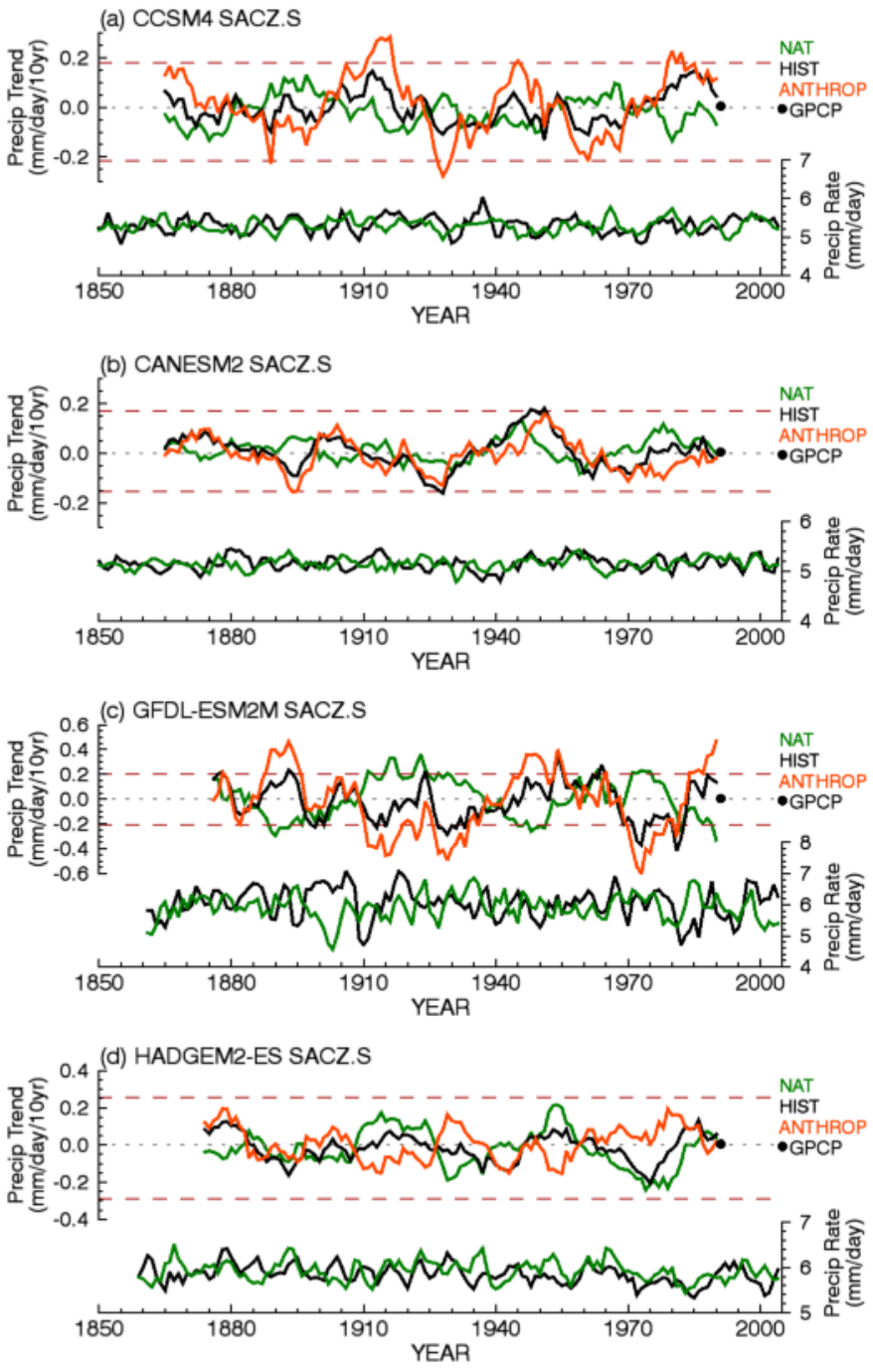

Figure 3.8 — As in Figure 3.7, for the southern margin of the SACZ

The role of natural variability on precipitation trends simulated by CCSM4 and GFDL-ESM2M is also evident in the 30 years moving trend calculated over the southern margin of the SACZ (Figures 3.8a and c). For both models, the trends simulated in their

respective HIST run seem more strongly correlated to changes in the anthropogenic forcing (orange line in Figures 3.8a and c), with the natural variability playing a minor role (green line in Figures 3.8a and c). It worth noticing that for the GFDL-ESM2M model, NAT is associated with negative precipitation trends over the entire SACZ region in recent years (compare Figure 3.7c and 3.8c), while the ANTHROP is associated with opposite trends in each margin. For CanESM2 and HadGEM2-ES, the 30-year moving trends estimated over the southern margin of the SACZ are close to zero after 1981 for all scenarios (Figures 3.8b and d) mostly due to the choice of the study area. Particularly for CanESM2, the largest precipitation trends occur over SESA and adjacent South Atlantic Ocean, to the south of the study area and are not captured by the spatial averages.

3.5.3. Internal Variability

Even though highly dependent on the definition of the study area, the 30-year moving trend (Figures 3.7 and 3.8) helps in understanding the influence of natural and anthropogenic forcing on the simulated trends. To investigate the relative importance of model's internal variability to the simulated trends, we compared 30-year precipitation trends spatially averaged over the margins of the SACZ in each scenario to the respective distribution of trends obtained from all consecutive 30-year periods in the PICONTROL (bars in Figures 3.9 and 3.10). In Figures 3.9 and 3.10, the "X" symbol represents the 30 years precipitation trend (1975-2004), spatially averaged over each margin of the SACZ. The multi member ensemble mean of these trends, averaged over all members of the ensemble for each model, is represented as a diamond. The spatially averaged precipitation trend obtained from the GPCP is also included as a black circle.

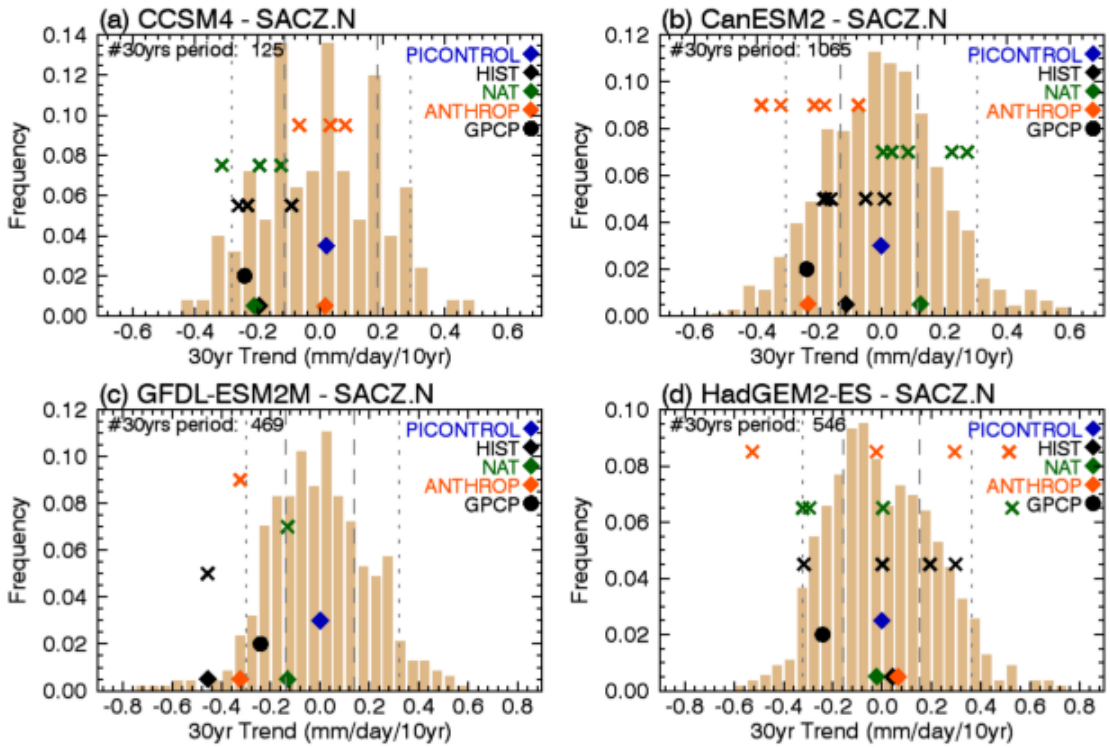

Figure 3.9 — Frequency distribution of 30 years trends for PICONTROL (bars), its 5th and 95th percentiles (dotted lines), and its lower and upper quartiles (dashed line), spatially averaged over the northern margin of the SACZ (black box in Figure 3.5) for each model: (a) CCSM4; (b) CanEMS2; (c) GFDL-ESM2M; and (d) HadGEM2-ES. Number of possible consecutive 30 years periods in PICONTROL for each model on the top left of each graphic. For each model, the "X" symbol represent the 30-year precipitation trend spatially averaged over the northern margin of the SACZ for each member of HIST (black diamond), NAT (green), and ANTHROP (HIST-NAT; orange) scenarios; and the diamonds represent the multi-member ensemble mean of the spatially averaged trends. The blue diamond represents the mean trend of PICONTROL, spatially averaged over each area and measures the model's drift. This value was subtracted from the frequency distribution and from each member's average before plotting. The black circle represents the spatially averaged 30 years trend for the GPCP and is plotted as a reference

For the northern margin of the SACZ, the trend distribution for the PICONTROL is symmetric (considering all models), with zero median (blue diamond in Figure 3.9), mean interquartile range (averaged over all models) of 0.28mm.day^{-1}10yr^{-1}, and mean range of 1.14mm.day^{-1}10yr^{-1}. Over the southern margin (Figure 3.10), the mean range of the trend distribution is smaller, 0.74mm.day^{-1}10yr^{-1}, with mean interquartile range of 0.17mm.day^{-1}10yr^{-1}, with the CCSM4 distribution showing a large negative skew (Figure 3.10a).

Among the four models investigated, GFDL-ESM2M has the largest negative spatially-averaged precipitation trend over the northern margin of the SACZ in HIST (black diamond and "X" symbols in Figure 3.9c). As this model has only one ensemble member, both the spatially averaged trend (black "X" symbol) and the multi-member ensemble mean trend (black diamond) are identical. The negative trend in HIST is mostly explained by anthropogenic-related forcing (orange diamond and "X" symbol in Figure 3.9c), which account for 71.2% of the total trend. Both HIST and ANTRHOP trends are below the 5th percentile of the trend distribution for PICONTROL (dotted line in Figure 3.9c), indicating that the influence of external forcing on the simulated trends are larger than the model's internal variability. The spatially averaged precipitation trend in NAT (green diamond and "X" symbol; Figure 3.9c) is also negative and accounts for the remainder of the HIST's precipitation trend.

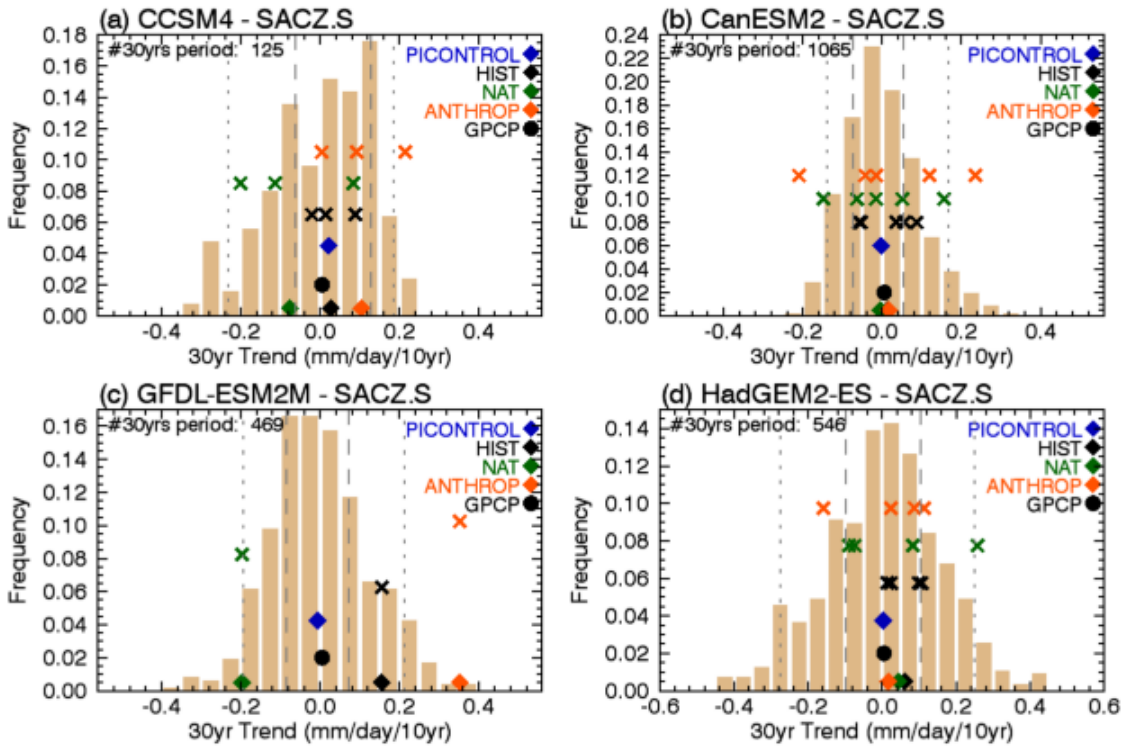

Figure 3.10 — As in Figure 3.9, for the southern margin of the SACZ

For CCSM4 and CanESM2 HIST, the multi member ensemble mean of the spatially averaged precipitation trend (black diamonds in Figures 3.9a and b) are negative over the northern margin of the SACZ. However, the multi-member ensemble mean trends of both models are larger than the 5^{th} percentile of the trend distribution for PICONTROL and not distinguishable from models' internal variability. The role of the natural variability in the trends simulated by these models is also evident in these graphics. For the CCSM4, the multi-member ensemble mean of the spatially averaged trends for NAT (green diamond in Figure 3.9a) is negative and with similar magnitude as the multi-member ensemble mean of the spatially averaged trends in HIST (black diamond in Figure 3.9a), resulting in close to zero spatially averaged trends due to ANTHROP (orange diamond in Figure 3.9a). Conversely, the multi-member ensemble mean of the spatially averaged trend for CanESM2 NAT is positive over the northern margin of the SACZ (green diamond in Figure 3.9b), partially offsetting the negative trends due to the anthropogenic forcing (orange diamond in Figure 3.9b). None of the multi member ensemble mean trends for both CCSM4 and CanESM2 models are large enough to be distinguishable from the model's internal variability, although the agreement on the sign of the spatially averaged trends among all members of each scenario and model ("X" symbols in Figures 3.9a and b) indicates that the trends are at least partially affected by external forcing.

For HadGEM2-ES, the spatially averaged precipitation trends for the northern margin of the SACZ show a large spread among the members of all scenarios ("X" symbols in Figure 3.9d), resulting in close to zero multi member ensemble mean (diamond in Figure 3.9d). These results emphasize the large uncertainty in the model's precipitation simulation for the region, with the model's internal variability prevailing over the external forcings.

The negative GPCP spatially averaged precipitation trend over the northern margin of the SACZ is located between the 5^{th} and 25^{th} percentiles of the trend distribution for PICONTROL for all models considered (black circle in Figure 3.9a-d). Assuming the distribution of trends in PICONTROL as a confidence interval for the GPCP as well, it is not possible to separate the forcings resulting in the precipitation trends from natural variability. CCSM4 HIST and CanESM2 ANTHROP multi-member mean of the spatially averaged trends closely reproduce the observed spatially averaged precipitation trend (Figures 3.9a and c, respectively).

Over the southern margin of the SACZ, only GFDL-ESM2M ANTHROP shows a positive spatially averaged trend above the 95^{th} percentile of the trend distribution for PICONTROL (orange diamond in Figure 3.10c). This trend is partially offset the natural variability (green diamond in Figure 3.10c), resulting in non-significant positive multi member ensemble mean trend in HIST (black diamond in Figure 3.10c). For the other models considered in this study, the large spread among the spatially averaged precipitation trends for each ensemble member and scenario ("X" symbols in Figure 3.10) results in close to zero multi member ensemble mean (diamonds in Figure 3.10) and indicates the influence of the models' uncertainties on the simulated trends.

3.6. Conclusion

Previous observational and climate model-based studies identified a poleward shift in the SACZ-related summer precipitation rate (Seth et al. 2010; Junquas et al. 2013; Diaz and Vera 2017; Talento and Barreiro 2017; Zilli et al. 2017a, b, in review). Over SESA, the increase in precipitation has been associated to tropical warming over equatorial Indian and eastern Pacific oceans (Junquas et al. 2013). Over EBr, the reduction in precipitation has

been related to a decrease in the frequency of the phase of the SACZ that favors precipitation over the region (Diaz and Vera 2017). Considering only the CMIP5 models that accurately reproduced the observed precipitation variability over the SACZ, the present study identified that the dipolar pattern consistent with the observed poleward shift in the SACZ precipitation has been partially modulated by anthropogenic-related forcings.

Among the 17 CMIP5 models considered in this study, 4 are able to accurately reproduce the observed SACZ climatology (CCSM4, CanESM2, GFDL-ESM2M, and HadGEM2-ES) and 3 of them correctly simulate the observed poleward shift of the SACZ. The multi-model mean trend of the 4 selected models also show evidence of the combined influence of anthropogenic forcing and natural variability on the SACZ-related precipitation trends. Even though most ensemble members of the 4 selected models correctly simulated the observed pattern of precipitation trends, the statistical significance of these trends in the multi member mean for each model and scenario is small, indicating that the model's internal variability and uncertainties still play an important role in the simulated trends. This is best exemplified by the differences among the ensemble members of the HadGEM2-ES scenarios, in which each member simulates precipitation trends with different spatial pattern and sign, resulting in weak trends over the SACZ region in the multi member ensemble mean. A similar problem is also evident in precipitation trends simulated by the other three models. The spatial pattern and the sign of the precipitation trends simulated by different ensemble members are similar but statistically significant at different parts of the study area, which results in a multi member ensemble mean trend that is not statistically significant. However, the similarity in the simulated precipitation trends among the ensemble members suggests the importance of anthropogenic forcing in modulating the sign of the trend.

Nonetheless, this study showed compelling evidence of the influence of anthropogenic forcing (increase in greenhouse gases concentration and land use change) on the poleward shift of the SACZ in the last 3 decades of the simulations. Over the northern (southern) margin, positive (negative) precipitation trends can be attributed to anthropogenic forcing, with the natural variability partially offsetting the simulated trends. Nevertheless, the discrepancy in the simulated precipitation over the region of interest is large, with only 3 out of 17 investigated CMIP5 models correctly reproducing the observed trends, suggesting that some important mechanisms related to variations in the position and intensity of the SACZ events may not be well represented by the models analyzed here.

The results presented here focused only on changes in average precipitation rate. Over the SACZ, the number of rainy days is decreasing (Zilli et al. 2017a) likely due to weaker northerly winds along the eastern Brazilian coast and reduced available moisture in lower-to-mid troposphere (Zilli et al. 2017b, in review). On the other hand, the intensity of extreme events is increasing over the region (Zilli et al. 2017a), suggesting a large influence of dynamic and thermodynamic forcing on the observed changes. Thus, besides correctly reproducing the observed average precipitation trends, it is necessary to access the accuracy of the CMIP5 models in reproducing the observed trends in extreme precipitation, as well as the dynamic and thermodynamic forcings associated to these events. A careful analysis of the mechanisms driving the observed and simulated changes in precipitation is also important to improve the quality of the climate simulation over the region, particularly along the transition zones such as the SACZ, where the uncertainty in simulations is large (Carvalho and Jones 2013; Jones and Carvalho 2013; Sánchez et al. 2015; Diaz and Vera 2017; de Barros Soares et al. 2017).

3.7. Appendix A – Precipitation trends in Natural and Anthropogenic Simulations

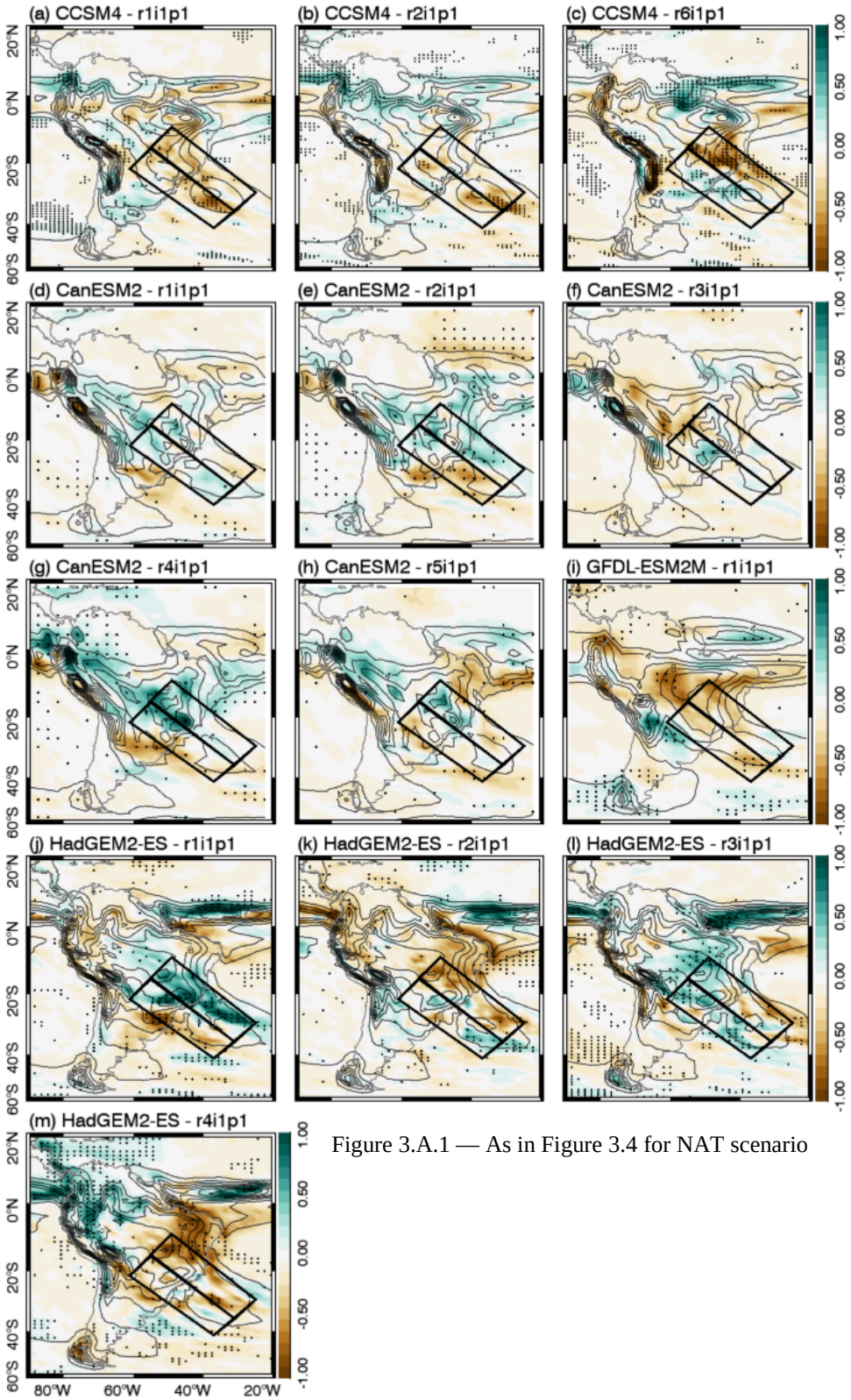

Figure 3.A.1 — As in Figure 3.4 for NAT scenario

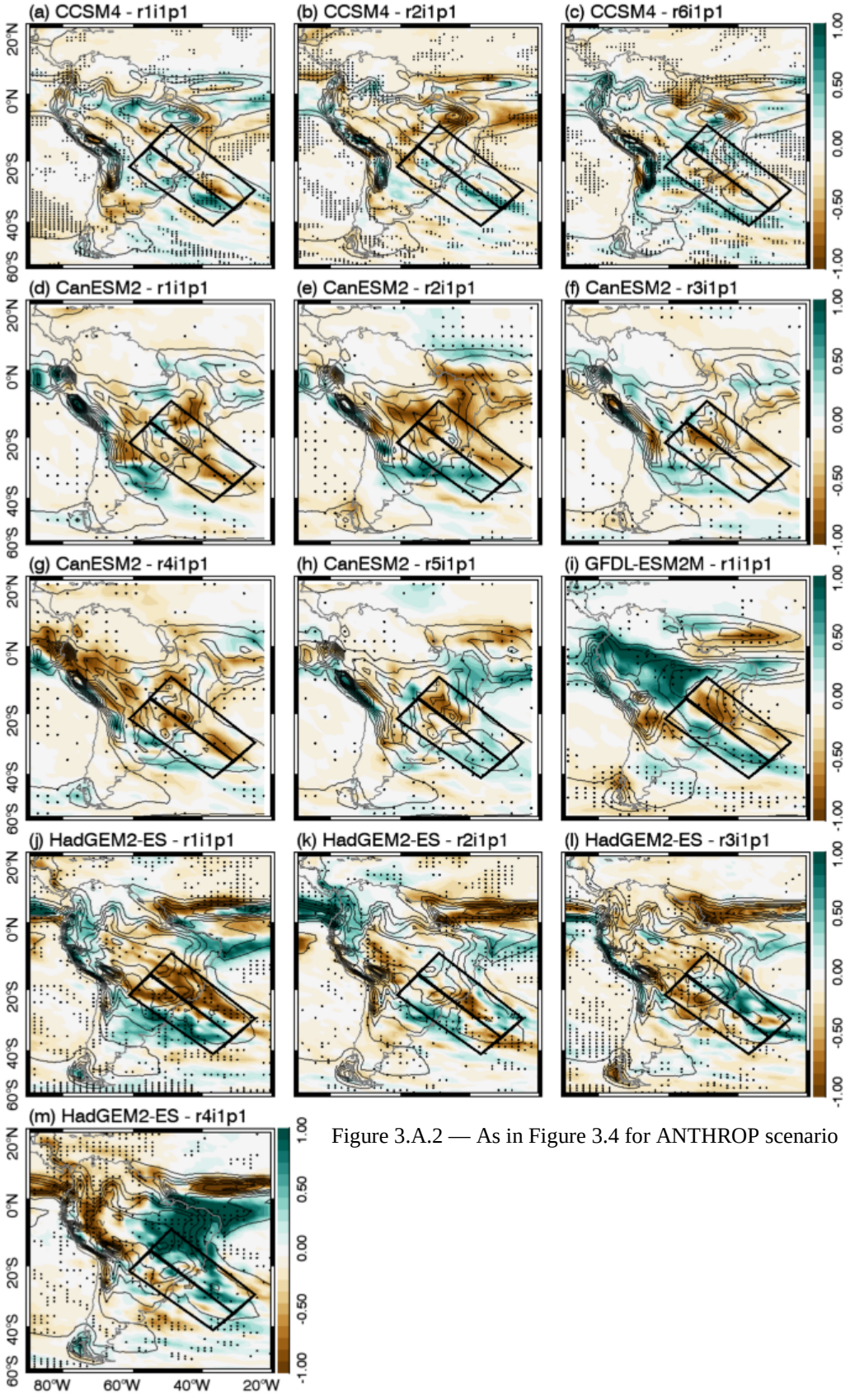

Figure 3.A.2 — As in Figure 3.4 for ANTHROP scenario

3.8. References

Adarsh S, Janga Reddy M (2014) Trend analysis of rainfall in four meteorological subdivisions of southern India using nonparametric methods and discrete wavelet analysis, Int J Climatol. doi: 10.1002/joc.4042

Barros V, Gonzalez M, Liebmann B, Camilloni I (2000) Influence of the South Atlantic Convergence Zone and South Atlantic sea surface temperature on interannual summer rainfall variability in Southeastern South America. Theor Appl Climatol 67:123-133

Barros V, Doyle M, Camilloni I (2008) Precipitation trends in southeastern South America: relationship with ENSO phases and with low-level circulation. Theor. App. Climatol 93:19-33. doi: 10.1007/s00704-007-0329-x

Bentsen M, Bethke I, Debernard JB, Iversen T, Kirkevåg A, Seland Ø, Drange H, Roelandt C, Seierstad IA, Hoose C, Kristjánsson JE (2013) The Norwegian Earth System Model, NorESM1-M – Part 1: Description and basic evaluation of the physical climate. Geosci Model Dev 6:687-720. doi:10.5194/gmd-6-687-2013

Bi D, Dix M, Marsland S, O'Farrell S et al (2013) The ACCESS coupled model: description, control climate and evaluation. Aust Meteorol Oceanogr J 63:41-64

Carvalho LMV, Jones C (2013) CMIP5 simulations of low level tropospheric temperature and moisture over tropical Americas. J Clim 26:6257-6286. doi: 10.1175/JCLI-D-12-00532.1

Carvalho LMV, Jones C, Liebmann B (2002) Extreme precipitation events in Southeastern South America and large-scale convective patterns in the South Atlantic Convergence Zone. J Clim 15:2377-2394

Carvalho LMV, Jones C, Liebmann B (2004) The South Atlantic Convergence Zone: intensity, form, persistence and relationships with intraseasonal to interannual activity and extreme rainfall. J Clim 17:88-108

Carvalho LMV, Jones C, Posadas AN, Quiroz R, Bookhagen B, Liebmann B (2012) Precipitation characteristics of the South American Monsoon System derived from multiple datasets. J Clim 25:4600-4620. doi: 10.1175/JCLI-D-11-00335.1

Carvalho LMV, Silva AE, Jones C, Liebmann B, Silva Dias PL, Rocha HR (2011) Moisture transport and intraseasonal variability in the South America Monsoon System. Clim Dyn 36:1865-1880. doi: 10.1007/s00382-010-0806-2

Cavalcanti I, Shimizu M (2012) Climate fields over South America and variability of SACZ and PSA in HadGEM2-ES. Am J Clim Change 1:132-144. Doi: 10.4236/ajcc.2012.13011

Chou S, Lyra A, Mourão C, Dereczynski C, Pilotto I, Gomes J, Bustamante J, Tavares P, Silva A, Rodrigues D, Campos D, Chagas D, Sueiro G, Siqueira G, Nobre P, Marengo J (2014a) Evaluation of the Eta simulations nested in three Global Climate Models. Am J

Clim Change 3:438-454. doi: 10.4236/ajcc.2014.35039.

Chou S, Lyra A, Mourão C, Dereczynski C, Pilotto I, Gomes J, Bustamante J, Tavares P, Silva A, Rodrigues D, Campos D, Chagas D, Sueiro G, Siqueira G, Nobre P, Marengo J. (2014b) Assessment of climate change over South America under RCP 4.5 and 8.5 downscaling scenarios. Am J Clim Change 3:512-527. doi: 10.4236/ajcc.2014.35043

Collins M, Tett SFB, Cooper C (2001) The internal climate variability of HadCM3, a version of the Hadley Centre coupled model without flux adjustments. Clim Dyn 17:61-81

Collins WJ, Bellouin N, Doutriaux-Boucher M et al (2011) Development and evaluation of an Earth-System model – HadGEM2. Geosci Model Dev 4:1051-1075. doi:10.5194/gmd-4-1051-2011

Cunningham CAC, Cavalcanti IFA (2006) Intraseasonal modes of variability affecting the South Atlantic Convergence Zone. Int J Climatol 26:1165-1180. doi: 10.1002/joc.1309

de Barros Soares D, Lee H, Loikith PC, Barkhordarian A, Mechoso CR (2017) Can significant trends be detected in surface air temperature and precipitation over South America in recent decades? Int J Climatol 37:1483–1493. doi:10.1002/joc.4792

Díaz LB, Vera CS (2017) Austral summer precipitation interannual variability and trends over Southeastern South America in CMIP5 models. Int J Climatol doi: 10.1002/joc.5031

Dufresne JL, Foujols MA, Denvil S et al (2013) Climate change projections using the IPSL-CM5 Earth System Model: from CMIP3 to CMIP5. Clim Dyn 40:2123-2165. doi 10.1007/s00382-012-1636-1

Dunne JP, John JG, Adcroft AJ et al (2012) GFDL's ESM2 Global Coupled Climate-Carbon Earth System Models. Part I: Physical Formulation and Baseline Simulation Characteristics. J Clim 25:6646-6665. doi: 10.1175/JCLI-D-11-00560.1

Fortin MJ, Dale MRT (2005) Spatial Analysis, a guide for ecologists. Cambridge University Press, Cambridge, UK. 380 p.

Gent PR, Danabasoglu G, Donner LJ, Holland MM, Hunke EC, Jayne SR, Lawrence DM, Neale RB, Rasch PJ, Vertenstein M, Worley PH, Yang Z, Zhang M (2011) The Community Climate System Model Version 4. J Clim 24:4973-4991. doi: 10.1175/2011JCLI4083.1

Giorgetta MA, Jungclaus J, Reick CH et al (2013) Climate and carbon cycle changes from 1850 to 2100 in MPI-ESM simulations for the Coupled Model Intercomparison Project phase 5. J Adv Model Earth Syst 5: 572–597. doi:10.1002/jame.20038.

Gocic M, Trajkovic S (2013) Analysis of changes in meteorological variables using Mann-Kendall and Sen's slope estimator statistical test in Serbia. Glob Planet Change 100:172-182. doi: 10.1016/j.gloplacha.2012.10.014

Grimm AM (2003) The El Niño impact on the summer monsoon in Brazil: regional processes versus remote influences. J Clim 16: 263-280

Grimm AM, Pal JS, Giorgi F (2007) Connection between spring conditions and peak summer monsoon rainfall in South America: role of soil moisture, surface temperature and topography in eastern Brazil. J Clim 20:5929-5945. doi: 10.1175/2007JCLI1684.1

Grimm AM, Saboia J (2015) Interdecadal variability of the South American precipitation in the monsoon season. J Clim 28:755-775. doi: 10.1175/JCLI-D-14-00046.1

Grimm AM, Zilli MT (2009) Interannual variability and seasonal evolution of summer monsoon rainfall in South America. J Clim 22:2257-2275. doi: 10.1175/2008JCLI2345.1

Gulizia C, Camilloni I (2015) Comparative analysis of the ability of a set of CMIP3 and CMIP5 global climate models to represent precipitation in South America. Int J Climatol 35:583-595. doi: 10.1002/joc.4005

Haylock MR et al. 2006. Trends in total and extremes South American rainfall in 1960–2000 and links with sea surface temperature. J Clim 19: 1490–1512, doi: 10.1175/JCLI3695.1.

Huffman GJ, Adler RF, Bolvin DT, Gu G (2009) Improving the global precipitation record: GPCP Version 2.1. Geophys Res Lett 36:L17808. doi:10.1029/2009GL040000.

Jain SK, Kumar V (2012) Trend analysis of rainfall and temperature data for India. Current Science 102:37-49

Jeffrey SJ, Rotstayn LD, Collier MA, Dravitzki SM, Hamalainen C, Moeseneder C, Wong KK, Syktus JI (2013) Australia's CMIP5 submission using the CSIRO Mk3.6 model. Aust Meteorol Oceanogr J 63:1-13.

Jones C, Carvalho LMV (2013) Climate change in the South American Monsoon System: present climate and CMIP5 projections. J Clim 26:6660-6678. doi: 10.1175/JCLI-D-12-00412.1

Jones CD, Hughes JK, Bellouin N et al (2011) The HadGEM2-ES implementation of CMIP5 centennial simulations. Geosci Model Dev 4:543-570. doi:10.5194/gmd-4-543-2011

Junquas C, Vera CS, Li L, LeTreut H (2012) Summer precipitation variability over Southeastern South America in a global warming scenario. Clim Dyn 38:1867-1883. doi: 10.1007/s00382-011-1141-y

Junquas C, Vera CS, Li L, LeTreut H (2013) Impact of projected SST changes on summer rainfall in Southeastern South America. Clim Dyn 40:1569-1589. doi: 10.1007/s00382-013-1695-y

Kodama YM (1992) Large-scale common features of subtropical precipitation zones (the Baiu Frontal Zone, the SPCZ and the SACZ) Part I: characteristics of subtropical frontal zones. J Meteor Soc Japan 70:813-835

Kodama YM (1993) Large-scale common features of subtropical convergence zones (the Baiu Frontal Zone, the SPCZ and the SACZ). Part II: conditions of the circulations for

generating the STCZs. J Meteor Soc Japan 75:581-610

Liebmann B, Jones C, Carvalho LMV (2001) Interannual variability of daily extreme precipitation events in the state of São Paulo, Brazil. J Clim 14:208-218

Liebmann B, Kiladis GN, Marengo JA, Ambrizzi T, Glick JD (1999) Submonthly Convective Variability over South America and the South Atlantic Convergence Zone. J Clim 12:1877-1891

Marengo JA, Liebmann B, Grimm AM, Misra V, Silva Dias PL, Cavalcanti I, Carvalho LM, Berbery E, Ambrizzi, T, Vera C, Saulo A, Nogues-Paegle J, Zipser E, Seth A, Alves L (2012) Review: recent developments on the South American Monsoon System. Int J Climatol 32:1-21. doi: 10.1002/joc.2254

Martin GM, Bellouin N, Collins WJ et al (2011) The HadGEM2 family of Met Office Unified Model climate configurations. Geosci Model Dev 4:723-757. doi:10.5194/gmd-4-723-2011

Mo K, Nogues-Paegle J (2001) The Pacific-South American modes and their downstream effects. Int J Climatol 21:1211-1229. doi: 10.1002/joc.685

Muza MN, Carvalho LMV, Jones C, Liebmann B (2009) Intraseasonal and interannual variability of extreme dry and wet events over Southeastern South America and the Subtropical Atlantic during austral summer. J Clim 22:1682-1699. doi: 10.1175/2008JCLI2257.1

Nogues-Paegle J, Byerle LA, Mo KC (2000) Intraseasonal modulation of South American summer precipitation. Mon Weather Rev 128:837-850

Nogues-Paegle J, Mo KC (1997) Alternating wet and dry conditions over South America during summer. Mon Weather Rev 125:279-291

Sakamoto TT, Komuro Y, Nishimura T, Ishii M, Tatebe H, Shiogama H, Hasegawa A, Toyoda T, Mori M, Suzuki T, Imada Y, Nozawa T, Takata K, Mochizuki T, Ogochi K, Emori S, Hasumi H, Kimoto M (2012) MIROC4h - A New High-Resolution Atmosphere-Ocean Coupled General Circulation Model. J Meteorol Soc Jpn 90:325-359. doi:10.2151/jmsj.2012-301

Sanchez E, Solman S, Remedio A, Berbery H, Samuelsson P, Rocha R, Mourão C, Li L, Marengo J, Castro M, Jacob D (2015) Regional climate modelling in CLARIS-LPB: a concerted approach towards twenty first century projections of regional temperature and precipitation over South America. Clim Dyn 45:2193-2212. doi: 10.1007/s00382-014-2466-0

Schmidt GA, Kelley M, Nazarenko L et al (2014) Configuration and assessment of the GISS ModelE2 contributions to the CMIP5 archive. J Adv Model Earth Syst 6:141-184. doi: 10.1002/2013MS000265

Sen PK (1968) Estimates of the regression coefficient based on Kendall's Tau. J Am Stat Assoc 63: 1379–1389.

Seth A, Rojas M, Rauscher SA (2010) CMIP3 project changes in the annual cycle of the South American Monsoon. Climatic Change 98:331-357. doi: 10.1007/s10584-009-9736-6

Skansi MM, BrunetM, Sigró J, Aguilar E, Groening JAA, Bentancur OJ, Geier YRC, Amaya RLC, Jácome H, Ramos AM, Rojas CO, Pasten AM, Mitro SS, Jiménez CV, Martínez R, Alexander LV, Jones PD. 2013.Warming and wetting signals emerging from analysis of changes in climate extreme indices over South America. Glob Planet Change 100: 295–307, doi: 10.1016/j.gloplacha.2012.11.004.

Talento S, Barreiro M (2017) Control of the South Atlantic Convergence Zone by extratropical thermal forcing. Clim Dyn. doi: 10.1007/s00382-017-3647-4

Taylor KE (2001) Summarizing multiple aspects of model performance in a single diagram. J Geophys Res 106(D7):7183-7192. doi:10.1029/2000JD900719

Taylor KE, Stouffer RJ, Meehl GA (2012) An overview of CMIP5 and the experiment design. Bull Am Meteorol Soc 93:485-498. doi: 10.1175/BAMS-D-11-00094.1

Vera C, Higgins W, Amador J, Ambrizzi T, Garreaud R, Gochis D, Gutzler D, Letternmater D, Marengo JA, Mechoso CR, Nogués-Paegle J, Silva Dias PL, Zang C (2006a) Toward a unified view of the American Monsoon System. J Clim 19:4977-5000. doi: 10.1175/JCLI3896.1

Vera C, Silvestri G, Liebmann B, Gonzales P (2006b) Climate Change Scenarios for Seasonal Precipitation in South America from IPCC-AR4 Models. Geophys Res Lett 33:L13707. doi: 10.1029/2006GL025759

Voldoire A, Sanchez-Gomez E, Salas y Mélia D et al (2013) The CNRM-CM5.1 global climate model: description and basic evaluation. Clim Dyn 40:2091-2121. doi: 10.1007/s00382-011-1259-y

Volodin EM, Dianskii NA, Gusev AV (2010) Simulating present-day climate with the INMCM4.0 coupled model of the atmospheric and oceanic general circulations. Izv Atmosph Ocean Phys 46:414-431. doi: 10.1134/S000143381004002X

Watanabe S, Hajima T, Sudo K, Nagashima T, Takemura T, Okajima H, Nozawa T, Kawase H, Abe M, Yokohata T, Ise T, Sato H, Kato E, Takata K, Emori S, Kawamiya M (2011) MIROC-ESM 2010: model description and basic results of CMIP5-20C3M experiments. Geosci Model Dev 4:845-872. doi: 10.5194/gmd-4-845-2011

Wilks DS (2011) Statistical methods in the atmospheric sciences. Vol. 100. Academic Press.

Yin L, Fu R, Shevliakova E, Dickinson RE (2013) How well can CMIP5 simulate precipitation and its controlling processes over tropical South America? Clim Dyn 41:3127-3143. doi: 10.1007/s00382-012-1582-y

Yukimoto S, Adachi Y, Hosaka M, Sakami T, Yoshimura H, Hirabara M, Tanaka TY, Shindo E, Tsujino H, Deushi M, Mizuta R, Yabu S, Obata A, Nakano H, Koshiro T, Ose T, Kitoh A (2012) A New Global Climate Model of the Meteorological Research Institute: MRI-CGCM3 – Model Description and Basic Performance. J Meteorol Soc Jpn 90:23-64. doi: 10.2151/jmsj.2012-A02

Zhang H, Delworth TL, Zeng F, Vecchi G, Paffendorf K, Jia L (2016) Detection, attribution, and projection of regional rainfall changes on (multi-) decadal time scales: a focus on Southeastern South America. J Clim 29:8515-8534. doi: 10.1175/JCLI-D-16-0287.1

Zhou J, Lau KM (1998) Does a monsoon climate exist over South America? J Clim 11:1020-1040

Zhou J, Lau KM (2001) Principal modes of interannual and decadal variability of summer rainfall over South America. Int J Climatol 21:1623-1644. doi: 10.1002/joc.700

Zilli MT, Carvalho LMV, Liebmann B, Silva Dias MA (2017a) A comprehensive analysis of trends in extreme precipitation over southeastern coast of Brazil. Int J Climatol. doi: 10.1002/joc.4840

Zilli MT, Carvalho LMV, Lintner BR (2017b) The poleward shift of South Atlantic Convergence Zone in recent decades. Clim Dyn, in review.

Conclusions

Current changes in the distribution and frequency of summer precipitation over Southeastern Brazil (SE Brazil) are of central importance for water management and natural disasters preparedness, particularly in the large urban areas. Thus, a better understanding of the effects of a warmer troposphere on the SACZ activity contributes to access the current and future changes in precipitation. ***This dissertation provides novel insights and improves the understanding of the consequences of climate change over eastern tropical South America with particular emphasis to the South Atlantic Convergence Zone through three interconnected research objectives:***

1. Provide a comprehensive analysis of the spatial variability of trends in observed precipitation over SE Brazil focusing on regional and local scales (Chapter 1).
2. Investigate decadal changes in the circulation features related to the position and intensity of the SACZ that influence dynamic and thermodynamic processes related to convection and precipitation over Eastern and SE Brazil (Chapter2).
3. Determine the contribution of natural variability and anthropogenic-related forcings on the precipitation trends through the evaluation of various global climate model simulations (Chapter 3).

The individual studies that comprise this dissertation represent a comprehensive analysis of the changes in SACZ activity and consequent effects in precipitation intensity, largely contributing to the scientific understanding of the impacts of climate change on the precipitation regime over eastern Brazil.

The observed changes in precipitation on SE Brazil during the wet season (October to March) have been identified in Chapter 1 of this dissertation. By applying robust statistical

analyses to rain gauges with more than 70 years of observed data, this work has identified a positive trend in both average and extreme precipitation over the coastal region of SE Brazil, as well as a pattern of spatial variability of these trends. Over the southern portion of the study region, this study has shown that the increase in total seasonal and average daily precipitation is related to an increase in the frequency and intensity of extreme events. Additionally, the analysis of individual stations has indicated negative trends in the number of light rainy days over large urbanized areas in the state of São Paulo. Over the northern portion, the percentage of rainy days and the number of light rainy days has been decreasing while the intensity and frequency of heavy rain has been increasing, resulting in fewer, but more intense precipitation events. This spatial pattern of precipitation trends suggests a poleward shift of the SACZ, which is favoring convective activity over the southern portion of the study region while inhibiting convection over the northern part.

Chapter 2 has investigated changes in the SACZ-related circulation resulting in the spatial patterns of precipitation trends over SE Brazil. In this chapter, the study area has been extended to capture changes along both margins of the SACZ and providing evidence of the poleward shift of convergence. By comparing decadal averages of precipitation and other atmospheric fields during austral summer (December to March), this study has identified a weakening of the poleward winds along the Eastern Brazilian coast and a drying of low-to-mid troposphere (700hPa) over the tropical Atlantic. The SACZ is formed by the convergence of northerly winds along the western flack of the SASH with southerly winds from the cyclonic circulation at the poleward side of the SACZ. Hence, a weakening of the northerly winds along the eastern Brazilian coast reduces the dynamic support necessary for convection and precipitation along the equatorward margin of the SACZ. Additionally, the

decrease in specific humidity at 700hPa over the tropical South Atlantic is indicative of an intensification of the subsidence that further contributes to the negative trends in precipitation by reducing the moisture transported into the convective margin. Both results suggest changes in the positioning and strength of the South Atlantic Subtropical High. The results support the hypothesis of a shift in the South Atlantic Convergence Zone position in recent decades, which is crucial to evaluate the consequences of climate change over populated areas in South America.

The final chapter of this dissertation has focused on attributing the causes of the poleward shift of the SACZ and consequent changes in precipitation. This work has evaluated the precipitation trends simulated by a set of state-of-art global climate models capable of correctly reproducing the observed precipitation variability over the region. The negative (positive) precipitation trends simulated over eastern Brazil (SESA) during the three last decades of the 20^{th} century can be attributed to anthropogenic forcing, such as changes in atmospheric composition and land use. These trends seem to be partially offset by natural variability. Even though the large uncertainties in the simulations prevents a precise definition of the contribution of each forcing to the simulated trends, the overall agreement among the models suggests that the poleward shift in the SACZ is enhanced by human-induced changes in the climate.

Collectively, the three chapters of this dissertation give novel insights into recent climate variability and change over eastern tropical South America. More importantly, this study investigates, for the first time, the influence of anthropogenic-related forcing on the poleward shift of the South Atlantic Convergence Zone that resulted in changes in precipitation intensity and frequency over Southeastern Brazil. These findings not only

advance the scientific community's understanding of the recent changes in extreme precipitation over populated areas, they also highlight possible implications of anthropogenic climate change to the SACZ activity. These results can potentially improve water management and increase preparedness of the population to precipitation-related natural disasters in future years.

Suggestions for future work

The research presented in this dissertation emphasizes the shift in the positioning of the South Atlantic Convergence Zone (SACZ) over Southeastern Brazil and consequent changes in the distribution and intensity of precipitation during austral summer, partially attributing it to anthropogenic climate change. Previous studies (Jones and Carvalho 2013; Rao et al. 2014) suggest that the duration and amplitude of the rainy season is increasing, with earlier onset and late demise of the South American Monsoon System. The results presented here indicate a spatial pattern of trends in the precipitation, affecting the intensity and the frequency of rainy events. However, changes in the observed onset and demise of the rainy season were not investigated. Future work would also benefit from higher quality precipitation data, including more rigorous quality control of the rain gauge measurements, correcting suspicious values and improving the spatial consistency of the observations.

The results presented here also suggest a reduction on the convergence along the equatorward margin of the SACZ, weakening the dynamic mechanisms related to convection triggering. However, these results were based on the analysis of few atmospheric levels and variables. A few studies (Lintner and Neelin, 2010; Ma et al. 2011) evaluated the consequences of an increase in the convective margin ventilation inducing thermodynamic conditions less favorable to deep convection along the SACZ. The convective margin

ventilation is associated with anomalies in the horizontal advection of moisture from the dry areas into the convection region, reducing precipitation (Chou and Neelin 2004; Held and Soden 2006; Chou et al. 2009). A thorough analysis of the dynamic and thermodynamic vertical profiles related to the advection of moisture along the SACZ equatorward margin would strongly contribute to the understanding of underlying mechanisms responsible for the observed trends in precipitation.

Previous studies (Kayano and Andreoli 2007; Krishnamurthy and Misra 2011; Grimm and Saboia 2015) suggested a modulation of the dipolar structure of the SACZ by coupled atmosphere-ocean modes on decadal to multi-decadal time-scales. Additionally, the intensity of the northerlies along the eastern Brazilian coast, related to the SACZ activity, is determined by the intensity and position of the South Atlantic Subtropical High (SASH; Kodama 1992, 1993). In turn, changes in the SASH intensity and positon have been associated to increase of condensation heating the tropics (Seth et al. 2010; Li et al. 2013) and to the poleward expansion of the Hadley circulation (Seidel and Randel 2007; Schneider et al. 2010). Thus, effort should be invested in identifying the causes of the observed changes in the dynamic and thermodynamic features associated with the shift in the SACZ position. The analysis of global and regional climate models simulations based on different scenarios could further characterize the effect of anthropogenic forcing on the changes in the local Hadley circulation.

Furthermore, the analysis of different scenarios of coupled climate model simulations could also improve the understanding of the spatial patterns of extreme precipitation trends over the tropics. This dissertation focused only on the trends in average precipitation trends. Continued effort should be invested in accessing the accuracy of the GCM in reproducing

the trends observed on extreme precipitation, as well as the dynamic and thermodynamic forcings associated to these events. A careful analysis of the mechanisms driving the observed and simulated changes in precipitation is also important to improve the quality of the climate simulation over the region, particularly along the transition zones such as the SACZ, where the uncertainty in simulations is large.

Additional effort should also be invested toward discussing and communicating the results of this dissertation, and future work, with climatologists and hydrologists working with water management and natural disaster preparedness in areas under the influence of the SACZ. Ultimately, the goal of this research is to provide climate information that is useful to the scientific community, as a whole, and that will improve the understanding of the current state and future fate of precipitation variability in Southeastern Brazil.

References

Chou C, Neelin JD (2004) Mechanisms of global warming impacts on regional tropical precipitation. J Clim 17:2688-2701

Chou C, Neelin JD, Chen C-A, Tu J-Y (2009) Evaluating the "Richer-Get-Richer" mechanism in tropical precipitation change under global warming J Clim 22:1982-2005. doi: 10.1175/2008JCLI2471.1

Grimm AM, Saboia J (2015) Interdecadal variability of the South American precipitation in the monsoon season. J Clim 28:755-775. doi: 10.1175/JCLI-D-14-00046.1

Held IM, Soden BJ (2006) Robust response of the hydrological cycle to global warming. J Clim 19:5686-5699.

Jones C, Carvalho LMV (2013) Climate change in the South American Monsoon System: present climate and CMIP5 projections. J Clim 26:6660-6678. doi: 10.1175/JCLI-D-12-00412.1

Kayano MT, Andreoli RV (2007) Relations of South American summer rainfall interannual variations with the Pacific Decadal Oscillation. Int J Climatol 27:531-540. doi: 10.1002/joc.1417

Kodama YM (1992) Large-scale common features of subtropical precipitation zones (the

Baiu Frontal Zone, the SPCZ and the SACZ) Part I: characteristics of subtropical frontal zones. J Meteorol Soc Jpn 70:813-835

Kodama YM (1993) Large-scale common features of subtropical convergence zones (the Baiu Frontal Zone, the SPCZ and the SACZ). Part II: conditions of the circulations for generating the STCZs. J Meteorol Soc Jpn 75:581-610

Krishnamurthy V, Misra V (2011) Daily atmospheric variability in the South American Monsoon System. Clim Dyn 37:803-819. doi: 10.1007/s00382-010-0881-4

Li W, Li L, Ting M, Deng Y, Kushnir Y, Liu Y, Lu Y, Wang C, Zhang P (2013) Intensification of the Southern Hemisphere summertime subtropical anticyclones in a warming climate. Geophys Res Lett 40:5959–5964, doi:10.1002/2013GL058124

Lintner BR, Neelin JD (2010) Tropical South America-Atlantic sector convective margins and their relationship to low-level inflow. J Clim 23:2671-2685. doi: 10.1175/2009JCLI3301.1

Ma HY, Ji X, Neelin J, Mechoso C (2011) Mechanisms for precipitation variability of the eastern Brazil/SACZ convective margin. J Clim 24:3445-3456. doi: 10.1175/2011JCLI4070.1

Rao V, Franchito S, Gan M, Gerolamo R (2014) Duration of the South America summer monsoon is increasing. Atmos Sci Lett 15:110-113. doi: 10.1002/asl2.476

Schneider T, O'Gorman PA, Levine XJ (2010) Water vapor and the dynamics of climate changes. Rev Geophys 48:RG3001. doi:10.1029/2009RG000302

Seidel DJ, Randel WJ (2007) Recent widening of the tropical belt: Evidence from tropopause observations. J Geophys Res 112:D20113. doi:10.1029/2007JD008861

Seth A, Rojas M, Rauscher SA (2010) CMIP3 projected changes in the annual cycle of the South American Monsoon. Clim Change 98:331–357. doi: 10.1007/s10584-009-9736-6